



School of Engineering & Design  
Electronic & Computer Engineering



MSc Distributed Computing Systems Engineering

Brunel University West London

Simulation and Performance Analysis  
of a Distributed Position Correction  
Scheme for Unmanned Aerial Vehicles

Dionysios Satikidis

Supervisor: Dr. Marios Hadjinicolaou

July / 2011

A Dissertation submitted in partial fulfillment of the  
requirements for the degree of Master of Science

School of Engineering & Design  
Electronic & Computer Engineering



MSc Distributed Computing Systems Engineering

Brunel University West London

Simulation and Performance Analysis  
of a Distributed Position Correction  
Scheme for Unmanned Aerial Vehicles

Dionysios Satikidis

Signature: \_\_\_\_\_

**Declaration:** *I have read and I understand the MSc dissertation guidelines on plagiarism and cheating, and I certify that this submission fully complies with these guidelines.*

---

# Abstract

This dissertation presents aspects of vision based movement detection, control systems, simulation methodology and test results for a distributed optical position correction scheme for Unmanned Aerial Vehicle(s) (UAV). A detailed physical model of a quadrocopter combined with a novel, simple and robust Proportional-Integral-Derivative (PID) control approach and a detailed configurable virtual camera environment were realised during this thesis, and provide an innovative method to simulate and test scenarios with different flight trajectories and sensor configurations. The content of this research is the exploratory work for the development of a vision-based stabilisation system for the University of Applied Sciences Esslingen (HSE) quadrocopter project.

The first part of this thesis contains the project organisation, the related tools and architectures, and presents the strengths and risks of the used simulation driven methodology. Afterwards, the literature review presents several technical topics of existing UAV techniques for vision-based stabilisation, and further methods for mathematical description of a quadrocopter, optical movement detection and suitable control. A detailed analysis of the existing architecture, the corresponding simulation containing the not-purchased vision module and the realisation of control and image processing modules are presented in the design and implementation chapter. Subsequently, test scenarios are derived from a set of vision-based navigation and correction implementations of other projects, and used to analyse the position correction scheme of the HSE quadrocopter simulation. The last part of this thesis gives an overview of the results and outcomes, and presents the upcoming projects which will be based on the results of this work. Finally, it gives an overview of the new possibilities to realise high complexity scientific projects using the introduced simulation architecture.

---

# Acknowledgements

I would like to thank the many people who have supported me and made this Master's Thesis possible. My girlfriend Sabine, and my parents Nikolaos and Kiriaki, an endless source of encouragement, support and love. I am grateful to my supervisor Dr. Marios Hadjinicolaou for his confidence in me and my project, and the priceless encouragement and support throughout my dissertation.

Special Thanks to Prof. Dr. Joerg Friedrich for his trust and support, and the chance to be responsible for the quadrocopter project of the Faculty of Information Technology HSE. It was an incomparable experience and a great honor. Further, I would like to thank Mr. Wiedenhoefer of the Faculty of Mechatronics, and Prof. Dr. Czarnetzki of the Faculty of Mechanical Engineering, for the great interdisciplinary project collaboration.

A special thanks to my project colleague Peter Beltz for his endless commitment in new quadrocopter developments and his patience to repair the crushed hardware again and again. Also, I am grateful to my project colleague Rafael Trybek for the excellent testing, demonstration flying and his great technical support.

Thanks to my Master colleagues Daniel Szabo, Florian Theis, Jian Wu and Daniel Tech. It was a great honor to work with you.

I want to thank Robert Czech for his endless dedication and great support. Finally, a special Thanks to my childhood friend Florian Mueller and to the other persons who have proofread and commented on this document. All remaining mistakes are mine.

# **Contents**

<b>List of Abbreviations</b>	<b>iv</b>
<b>List of Symbols</b>	<b>viii</b>
<b>List of Figures</b>	<b>xii</b>
<b>References</b>	<b>1</b>
<b>Bibliography</b>	<b>10</b>

# List of Abbreviations

<i>I/O</i>	Input/Output
4GL	Fourth Generation Language
ADC	Analog to Digital Converter
ALGO	Algorithm
API	Application Programming Interface(s)
BDM	Background Debug Mode
BMOF	Block Matching Optical Flow
BS	Block Size
CACD	Camera Calibration Domain
CCU	Central Control Unit
CLCS	Closed Loop Control System(s)
CMOS	Complementary Metal Oxide Semiconductor
COOF	Corner Detection Optical Flow
CT	Cycle Time(s)
CV	Computer Vision
DMS	Deadline Monotonic Scheduling
DOF	Degrees of Freedom
DOSEK	Didactic OSEK
DSM	Domain Specific Modelling
DSP	Digital Signal Processor

## LIST OF ABBREVIATIONS

---

ECT	Enhanced Capture Timer
EOM	Equations of Motion
EVTF	Error-Value-Transfer-Function
FNC	Flow Number Calculation
FOE	Focus Of Expansion
FPGA	Field-Programmable Gate Array
FPS	Frames per Second
GAV	Generalized Acceleration Vector
GPS	Global Position System
GPV	Generalized Position Vector
GUAV	Gliding Unmanned Aerial Vehicle(s)
GUI	Graphical User Interface
GVV	Generalized Velocity Vector
HAL	Hardware Abstraction Layer
HighGUI	High Graphical User Interface
HIL	Hardware In the Loop
HSE	University of Applied Sciences Esslingen
HUAV	Hovering Unmanned Aerial Vehicle(s)
HWBIP	Hardware-Based Image Processing
IIC	Inter-Integrated Circuit
IMU	Inertial Measurement Unit

## LIST OF ABBREVIATIONS

---

IS	Image Size
ISR	Interrupt Service Routine
LSb	Least Significant bit
MATLAB	MATrix LABoratory
MAV	Micro Aerial Vehicle(s)
MBD	Model Based Design
MC	Microcontroller
MCU	Microcontroller Unit
MEMS	Micro-Electro-Mechanical System
MIMO	Multiple-Input and Multiple-Output
MLL	Machine Learning Library
OC	Optical Correction
ODE	Ordinary Differential Equation(s)
OF	Optical Flow
OFCA	Off-board Camera
OFIP	Off-board Image Processing
ONCA	On-board Camera
ONIP	On-board Image Processing
OpenCV	Open Computer Vision
OSEK	Offene Systeme und Schnittstellen für die Elektronik im Kraftfahrzeug
PCB	Printed Circuit Board

## LIST OF ABBREVIATIONS

---

PID	Proportional-Integral-Derivative
RANSAC	Random Sample Consensus
RF	Radio Frequency
RPM	Revolutions per Minute
SBC	Single Board Computer(s)
SCI	Serial Communication Interface
SISO	Single-Input and Single-Output
SLAM	Simultaneous Localization And Mapping
SOAD	Shift of the Optical Axis Domain
SPI	Serial Peripheral Interface
SVTF	Set-Value-Transfer-Function
SWBIP	Software-Based Image Processing
TF	Transfer Function
Tform	Transformation Matrix
TT	Time Triggered
UAV	Unmanned Aerial Vehicle(s)
UND	Underground
VIP	Video and Image Processing
WRT	with respect to
XML	Extensible Markup Language

# List of Symbols

$X_E$	X-axis WRT E-frame
$Y_E$	Y-axis WRT E-frame
$Z_E$	Z-axis WRT E-frame
$\phi$	Angular quadrocopter position around $X_E$ WRT E-frame (Roll)
$\theta$	Angular quadrocopter position around $Z_E$ WRT E-frame (Yaw)
$\psi$	Angular quadrocopter position around $Y_E$ WRT E-frame (Pitch)
$x_e$	Linear quadrocopter position along $X_E$ WRT E-frame
$y_e$	Linear quadrocopter position along $Y_E$ WRT E-frame
$z_e$	Linear quadrocopter position along $Z_E$ WRT E-frame
$\dot{x}_e$	Linear quadrocopter velocity along $X_E$ WRT E-frame
$\dot{y}_e$	Linear quadrocopter velocity along $Y_E$ WRT E-frame
$\dot{z}_e$	Linear quadrocopter velocity along $Z_E$ WRT E-frame
$\ddot{x}_e$	Linear acceleration of quadrocopter along $X_E$ WRT E-frame
$\ddot{y}_e$	Linear acceleration of quadrocopter along $Y_E$ WRT E-frame
$\ddot{z}_e$	Linear acceleration of quadrocopter along $Z_E$ WRT E-frame
$X_B$	X-axis WRT B-frame
$Y_B$	Y-axis WRT B-frame
$Z_B$	Z-axis WRT B-frame
$p$	Angular quadrocopter velocity around $X_B$ WRT B-frame (Roll)
$q$	Angular quadrocopter velocity around $Y_B$ WRT B-frame (Pitch)
$r_g$	Angular velocity $r$ measured by gyroscope

## LIST OF SYMBOLS

---

$r_{of}$	Angular velocity $r$ measured by optical flow sensor
$r$	Angular quadrocopter velocity around $Z_B$ WRT B-frame (Yaw)
$x_b$	Linear quadrocopter position along $X_B$ WRT B-frame
$y_b$	Linear quadrocopter position along $Y_B$ WRT B-frame
$z_b$	Linear quadrocopter position along $Z_B$ WRT B-frame
$u$	Linear quadrocopter velocity along $X_B$ WRT B-frame
$v$	Linear quadrocopter velocity along $Y_B$ WRT B-frame
$w$	Linear quadrocopter velocity along $Z_B$ WRT B-frame
$\dot{u}$	Linear quadrocopter acceleration along $X_B$ WRT B-frame
$\dot{v}$	Linear quadrocopter acceleration along $Y_B$ WRT B-frame
$\dot{w}$	Linear quadrocopter acceleration along $Z_B$ WRT B-frame
$\omega$	Speed of rotation
$\Delta\omega$	Deviation of rotation speed
$\xi$	GPV WRT E-frame
$\dot{\xi}$	GVV WRT the E-frame
$\nu$	GVV WRT the B-frame
$J_\Theta$	Transformation matrix from B-frame to E-frame
$R_\Theta$	Rotation transformation matrix from B-frame to E-frame
$T_\Theta$	Translation transformation matrix from B-frame to E-frame
$\Gamma^E$	Linear position vector WRT the E-frame
$\Theta^E$	Angular position vector WRT the E-frame
$V^B$	Linear velocity vector WRT the B-frame

## LIST OF SYMBOLS

---

$\omega^B$	Angular velocity vector WRT the B-frame
$\ddot{\Gamma}^E$	Linear acceleration vector WRT the E-frame
$\dot{\Gamma}^E$	Linear velocity vector WRT the E-frame
$M_B$	System inertia matrix WRT the B-frame
$M_H$	System inertia matrix WRT the H-frame
$C_B(\nu)$	Coriolis-centripetal matrix WRT the B-frame
$C_H(\zeta)$	Coriolis-centripetal matrix WRT the H-frame
$m$	Mass of body
$I_{n \times n}$	Identity matrix of dimension n times n
$I$	Body inertia matrix
$G_B(\xi)$	Gravitational vector WRT the B-frame
$G_H$	Gravitational vector WRT the H-frame
$O_B(\nu)$	Gyroscopic propeller matrix WRT B-frame
$O_H(\zeta)$	Gyroscopic propeller matrix WRT H-frame
$\Omega$	Sum of propellers' speed
$E_B$	Movement matrix WRT B-frame
$E_H(\xi)$	Movement matrix WRT H-frame
$b$	Factor of thrust
$d$	Factor of drag
$l$	Distance between centre of quadrocopter and centre of propeller
$\dot{v}$	GAV WRT B-frame
$\zeta$	GVV WRT H-frame

## LIST OF SYMBOLS

---

$\dot{\zeta}$	GAV WRT H-frame
$F^B$	Forces vector of quadrocopter WRT B-frame
$\tau^B$	Torques vector of quadrocopter WRT B-frame
$\dot{V}^B$	Linear acceleration vector WRT the B-frame
$\dot{\omega}^B$	Angular acceleration vector WRT the B-frame
$U_1$	Vertical thrust WRT the B-frame
$U_2$	Roll torque WRT the B-frame
$U_3$	Pitch torque WRT the B-frame
$U_4$	Yaw torque WRT the B-frame
$F_{n\{X_B, Y_B, Z_B\}}$	Thrust component of rotor n along $X_B$ , $Y_B$ or $Z_B$
$S^2_{N-1}$	Bias-corrected Sample Variance(s)

# **List of Figures**

## Introduction

In recent years, the interest in robotic science and the development of robots enormously increased. Reasons for that are the unstoppable technological progress in hard-and software techniques, but also the ambition to replace humans with machines in dangerous, monotonous or unreachable industrial environments (medical, space, aviation and so forth). One area of these interests is the aerial platform and the realization of UAV, which are mostly controlled via remote control or fly autonomous. These aircraft vehicles have several capabilities, like in military or rescue operations, with special environments like a burning house. For such indoor operation, it is important to realise that some kinds of feedback sensors, like GPS-sensors, could not work satisfactory. In such cases, UAV face problems with their self-stabilization, because their physical behaviour is generally unstable [39, p.1 Introduction]. Most of the attempts to stabilize UAV work with a clever combination of sensor equipment and control algorithms. Mostly this controller uses an Inertial Measurement Unit (IMU) which is mounted on board and includes acceleration sensors to detect movements in the given Degrees of Freedom (DOF).

## CHAPTER 1 INTRODUCTION

---

Current acceleration sensors, which are used for this purpose, are Micro-Electro-Mechanical System (MEMS) or fiberoptic sensors which have a finite precision and unacceptable error propagation in case of integration for velocity or position detection [37, pp.11-13 Function Principles of MEMS, Sources of Error]. This problem also is a field of research for the Quadrocopter project of the HSE [1, Website]. The goal of this Master's Thesis is to research the topic of flight stabilisation and error drift elimination with an optical sensor. This approach has to be tested and evaluated with the implementation of a simulation focused on the behaviour of the flight dynamics in relation to the quality of the optical measurements and the control system of the quadrocopter.



**Figure 1.1:** HSE Quadrocopter

## 1.1 CONTEXT OF THE PROJECT

---

### 1.1 Context of the Project

The quadrocopter project of the HSE was launched with the goal to build a system from the scratch, which is developed by students, scientific workers and Professors. In a prior project, the Printed Circuit Board (PCB), which contains the parts necessary to control the quadrocopter, was designed by students at the faculty of Mechatronics and Electrical Engineering in Goeppingen. Back then, these project groups' focuses were on the simulation, implementation of basic functions and visualization of the actual condition of the aircraft. The first two project groups already show their results, a multidisciplinary development including hardware design, application development, embedded programming, simulation and the interfaces between these special fields. In the year 2009, the Faculty of Information Technology adopted the development of the project, with the aim to solve problems which came up in the previous development process and to redesign the soft- and hardware architecture. So a new hardware design was developed in a corporation between the two faculties, with the outcome of a Central Control Unit (CCU) which can detect inertial movements in six DOF and can control the four actuators of the quadrocopter via so-called "brushless controllers". One of the biggest unresolved problems so far is the development of a robust controller and the elimination of drifts, which especially come up at the hovering state. The practice and experience of previous developments show that it is indispensable to proof new developments with a simulation before they will be realized at the real UAV. So the main topic and focus of this Master's Thesis will be on the development of a simulation that shows potential solutions of the mentioned problems, and the research and evaluation for the outcome results.

### 1.2 Problem Description

Improvements in high density power storage, integrated miniature actuators and sensors facilitate the development of Micro Aerial Vehicle(s) (MAV) and new areas of research for unmanned and autonomous flying systems [50, p.1 Introduction]. This new area of interest also brought a new area of problems. One of these is the fact that the pilot of the aerial vehicle does not exist, either because the UAV flies autonomous or because the pilot observes and controls the UAV via remote control. In both cases, it is necessary that the UAV system can detect its absolute position, to provide the pilot with a better quality of control or, furthermore, to manoeuvre autonomous. The following articles also describe this problem with different views and approaches [?, p.2 Localization and path planning] [36, p.1 High precision aircraft positioning] [53, p.2 Teleoperated Robot Control].

This necessity of location determination leads to the requirement of a measurement unit which provides the possibility to detect the movements in the given DOF. Because of low-cost and low-complexity reasons, the most popular components which are used to reach a nearly satisfactorily level of flight stabilisation are inertial sensors. These sensors, altogether called IMU, have the ability to detect the acceleration or velocity of translational or rotational movements. Furthermore, a control system can be used in a closed loop together with the IMU and theoretically can correct nearly every disturbance in a continual system [51, pp.45-64 System Control] [43, pp.49-51 Control Strategy].

### **1.3 AIMS AND OBJECTIVES**

---

The resolution limitation of the sensors and the necessity of integrating the acceleration values for position and velocity determination have a big impact in aspects of error propagation and detection of smoothly movements in real systems [12, p.5 Low-acceleration Drift]. The quadrocopter of the HSE also includes an IMU for stabilisation and faces the same problems. These problems can be eliminated with the extension of an optical system, which can track the absolute position of the UAV ego-motion.

### **1.3 Aims and Objectives**

The aim of this dissertation is to provide a simulation architecture that can be used as prototype development platform for a distributed visual movement detection and control of a quadrocopter. Furthermore, the characteristics of the distributed image processing and movement detection have to be analysed in relation to the variation of configurations and critically assessed.

One essential objective is for the configuration of the simulating components to provide the option to simulate a range of hardware components that have not been purchased yet. By way of example, the simulation of the on-Board camera has to provide options of configuration for the image size, underground structure and so on. The simulation of the communication between UAV and host also has to provide a variation of transmission rate, or abstracted as frame rate, and further behaviour which could affect the visual movement detection at the base station. The efficiency in relation with the quality of functionality is an important indicator for the success and acceptance of the distributed movement detection

### **1.3 AIMS AND OBJECTIVES**

---

approach.

### **1.3 AIMS AND OBJECTIVES**

---

Therefore it is important to get an insight on the possible characteristics of the simulated components with the result to find a solution that satisfies the efficiency and quality aspects.

Another important objective is for the interfaces between the simulating components to be clearly specified and allow a way of modular exchangeability of simulation components with the real objects. This purpose has to allow a more precise investigation of the behaviour of the real hardware related components, and the option to test software for the UAV target, like the On-Board control algorithm, at the base station.

The realisation of the simulation therefore has to provide an encapsulated and flexible architecture, and has to simulate behaviour like delays and jitters for simulated components. Thereby, the simulation has to adjust a real-time-behaviour into the complete simulated environment and, allow measurements and predictions about feasibilities with the simulated configuration.

# **Methodology and Project Organisation**

This chapter introduces development methods, tools and frameworks, which were used in this project. Furthermore, it shows the individual usage combinations of the presented methods and the project plan. Thereby, this plan presents the effective in comparison to the planned process of this project, visualised in a Gantt chart.

## **2.1 Software Development Process**

Mechatronic projects combine mechanical, electronic and software modules, which mostly are strongly related to each other. To solve problems of parallel development and a test driven architecture, the method Model Based Design (MBD) is introduced and described here. This method is combined with the spiral model and builds an individual software development method for this project. The motivation thereby is to combine the strengths of a simulation driven MBD with the advantageous evolutionary structure of the spiral model.

## 2.1 SOFTWARE DEVELOPMENT PROCESS

---

### 2.1.1 Model Based Design

MBD is a popular method to encounter problems which come up in the development of mechatronic products. These systems always involve mechanical, electrical, control and embedded components which are developed in different teams of engineers with a specialised focus on one part of the complete project. Some of these components are dependent on the results of other components before they can be developed. This problem can be solved with MBD and the possibility to develop modules of the complete project by simulating their environment, so the development can run highly parallel with the benefit that the modules can be continuously tested in each phase of the project [23, pp.1-2 Challenges of mechatronic product development]. Beside the direct challenges of mechatronic projects, problems also exist with the multiple domain modelling and development notations and languages. Legacy attempts almost used several domain solutions and mapped these from the idea domain into the solution domain. The problem in doing so is the additional effort to spit up the problem in domain terms and to map the outcomes together. So another concept, which is adopted by modern MBD architectures is to create in a Domain Specific Modelling (DSM) language, a model which is generated to code from the domain-specific framework and to use the benefit to model the functionality and not indirect the code (See figure ??<sup>1</sup>)[56, pp.55-60 Chapter 3.3 Difference from other modelling approaches]. One of the biggest disadvantages of MBD architectures is that the DSM language is not as fine-grained and low-level as classic programming languages.

---

<sup>1</sup>This figure is derived from [55, p.13 Modelling functionality vs. modelling code]

## 2.1 SOFTWARE DEVELOPMENT PROCESS

This can cause problems, especially in projects with very special requirements to the functionality which can not be reflected without a workaround into the DSM language.

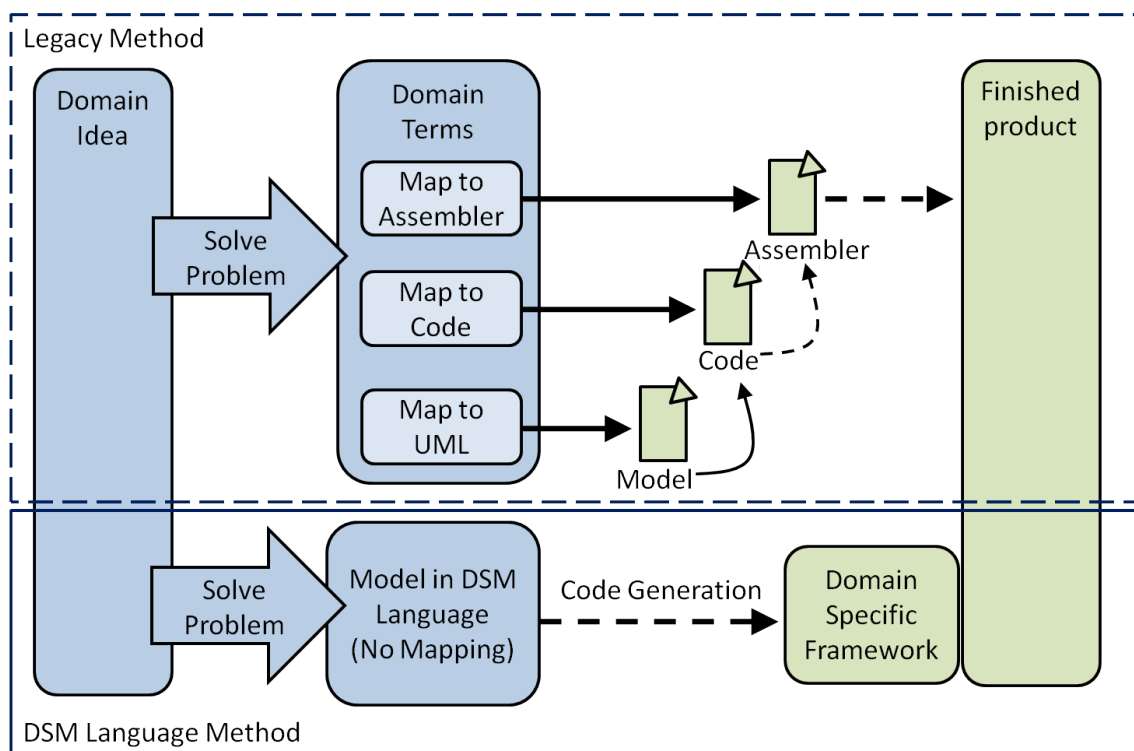


Figure 2.1: Legacy DSM vs. DSM Language approach

The development section in figure ?? includes the phases and the corresponding key capabilities of MBD. The first phase of MBD is the realisation of the researched and required components into a simulation environment. Thereby physical components, environmental models and algorithms are abstracted into systems by using domain-specific modelling tools with well defined edges and intercommunication. The developed systems can be tested during the design phase simultaneously to analyse the system performance and correctness.

## 2.1 SOFTWARE DEVELOPMENT PROCESS

---

Other key capabilities of MBD are given in the implementation phase. Mostly, MBD tools allow to generate embedded code from the designed systems or to combine handwritten code with the built simulation of the design phase. So the implemented modules can be similarly tested in the adopted simulation environment. Finally, components that have passed the tests at the implementation phase can be integrated together. Ultimately, the final product can also be tested with the MBD tool by simulating the environment of the product, e.g. in a Hardware In the Loop (HIL) test bench. [2, Model Based Design, MathWorks]

### 2.1.2 Spiral Model

Most of the UAV stability and movement detection approaches were developed iterative under consideration of the upcoming problems and obstacles [25, 24, Iterative Development, Single and Dual Camera Feedback] [57, 58, Iterative Development, Landing and Position Control Development]. This procedure model will also be appropriate for this project, because the potential risks are difficult to identify. So the outcome of the development process has to be a prototype that can be evaluated, tested and extended. A process model, which provides an appropriate structure to face the iterative prototyping strategy under consideration of the risk-aspects, is given with the spiral model. The classic spiral model has typically four phases in which the product is developed in an incremental evolutionary process. Derivates of this classic model, for a customer evaluation focused on quality improvements, may have three, five or six phases. In the context of this project, the classic four phases spiral model is used for scientific and feasibility studies and does not have to provide further customer communication

## 2.1 SOFTWARE DEVELOPMENT PROCESS

phases [48, pp.36-38 The Spiral Model].

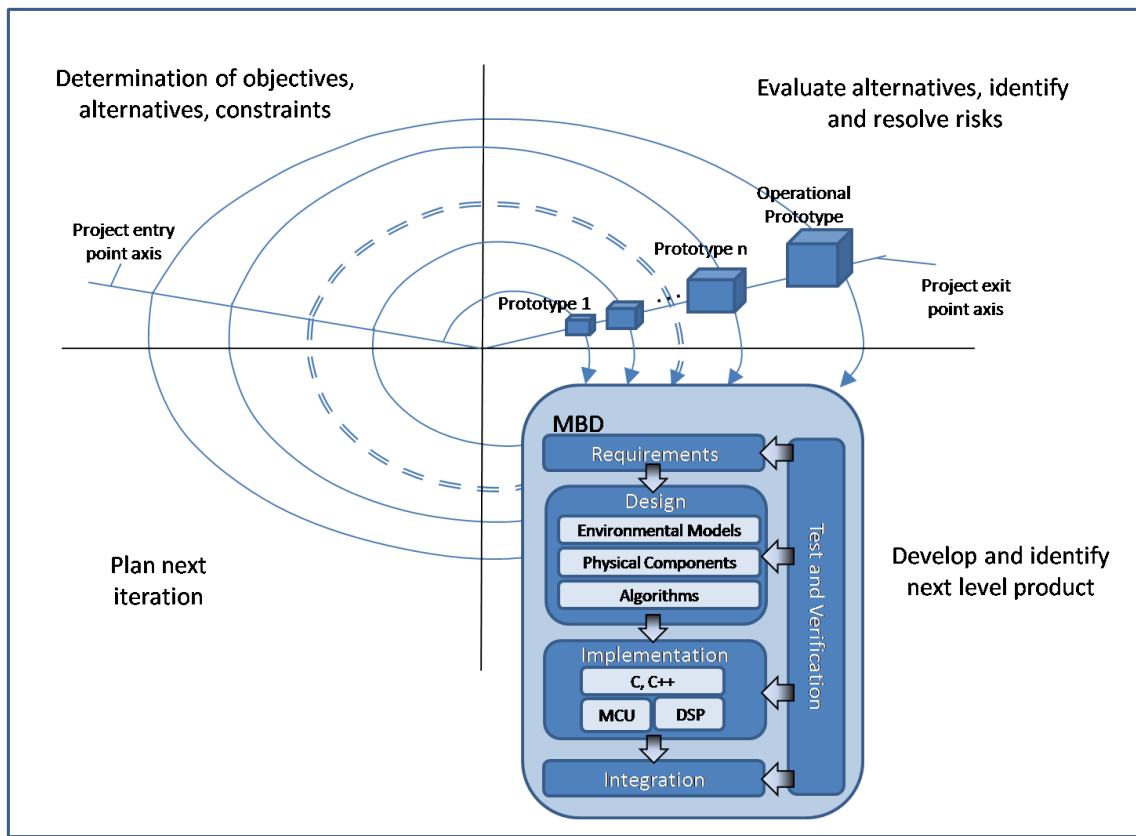


Figure 2.2: The Spiral Model in combination with Model Based Design

A typical cycle of the four phases spiral model (??) begins with the identification of the objectives which have to be elaborated, like performance, functionality, flexibility and so on. The next step is to evaluate the alternatives in relation to the objectives and constraints, and to determine significant sources of risks. After that, the next level iteration of the product is planned. In the special case of this project, it is advantageous to use MBD in this phase by using the results of the previous phase as input. This input can be a planned prototype, or requirements that describe the changes to be executed. The output of the MBD phase can be used again in the planning phase for the next iteration [11, pp.64-69 Spiral Model of the Software Process].

### 2.2 Tools and Architectures

An overview of tools and architectures, which are analysed and used in the context of this project, is the main topic of this chapter. Thereby the detailed components of the presented architectures are examined with the focus of extensibility, exchangeability, modularity and so far.

#### 2.2.1 MATLAB/Simulink

The software package MATrix LABoratory (MATLAB)<sup>2</sup>, developed by the company MathWorks<sup>3</sup>, stands for solutions of high-performance numerical computation and visualisation. Thereby MATLAB's main features and capabilities can be summarized in the groups visualized in figure ??<sup>4</sup>. MATLAB's built-in functions provide tools for linear algebra computations, data analysis, signal processing, optimisation, numerical solution of Ordinary Differential Equation(s) (ODE) and further types of scientific computation. For visualisation, MATLAB supports numerous graphic functions for 2-D and 3-D graphics and animations. Modules programmed in C/C++ or Fortran can be integrated into MATLAB by using the external interface using the Mex-files. This facility allows to simulate the environment of an embedded algorithm and to test it, to include legacy modules of previous developments or libraries which are programmed in the supported languages.

---

<sup>2</sup>See [4, MATLAB]

<sup>3</sup>See [6, The MathWorks, Inc.]

<sup>4</sup>This figure is derived from the schematic diagram presented in [44, A schematic diagram of MATLAB'S main features]

## 2.2 TOOLS AND ARCHITECTURES

MATLAB also provides an own Fourth Generation Language (4GL)(also denoted as MATLAB) DSM language for programming focused on the fast development of functions or applications. Various toolboxes of MATLAB allow the development of special applications such as symbolic computations, image processing, statistics etc. and reflect the idea of DSM. The list of toolboxes keeps growing over time and releases of MATLAB [44, p.3 What is MATLAB?]. Beside the programming interface of MATLAB, Simulink provides an environment for multi-domain simulation and MBD of dynamic embedded systems. This graphical interface also provide easy access to the complete MATLAB continuum of tools<sup>5</sup>.

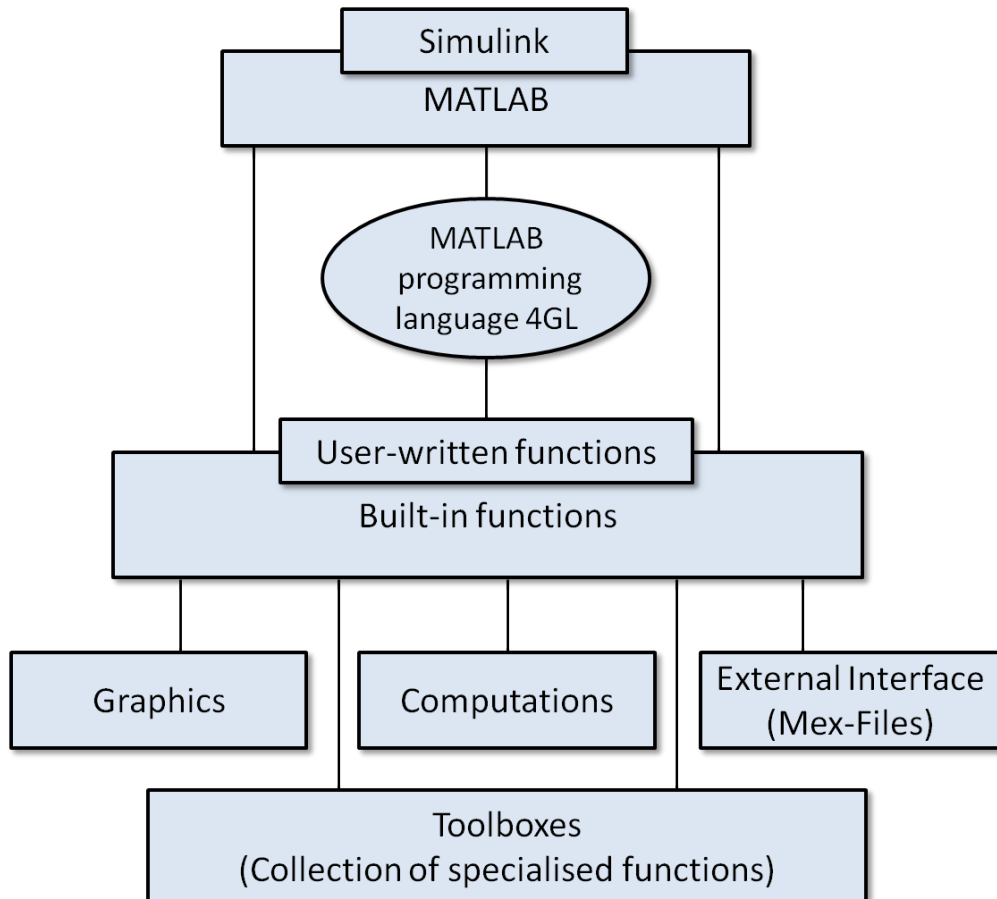


Figure 2.3: MATLAB/Simulink's schematic diagram of main features

<sup>5</sup>See [5, Simulink]

### 2.2.2 OpenCV

Open Computer Vision (OpenCV)<sup>6</sup> is one of the most popular open source computer vision libraries for scientific and industrial projects. It contains over 500 functions that span many areas in computer vision such as medical imaging, factory product inspection, security, camera calibration, stereo vision, robotics and so on. The main components of OpenCV are visualized in figure ??<sup>7</sup>. The component Computer Vision (CV) contains the basic image processing and higher-level computer vision algorithms. Another important part strongly related to computer vision is the machine learning ability. So OpenCV provides statistic classifier and clustering tools which allow this ability in the Machine Learning Library (MLL) component. OpenCV's Input/Output (*I/O*) component High Graphical User Interface (HighGUI) contains functions and routines for fast loading and storing of image or video data and a Graphical User Interface (GUI). Finally, the core data structures and algorithms are located in the component CX-CORE which supports data transforms, matrix algebra, object persistence, memory management, error handling and further core capabilities [27, pp.1-33 Chapter 1, Overview].

---

<sup>6</sup>See [3]

<sup>7</sup>This basic structure overview bases on the figure presented in [27, p.33 Chapter 1, The basic structure of OpenCV]

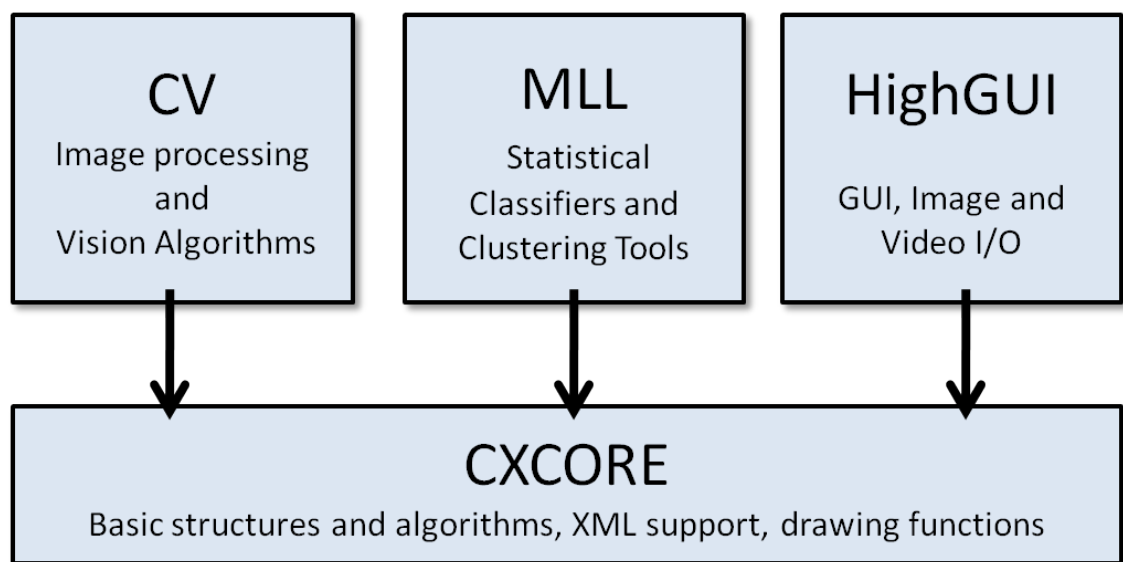


**Figure 2.4:** OpenCV's basic structure

## 2.3 Strengths and Risks

As mentioned in chapter ??, the strengths of MBD are the possibility of parallel development of mechatronic, electrical or software components, and the test facility during each phase that is presented in the MBD process in ???. Beside this advantages, MBD bases on the strategy to create simulations of components and to refine these from an abstract level to a more detailed level and finally to the real execution environment. Thereby, this way of development can include risks which can lead, at the worst, to a restart of the project development. As presented in the spiral process model, risks should be analysed and classified in a previous phase before development. Related to the simulation development of this project, the most important risks are analysed in ??<sup>8</sup>.

---

<sup>8</sup>Related risk preventions and provisions are shown in ??, ??, ??, ??

## 2.3 STRENGTHS AND RISKS

---

The analysis thereby includes the identified risk, the effect, which can raise if the risk becomes real, the classification of the risk related to the seriousness, and the strategy which should be executed if the risk occurs or to prevent the risk. The corresponding risk preventions in this work are presented with references to the corresponding chapters. Furthermore, the classification shows if the risk is ignorable, threatens to delay the project could even lead to a catastrophic project fail.

graphic/RiksAnalysisTable.pdf

**Figure 2.5:** Possible risks, effect, classification and solution strategy

### 2.4 Project Management

Based on the spiral model presented in ??, the project plan executed in this Master's Thesis project includes one circle of all phases and ends with the release of the first prototype and the corresponding research and documentation. The Gantt chart, shown in figure ??, visualises the original planned and the truly executed project plan <sup>9</sup>. Regarding the first few tasks of analysis and research of relevant topics, the time resources were guessed quite good because the time-drift between the issues adds up to only few days. After the second milestone, which symbolises the start of the MBD phase, the time miscalculation increases dramatically.

A reason for that could be the missing practical experience and the necessity to gain new knowledge of architectures and tool-kits of the MBD tool which were not expected before. This experience shows that more time has to be planned in the context of a project like this, to research which components should be used and to get familiar with these. Furthermore, it is interesting to see that the parallel tasks, which include two parallel lines for documentation and parallel research, could be executed as planned for the interim report and final dissertation.

The characteristic not expected of these parallel tasks was the fact that the modelling and research parallel to the documentation took nearly the same time. A reason for that is the fact that the research results show mostly unexpected phenomena which were examined more closely to find out the reasons for these effects.

---

<sup>9</sup>The original planned tasks/milestones are grey/white and the truly executed are red/blue/black

## 2.4 PROJECT MANAGEMENT

---

Another reason of delay was the expectation that most of the needed components could only be designed with the MBD tool, and the execution code of the simulation can be generated automatically. But some of the needed functions were not supported by the framework, which lead to the necessity to implement the components manually. Overall, the expected critical path (red) was correct, because the documentation of the dissertation claimed the biggest time resources and delays. This could base on the fact that the complex parts of this dissertation are difficult to be presented and reduced so the reader has the chance to understand the presented material.

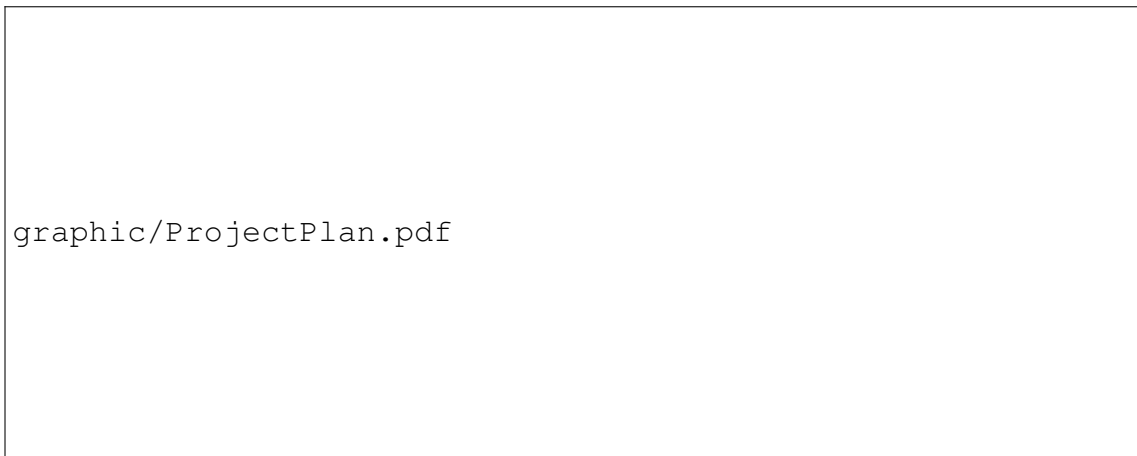


**Figure 2.6:** Executed project plan with time drifts (Gantt Chart)

## Literature Review

The realization of a distributed optical error correction scheme for UAV contains several challenges of different topics of technical information technology, which have to be introduced for this project in the context of a literature survey. These topics are related to the focus to create a simulation. That means the theory of function and the complexity of these topics should be examined, as also the possibilities of simplification.

The first part of the survey will introduce the basic quadrocopter flight dynamics and approaches to derive the mathematical model of motion. The result of this model will be the Equations of Motion (EOM) in a form which can be used for simulation and reflects as much as possible the reality.

A comparison between the researched existing visual approaches for error correction of UAV, will be the focus of the second part of this survey. Thereby, the strengths and weaknesses in focus of different aspects have to be given. Furthermore, this part will introduce optical movement detection technique which will be investigated here under consideration of the limitations and the abstraction of the reality.

## 3.1 QUADROCOPTER FLIGHT DYNAMICS

---

Finally, the third part of the survey will give an overview of control approaches in, which the determined movement detection values can be processed for aircraft stabilisation. Further methods will be introduced, which allow to measure and classify the performance of a control system and its characteristics under consideration of digitalisation aspects.

### 3.1 Quadrocopter Flight Dynamics

The following chapters examine the principles and flight dynamics of the quadrocopter system, and further presents a mathematical model, which describes the desired movements in different frames. This mathematical model bases on several researches, found in focus of this review, and provides the basis needed for a time- variant realisation of a simulation.

#### 3.1.1 Principles

For a better appreciation of the quadrocopter flight dynamics, the following figure<sup>1</sup> visualizes the influence of thrust in relation to the movements in the DOF. Thereby the values of  $\omega$  [rad/sec]represents the least needed speed of rotation, for creating the required thrust for the hovering state. This can be described as a state, in which the forces in x- and y-axis equal zero and the uplift force in direction of the z-axis has the same absolute value as the gravitational force.

---

<sup>1</sup>This picture extends the pictures presented in[59, pp.8-11 Basic concepts]

### 3.1 QUADROCOPTER FLIGHT DYNAMICS

The value of  $\Delta\omega$  characterizes the purposed deviation of the required rotation speed in hovering state and is used for navigation of the quadrocopter.

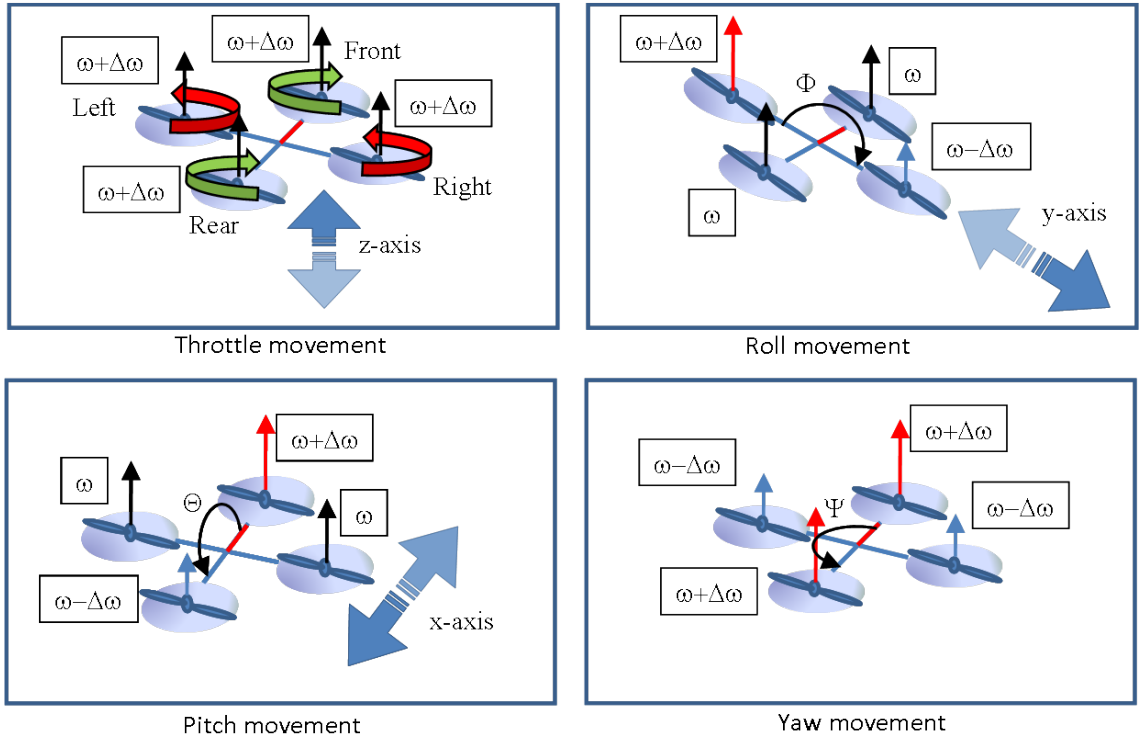


Figure 3.1: Degrees of Freedom of a quadrocopter

To keep the equilibrium of rotational kinematics and to prevent self-rotation, the motor direction of rotation equals crosswise. The quadrocopter has six DOF which can be distinguished as angular and translational movements. Translational movements can be executed in x-, y- and z- axis. Accelerating all rotors with the same speed  $\omega$  to the value of  $\Delta\omega$  will affect a throttle movement  $U_1$  [N] in z-direction. Movements to the negative direction of the z-axis are possible, if the summarised thrust of the four rotors is smaller as the gravitational force of the aerial vehicle. The roll movement  $U_2$  [N m] can be described as a change of the angle around the x-axis.

### 3.1 QUADROCOPTER FLIGHT DYNAMICS

---

Thereby the left and right rotors execute a force difference by slowing down the one and simultaneous increasing the other speed with  $\Delta\omega$ . Related to the thrust difference and angular movement, the aerial vehicle creates a force in the direction of the y-axis. Equivalent to roll, the pitch movement  $U_3$  [N m] is executed with a change of the angle around the y-axis. Also the pitch movement creates a translational movement across the x-axis. Pitch and roll can only reach a stable angular state and accelerate to the x- or y-axis, if the value of  $\Delta\omega$  is the same at the diagonal rotors. Otherwise, the quadrocopter would pure rotate across the corresponding axis. The yaw movement  $U_4$  [N m] is a rotation around the z-axis. This angular movement results in combination of pairwise different thrusts and takes as long as these thrusts are different<sup>2</sup>.

#### 3.1.2 Equations of Motion

Simulations of dynamic systems are based on physical models which describe their motion. So the behaviour of the quadrocopter also can be described by using EOM, with respect to (WRT) the input parameters of the model. Thanks to these equations, it is viable to predict and define the positions, velocities and accelerations of the quadrocopter by investigating the four motor speeds. Bouabdallah [51, pp.15-24 System Modelling] demonstrates two methodologies to derive the EOM with the Newton-Euler and Euler-Lagrange formalism.

---

<sup>2</sup>The theory and the identifiers of this chapter bases on [59, pp.8-11 Quadrotor model and system]

### 3.1 QUADROCOPTER FLIGHT DYNAMICS

---

The Euler-Lagrange formalism derives the EOM by calculating the difference of the kinetic and potential energy of the system under consideration of the general coordinates and forces<sup>3</sup>. The Newton-Euler formalism bases on the Newton-Euler equations [49, p.106 The original recursive Newton-Euler equations] which describe the combined translational and rotational dynamics of a rigid-body WRT the centre of mass. Both formalisms follow different approaches to derive the EOM, but are based on the same coordinate systems. These two coordinate systems have different origins and describe movements from different perspectives. One coordinate system can be considered as observer perspective to the quadrocopter because it describes the absolute position in space and is called earth inertial frame (E-frame).

In contrast to that, the second coordinate system is a body fixed frame (B-frame) and is defined as system of relative movements which originates in the middle of the symmetric rigid quadrocopter body<sup>4</sup>. Bresciani [59, pp.8-23 Quadrotor model and system] shows in his work the identification and derivation of the EOM by using the Euler-Newton formalism and gives reasons why EOM are more conveniently formulated in the B-frame or further in a mixture called hybrid frame (H-frame)<sup>5</sup>. A part of these congenial reasons focus the simplicity to convert on-board measurements to the B-frame coordinates and the matter of fact that the control forces almost are given in B-frame. The other part describes simplifications in the mathematical derivation causes of B-frames symmetrical behaviour and the time invariance of the inertias<sup>6</sup>.

---

<sup>3</sup>See [20, pp. 218-219 The Lagrangian Method]

<sup>4</sup>An origin which is coincidence to the centre of mass simplifies the Newton-Euler equation enormous, See [49, p.98 The original recursive Newton-Euler equations]

<sup>5</sup>See [59, p.19 Hybrid frame]

<sup>6</sup>See [59, p.12 Conveniently formulated EOM]

### 3.1 QUADROCOPTER FLIGHT DYNAMICS

In the following figures<sup>7</sup>, we can see the both coordinate systems and the movements in the DOF which are interesting.

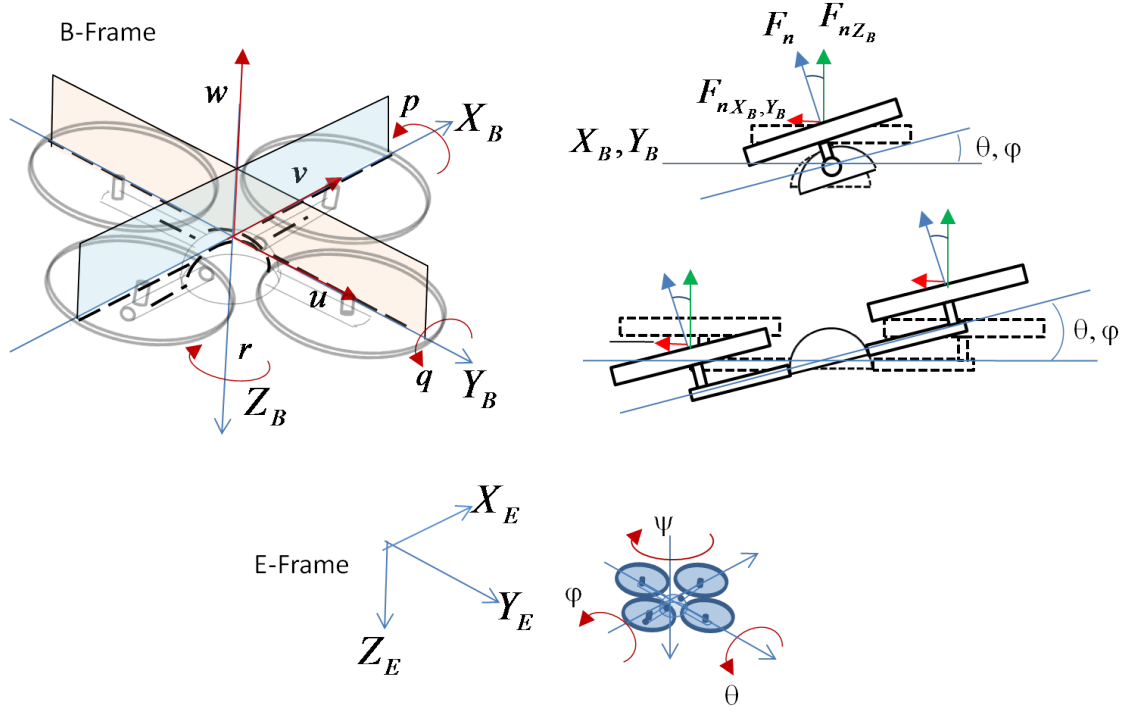


**Figure 3.2:** Quadrocopter movements and coordinate systems

The starting point of Brescianis derivation is to define an equation, which describe a generic 6 DOF rigid-body (See ??) with the Generalized Velocity Vector (GVV)  $\dot{\xi}$  WRT the E-frame, the GVV  $\nu$  WRT the B-frame and the generalized matrix  $J_\Theta$  which includes the rotation and the translation submatrix  $R_\Theta, T_\Theta$  which transforms  $\nu$  to  $\dot{\xi}$  (See ??). The definition of the GVV and the Generalized Position Vector (GPV) WRT the corresponding frames are visualized in figure ?? and can be described with the equations ?? and ???. Thereby  $\dot{\xi}$  is composed of the linear position vector  $\Gamma^E$  [m] and the angular position vector  $\Theta^E$  [rad]. Similar to the position vector, the velocity vector is composed of a linear velocity vector

<sup>7</sup>This picture extends the coordinate system picture presented in[51, p.20 OS4 coordinate system]

### 3.1 QUADROCOPTER FLIGHT DYNAMICS

---

$V^B$  [m/s] and an angular velocity vector  $\omega^B$  [rad/sec].

### 3.1 QUADROCOPTER FLIGHT DYNAMICS

---

The essence frame of interest is a mixture of the both mentioned frames, called H-frame, which contains the linear velocity vector  $\dot{r}^E$  [m/s] from E-frame and the angular velocity vector  $\omega^B$  [rad/s] from B-frame [??](#). Brescianis interest was to define a frame which can be transferred to an acceleration vector WRT the H-frame and to facilitate the EOM under consideration of typical IMU values of a quadrocopter.

Bresciani uses the Euler-Newton equations (See [??](#))<sup>8</sup> to derive the matrix form which is composed of the system inertia matrix  $M_B$  and a Coriolis-centripetal matrix  $C_B(\nu)$ . A 6 DOF rigid-body dynamics system inertia matrix takes the mass of the body  $m$ <sup>9</sup> [kg] and its inertia  $I$  [Nm s<sup>2</sup>] into account.

Furthermore Bresciani recognized that the quadrocopter dynamics can be divided to three contributors which describe the gravitational vector  $G_B(\xi)$ <sup>10</sup>, the gyroscopic torque  $O_B(\nu) * \Omega$ <sup>11</sup> and the movement vector with the inputs of the system  $E_B * \Omega^2$ (See [??](#))<sup>12</sup>. So it is possible to create a relation between the Newton-Euler equations (See [??](#)) and the sum of these three contributors ([??](#)), to isolate the Generalized Acceleration Vector (GAV)  $\dot{v}$ , and to derive the EOM WRT the B-frame (See [??](#)).

---

<sup>8</sup>See [59, p.13 The dynamics of a generic 6 DOF rigid-body]

<sup>9</sup>The notation  $I_{3x3}$  means 3 times 3 identity matrix (See  $I_{n \times n}$ )

<sup>10</sup> $G_B(\xi)$  considers the acceleration of gravity  $g$  [m/s<sup>2</sup>] and influences the linear forces, See [59, p.15 The gravitational vector]

<sup>11</sup> $O_B(\nu) * \Omega$  considers the gyroscopic effects of the propeller rotation which influence the angular forces. Thereby  $O_B(\nu)$  is the propeller matrix and  $\Omega$  [rad/s] the propellers' speed vector See [59, p.16 The gyroscopic torque]

<sup>12</sup>The constant matrix  $E_B$  ?? includes the thrust  $b$  [Ns<sup>2</sup>],  $d$ [Nm s<sup>2</sup>]and  $l$  [m] (distance between the center of the quadrocopter and the center of a propeller) factors of the input system. The inputs are given with  $\Omega^2$  because the forces and torques are proportional to the squared propellers' speed, See [59, pp.129-135 Aerodynamics calculation]

### 3.1 QUADROCOPTER FLIGHT DYNAMICS

Equivalent to that, the substitution of GAV  $\dot{\nu}$  with GAV  $\dot{\zeta}$  WRT the H-frame in ??, gives an equation which can be solved to  $\dot{\zeta}$  for the determination of the required EOM and a quadrocopter model with typical IMU values (See ??).

$$\begin{array}{c}
 \dot{\zeta} = J_{\Theta} * \nu \quad (3.1) \\
 \downarrow \\
 \begin{aligned}
 \zeta &= \begin{pmatrix} \Gamma^E \\ \Theta^E \end{pmatrix} = \begin{pmatrix} x_e \\ y_e \\ z_e \\ \phi \\ \theta \\ \psi \end{pmatrix} \quad (3.2) \\
 J_{\Theta} &= \begin{pmatrix} R_{\Theta} & 0_{3x3} \\ 0_{3x3} & T_{\Theta} \end{pmatrix} \quad (3.3) \\
 \nu &= \begin{pmatrix} V^B \\ \omega^B \end{pmatrix} = \begin{pmatrix} u \\ v \\ w \\ p \\ q \\ r \end{pmatrix} \quad (3.4)
 \end{aligned}
 \end{array}$$
  

$$\begin{array}{c}
 \zeta = \begin{pmatrix} \dot{\Gamma}^E \\ \omega^B \end{pmatrix} = \begin{pmatrix} \dot{x}_e \\ \dot{y}_e \\ \dot{z}_e \\ p \\ q \\ r \end{pmatrix} \quad (3.5) \\
 \downarrow \\
 \begin{aligned}
 \begin{pmatrix} F^B \\ \tau^B \end{pmatrix} &= \begin{pmatrix} m * I_{3x3} & 0_{3x3} \\ 0_{3x3} & I \end{pmatrix} \begin{pmatrix} \dot{V}^B \\ \dot{\omega}^B \end{pmatrix} + \begin{pmatrix} \omega^B \times (m * V^B) \\ \omega^B \times (I * \omega^B) \end{pmatrix} \quad (3.6) \\
 &= M_B * \dot{\nu} + C_B(\nu) * \nu = G_B(\zeta) + O_B(\nu) * \Omega + E_B * \Omega^2
 \end{aligned}
 \end{array}$$
  

$$\boxed{
 \begin{array}{l}
 M_H * \dot{\zeta} + C_H(\zeta) * \zeta = G_H + O_H(\zeta) * \Omega + E_H(\zeta) * \Omega^2 \quad (3.7) \\
 \dot{\nu} = M_B^{-1} * (-C_B(\nu) * \nu + G_B(\zeta) + O_B(\nu) * \Omega + E_B * \Omega^2) \quad (3.8) \\
 \dot{\zeta} = M_H^{-1} * (-C_H(\zeta) * \zeta + G_H + O_H(\zeta) * \Omega + E_H(\zeta) * \Omega^2) \quad (3.9)
 \end{array}
 }$$

### 3.1 QUADROCOPTER FLIGHT DYNAMICS

---

The following equations show the derived EOM of the GAV  $\dot{\zeta}$  WRT the H-frame. Apparent from the rotational DOF of the quadrocopter, the linear accelerations  $\dot{\Gamma}^E$  WRT the E-frame are influenced by a trigonometrical equation of the angles  $\Theta^E$  and the sum of the uplift forces  $U_1$ . This behaviour is also visualized in the cross-sectional and front side view WRT the specific angle and B-frame axis in the figure ???. Further the equations show the angular accelerations  $\dot{\omega}^B$  WRT the B-frame and the corresponding influences which derive from the propellers' force constellation  $U_1, U_2, U_3, U_4$ (See chapter ??), the angular velocities from  $\omega^B$  and the body inertias WRT the mass axis<sup>13 14 15 16</sup>.

$$\dot{\zeta} = \begin{pmatrix} \ddot{x}_e \\ \ddot{y}_e \\ \ddot{z}_e \\ \dot{p} \\ \dot{q} \\ \dot{r} \end{pmatrix} = \begin{pmatrix} (\sin\psi\sin\phi + \cos\psi\sin\theta\cos\phi)\frac{U_1}{m} \\ (-\cos\psi\sin\phi + \sin\psi\sin\theta\cos\phi)\frac{U_1}{m} \\ -g + (\cos\theta\cos\phi)\frac{U_1}{m} \\ \frac{I_{YY}-I_{ZZ}}{I_{XX}}qr - \frac{J_{TP}}{I_{XX}}q\Omega + \frac{U_2}{I_{XX}} \\ \frac{I_{ZZ}-I_{XX}}{I_{YY}}pr + \frac{J_{TP}}{I_{YY}}p\Omega + \frac{U_3}{I_{YY}} \\ \frac{I_{XX}-I_{YY}}{I_{ZZ}}pq + \frac{U_4}{I_{ZZ}} \end{pmatrix} \quad (3.10)$$

---

<sup>13</sup>The formula ?? bases on [59, p.21 The GAV WRT H-frame]

<sup>14</sup> $J_{TP}$  [N m s2] is the total rotational moment of inertia around the propeller axis, See [59, p.16 Propeller inertia]

<sup>15</sup> $I_{XX}, I_{YY}, I_{ZZ}$  [kg m2] are moments of inertias around the specific axis, See [59, p.136 Inertia matrix]

<sup>16</sup>The identifiers of this chapter are derived from [59]

$$U_B = E_B \Omega^2 = \begin{pmatrix} 0 \\ 0 \\ U_1 \\ U_2 \\ U_3 \\ U_4 \end{pmatrix} = \begin{pmatrix} 0 \\ 0 \\ b(\Omega_1^2 + \Omega_2^2 + \Omega_3^2 + \Omega_4^2) \\ lb(-\Omega_2^2 + \Omega_4^2) \\ lb(-\Omega_1^2 + \Omega_3^2) \\ d(-\Omega_1^2 + \Omega_2^2 - \Omega_3^2 + \Omega_4^2) \end{pmatrix} \quad (3.11)$$

## 3.2 Vision-based Sensors

This chapter introduces why visual sensors are interesting in actual technological developments of UAV systems, which approaches exist and what the benefits and drawbacks are. The mentioned approaches are separated thereby in several domains and compared with each other. The outcomes of this review about vision-based sensors and the related topics, include some decision criteria of the realised approach in focus of this project.

### 3.2.1 Motivation

An enormous quantity of researches, which is sponsored by industry companies and universities, was executed to find a better approach to stabilize UAV by using different sensors. Movement detection approaches, which are ultrasonic, sonar or Radio Frequency (RF) based show that it is necessary to have known reference points to get a reliable result [35, p.2 Ultrasound indoor localization with

### 3.2 VISION-BASED SENSORS

---

reference points][42, pp.4-5 Radio Model Localization]. The problem of these approaches is that the environment has to be prepared before the UAV flight. This preparation is a drawback in point of flexibility in different operation places. Anyway, approaches with ultrasonic, RF or sonar sensors show that the localization of UAV needs a kind of global feedback to correct the UAV absolute position. One of the first motivations for a vision-based sensor was presented by Ettlinger et al. [52, pp.1-2 Visual-Based Localization and Control].

## 3.2 VISION-BASED SENSORS

---

In this paper, the authors suggest that vision is the only practical solution for obstacles of reference free flight stability, and showed an On-board approach for a Gliding Unmanned Aerial Vehicle(s) (GUAV) by detecting the horizon with a forward looking camera and estimating and control the flight attitude[12, p.27 Vision Sensors]. The intention of a reference free vision-based stability approach, for solving the IMU error drift, is the motivation for the investigation of visual approaches, which will be introduced and compared in this chapter.

### 3.2.2 Distribution and Implementation Approaches

This chapter focus the comparison of different approaches of vision sensors' implementations and distributions, which were researched in several scientific works. These approaches are separated in distribution approaches (Off-board Image Processing (OFIP), On-board Image Processing (ONIP), On-board Camera (ONCA), Off-board Camera (OFCA)), as visualized in figure ??, and the implementation approaches Hardware-Based Image Processing (HWBIP) and Software-Based Image Processing (SWBIP). Problems, such as a limited power resource, a poor level of algorithm complexity for ONIP resulting from the limited calculating On-Board performance and the endeavour to economise weight, lead to outsourcing the image processing to a remote system via a wireless communication, which is not concerned to the On-Board problems. A drawback of this approach was examined by Langer et al. [57, pp.5-7 Off-Board Image Processing] which use OFIP to track a landing pad for autonomous landing and show that the wireless transmission delay has an impact on the sampling rate of the algorithm.

### 3.2 VISION-BASED SENSORS

Tippetts [12, p.27 Vision Sensors] mentions in his work the limitation of the wireless communication in OFIP as a drawback for range of the aircraft<sup>17</sup>. The OFCA approach was researched by Altug et al. [25, p.76 Localization and Control with an Off-Board camera], with the result of a less sensitive feature detection and position localization compared to the ONCA approach. OFCA tracking is shown in the developments of extremely reliable and precise localization of a UAV and is used in the development of aggressive autonomous flights of multiple MAV in the experiments of Mellinger et al. [18, Trajectory Generation and Control with Off-Board cameras] [17, pp.363-364].

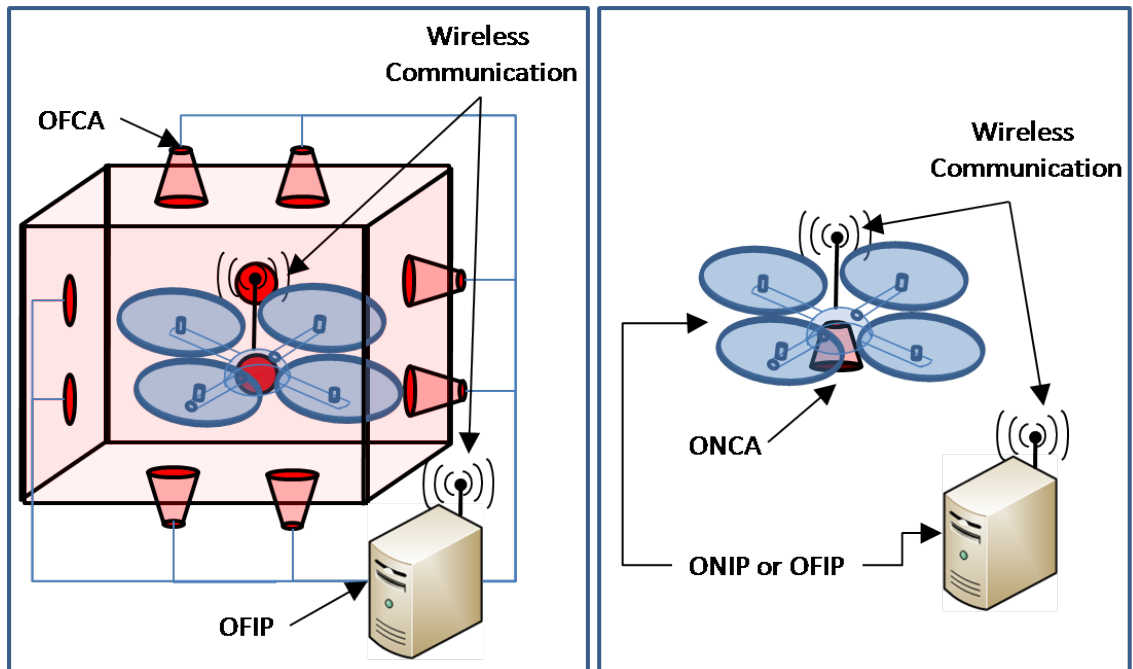


**Figure 3.3:** On- and Off-Board camera and motion tracking system approach

The advantage of OFCA tracking system is that the image capturing and position tracking is executed outside the UAV and prevents complex On-Board calculations for movement and position estimation<sup>18</sup>.

<sup>17</sup>The comparison of OFIP and ONIP approaches is visualized in ??

<sup>18</sup>This approach focus the E-frame localisation and is robust against position drifts and errors

## 3.2 VISION-BASED SENSORS

---

The disadvantage of this OFCA method is that they need a special flying environment, which is build up with an OFCA motion tracking system<sup>19</sup> [?, pp.1-2 The GRASP Testbed]. Tippetts [12, pp.21-22 On-Board image processing with an FPGA] realised an ONIP approach with a Field-Programmable Gate Array (FPGA), which uses a complex feature tracking algorithm, but runs with high sampling rate<sup>20</sup>.

The characteristics of the feature tracking with a FPGA can result a fast movement tracking method, but it is not an efficient method in the focus of power consumption because the hardware is not optimised for the image processing tasks. In contrast to the drawbacks of FPGA, Langer et al. [58, On-Board image processing with mice sensors] and Beyeler et al. [8, pp.4-5] showed an approach for detecting the spatial movement of a UAV with optical mice sensors, which have an optimized hardware for image processing and are lightweight.

These sensors calculate the optical flow of the captured images and estimate the movement direction of the UAV in hardware and can provide a high sample rate. In contrast to the fast movement detection, a disadvantage is that these sensors have limitations related to the operating environments. These limitations are the concrete light and distance range which is required from the manufacturer [?, pp.7-15 Limitations of the operating environment][58, p.6 Performance of the optical flow based position controller]

SWBIP approaches have a more flexible extension and change behaviour for prototyping of vision-based solutions, but they don't work as fast as HWBIP ap-

---

<sup>19</sup>The comparison of OFCA and ONCA approaches is visualized in ??

<sup>20</sup>In this case a high sampling rate means that the image processing runs nearly equal to the sampling rate of the IMU

### 3.2 VISION-BASED SENSORS

---

proaches.

## 3.2 VISION-BASED SENSORS

Stowers et al. [34] realized a heading estimation for a quadrocopter with an on-board Single Board Computer(s) (SBC) which runs the open source computer vision toolkit OpenCV [3]. This software based image processing approach shows strengths in the modularity of the image processing architecture and in the interchangeability of the vision system<sup>21</sup> [34, pp.1-6 Software Based Vision Processing][27, Software Structure and Portability]. Figure ?? includes the summary of the examined approaches of this chapter. We can see that no approach has outstanding set of beneficial characteristics. Each approach brings advantages and disadvantages, so the decision of the appropriate approach relates to the focus of investigation.

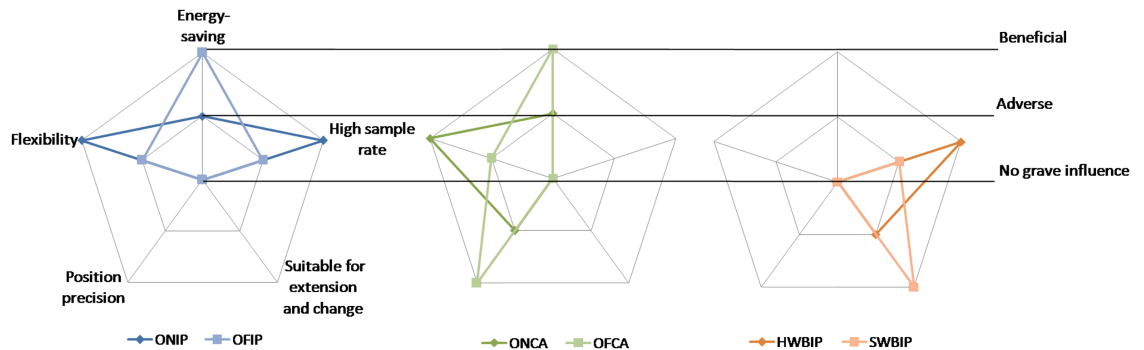


**Figure 3.4:** A comparison of the distribution behaviour of vision sensors

### 3.2.3 Vision-based Movement Detection Algorithms

Sequential captured images contain a huge amount of information about the absolute and relative movement of objects in every direction.

<sup>21</sup>The comparison of HWBIP and SWBIP approaches is visualized in ??

### 3.2 VISION-BASED SENSORS

---

So several vision-based movement detection approaches were researched in the topic of UAV stability with different requirements to the information which extracted from the vision process<sup>22</sup>. A simple approach for a relative vision based control of a UAV was implemented by Boabdallah [51, pp.110-114 Position Sensor] using a down looking camera and the Canny edge detector [33] and the Douglas Peuker Algorithm for curve equalisation [22]. The drawback of this approach is that the field of vision must contain forms with edges which mean that the approach cannot result a satisfactory result if no edges are detected.

A further approach for detecting relative movements and to build up a map for autonomous navigation, is visual Simultaneous Localization And Mapping (SLAM). This approach tracks features in the field of vision and reconstructs the relation to the tracked features of previous images. The realization of SLAM [14] in a UAV was executed in the work of Bloesch et al. [39] under consideration of real-time characteristics. The behaviour of the algorithm shows that the localization of the tracked features and the simultaneous mapping has a big impact at the time delay of the calculation.

So the experiments and the control algorithms were researched and designed for 7.5Hz sample rate. Another popular tracking method for movement detection is given with the Optical Flow (OF), which can be described as movement observation of tracked objects or pixels in a sequence of images. Algorithms to calculate the OF were introduced by Horn and Schunk [?], Lucas and Kanade [16]. A few years after introducing the Lucas-Kanade-Algorithm, Lucas described the theoretical approach of visual navigation by using the OF. Thereby he described the

---

<sup>22</sup>These investigated approaches are visualized in figure ???. This figure includes pictures presented in [Jea11, SLAM][28, Edge detector][31, p.27 Horn and Schunck optical flow]

### 3.2 VISION-BASED SENSORS

---

possibility to detect movements and to calculate correspondence velocities.

## 3.2 VISION-BASED SENSORS

These velocities can be combined to a vector field which can describe movements in every direction [15, pp.40-45 Optical Navigation Theory].

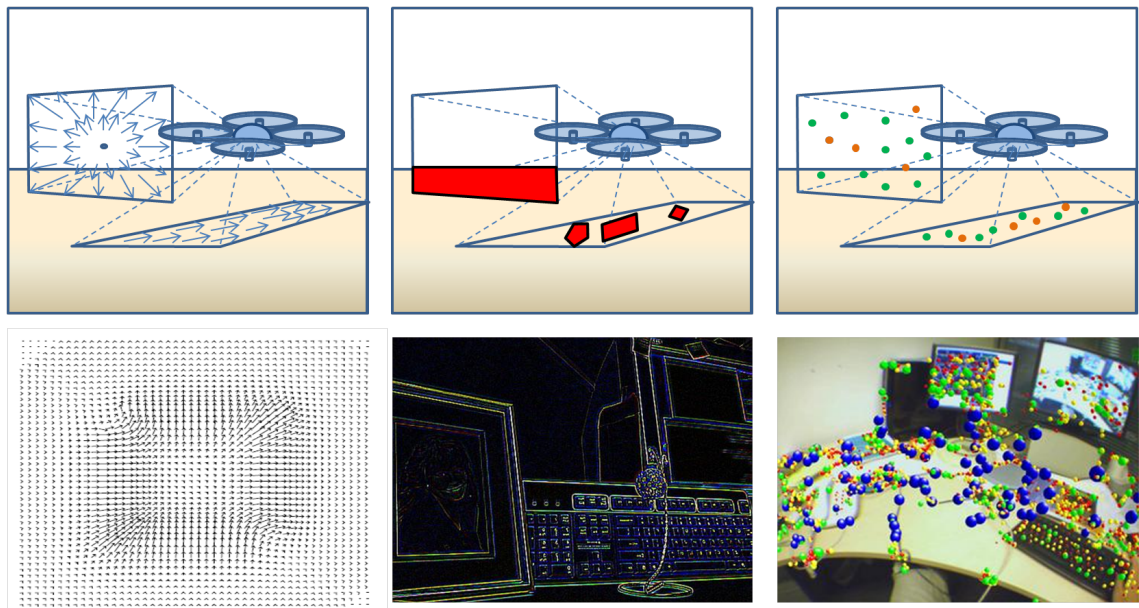


**Figure 3.5:** Examples for UAV stabilisation with Optical Flow, Edge detection and SLAM

### 3.2.4 Optical Flow

Researches which are related to image processing, mostly use camera models to reduce the complexity of the reality. This approach is also practicable in researches with OF. The figure ?? visualizes a camera model with a spherical image plane, which illustrates a complex real camera and a flat image plane, that simplifies the complex model. Such simplification is achievable, if a mathematical transformation of the image plane can result a distortion-free image plane. Fach [37, pp.29-31 Chapter 3.3, Distortions] classifies reasons for distortions in a Camera Calibration Domain (CACD) and the Shift of the Optical Axis Domain (SOAD). Pincushion- and barrel- distortions are summarized as radial distortions

### 3.2 VISION-BASED SENSORS

---

and caused by focal distance in relation to the captured image dimension.

### 3.2 VISION-BASED SENSORS

---

Further decentering distortions are based on the wrong alignment of the optical axis to the projected plane. Further Fach [37, pp.29-31 Matchematical description of distortions] shows that these distortions of a physical camera can be eliminated with the equations shown in appendix ???. Thereby, the problem of distortions is reduced to a factorisation of each distorted coordinate of the complete image. This process can be executed in the initial camera calibration phase, to eliminate distortions of the physical behaviour of the lenses and the image plane of the camera, and further in situations in which the camera is moved not planar to the projected plane. In the second case a fixed IMU of the camera system can provide the difference to the orthogonal gravity vector  $g$ , and can allow the transformation of the captured image in real time<sup>23</sup>.

Following, the OF projection suggested by Wei [?, pp.71-96 Obstacle Detection Using Optical Flow], is described as a 2D-projection on the image plane of a 3D motion in the real world. Thereby Wei uses the ideal perspective projection model to introduce the projection of a point  $P = (X, Y, Z)$ , from the camera frame into the image frame  $p = (x, y, f)$  where  $f$  is the focal length. The OF definition is derived with the assumption that the point  $P$  moves in the time  $t'$  to the Point  $P'$  with the corresponding projection on the image plane  $p$  and  $p'$ .

The velocity on the image plane can be calculated as  $v = p - p' = (x, y, 0)^T - (x', y', 0)^T$ , where the component of  $z$  is cancelled out causing the 2D projection. Wei uses this projection to describe the problem of retrieving the OF velocity with 6 DOF.

---

<sup>23</sup>Such a camera was introduced in the year 2009 as standalone system from Fraunhofer Institute for Manufacturing Engineering and Automation ,See [13, pp.1-2]

## 3.2 VISION-BASED SENSORS

Further Wei described that researches, related to the OF velocity determination, only can based on a reduced DOF model<sup>24</sup>.

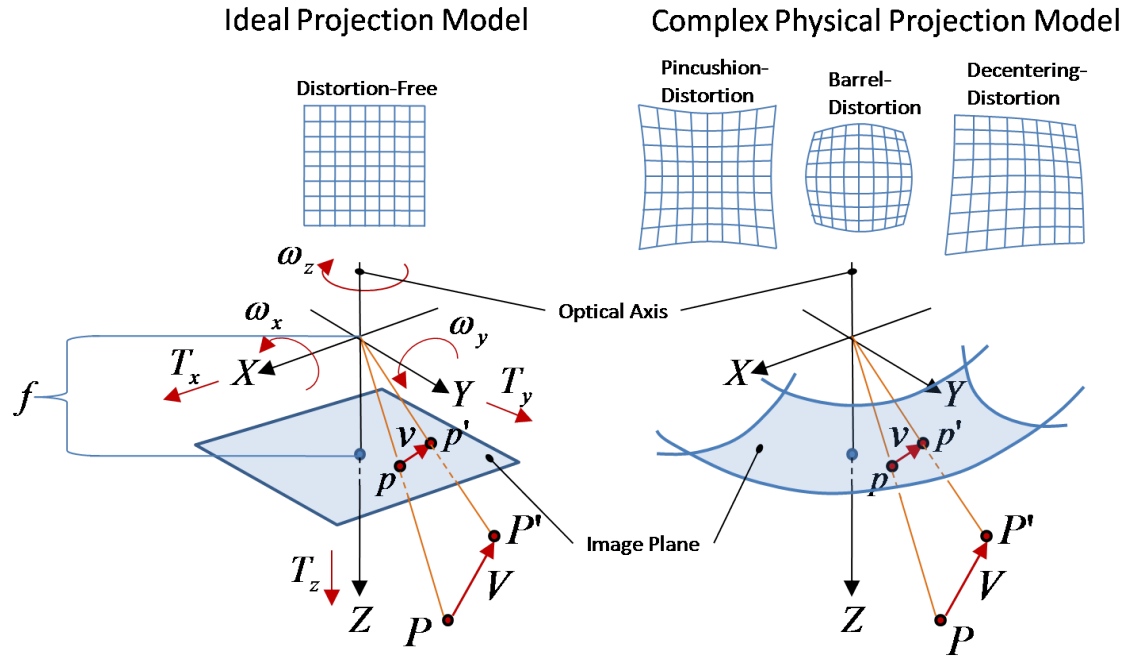


**Figure 3.6:** Complex Physical and Reduced Projection Camera Model

After introducing the projection camera models, the possibilities of OF determination can be focused with a top-down separation of algorithm classifications. These classification groups OF algorithms to feature based, gradient based and correlation based methods. Feature based OF algorithms usual execute three steps for the determination of the OF field. At first, the images of a sequence are scanned for good features. Such features can be corners or regions of contrast peaks. Further found features are compared trough the image sequence with the result to determine for each step an OF vector field.

---

<sup>24</sup>The DOF of a ideal projection model are shown in figure ?? The can be summarised in a translation vector  $T = (T_x, T_y, T_z)^T$  and a rotational vector  $\omega = (\omega_x, \omega_y, \omega_z)^T$ , See [?, pp.74-77 Motion Model Deduction]

## 3.2 VISION-BASED SENSORS

The feature based OF is robust against the aperture problem, which implies that just a part of the orthogonal movements can be detected in a image sequence with edges [9, p.24].

The figure ??<sup>25</sup> visualises the peaks of contrast regions. In this case the three hot-air balloons, in the square of the image, can be used as good features. Based on this example, the drawback of the feature based OF is given in cases, if no features can be found.

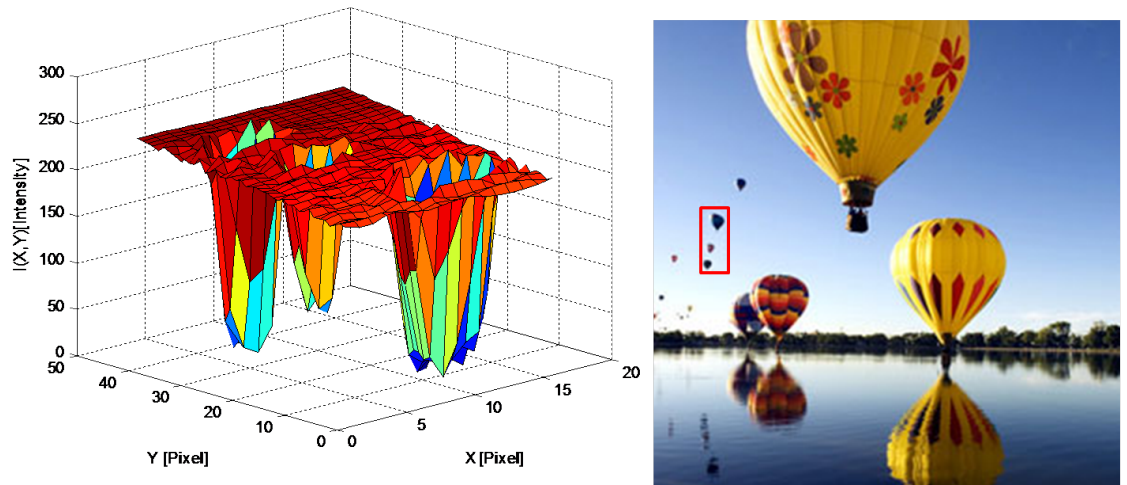


**Figure 3.7:** Detected features visualised as peaks

In contrast to that the gradient based algorithms can determine a optical flow field with no found features. This characteristic bases on the calculations of such algorithms, which use the intensity of images to determine the vector field. Thereby the movements of the intensities are determined with executing a minimising algorithm to the neighbourhood intensities. These determination is related to the disadvantage of intensive calculation complexity, which can be a drawback for real-time applications [?] [16].

<sup>25</sup>The presented image is downloaded from the website: <http://www.1800skyride.com/>

### 3.2 VISION-BASED SENSORS

An approach to improve the calculation complexity of the gradient based OF determination, is given with the pyramids approach of Lucas and Kanade [16] (See figure ??). The approach thereby downscales the pixel resolution with grouping pixels into blocks, with the average grayscale, and refines the image more and more until the intensity distances are determined satisfactory.

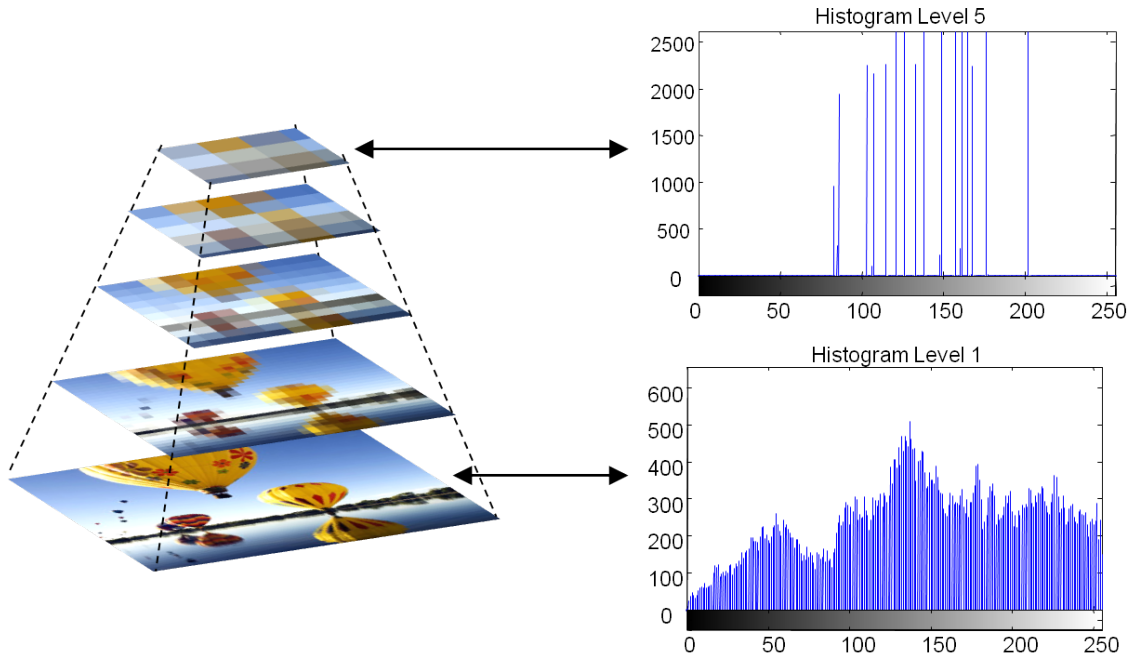


**Figure 3.8:** Lucas-Kanade-Algorithm with Pyramidal Scaling

Correlation based approaches use the strategy of searching and matching segments through a image sequence. Such algorithms work satisfactory, if the distribution of intensity in the processed regions of the image is constant over time. Another more conventional name for this kind of algorithm is block matching (See figure ??). Thereby the algorithm tries to match blocks from previous to the actual image in the defined section. The block size and the corresponding search section influences the calculation time of processing. The result of the block matching algorithm is the vector shift of the blocks. This shift can be transformed in relation to the sample rate to the velocity vector field OF.

## 3.2 VISION-BASED SENSORS

One of the biggest advantages of correlation based approaches is the simplicity of processing and the uncomplex mathematical theory which allows a fast and easy evaluation of the process. Drawbacks of this approach are the memory intensity as well as the error sensibility which bases on wrong matches. Further the execution time characteristic of such approaches is related to the search algorithms and the realisation. Generally, all approaches introduced in this chapter can be configured and executed unprofitable to the characteristics of the incoming image sequence, which can further be a reason for unsatisfactory results.

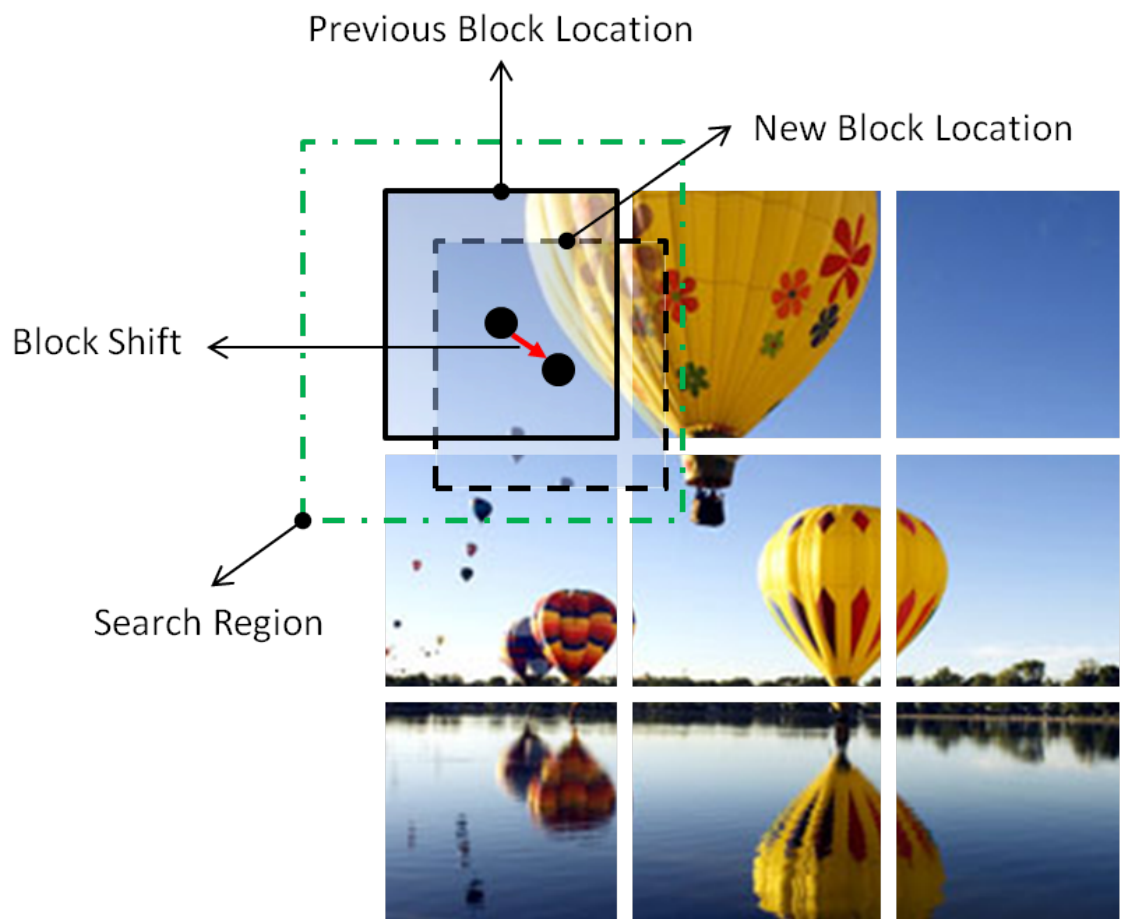


**Figure 3.9:** Block Matching Algorithm

### 3.3 CONTROL SYSTEM CHARACTERISTICS

---

## 3.3 Control System Characteristics

This chapter focus several aspects of control systems, which are frequently used in UAV projects. At first, different control architectures are examined, compared and discussed. Further, several methods of analysis and design of control systems are presented with the aim to show how such systems can be designed, robust and stable, using different strategies in different domains. Another focus, which is introduced with the multiple domain analysis of this chapter, is the methodology and analysis of discrete time-variant control systems.

### 3.3.1 Control Approaches

The closed loop feedback architecture is an approved method for controlling systems, that is nearly used in the most of the systems controls in industry and society. So the most of the researches in the UAV stabilisation topic were, and still are, executed with closed loop control architectures, which are built up as Multiple-Input and Multiple-Output (MIMO) or as multiple Single-Input and Single-Output (SISO) systems. The differences between the researched approaches are the amount of inputs and outputs of the physical process, the type of controller, the used measurements and the sampling rate. Thereby the type and behaviour of the controller is close related to the measurements and the physical process [46, p.3]. The classical control approach using PID controller was researched in several Hovering Unmanned Aerial Vehicle(s) (HUAV) projects [61, pp.24-31] [51, pp.43-68]. These researches show that the classical PID controller is not robust enough to handle with complex models which include several inte-

### 3.3 CONTROL SYSTEM CHARACTERISTICS

---

gration states, but has to be transformed to cascaded PID controller.

### 3.3 CONTROL SYSTEM CHARACTERISTICS

---

Basically the implementation of a PID controller can be executed with the determination of three parameters for the given process. These parameters are the proportional, integral and derivative gain of the controller, which have an impact on the dynamic behaviour of the controlled value [46, pp. 695-698 PID Controllers]. Another approach for control improvement was introduced by Luenberger [19] and describes a closed loop control approach called state-observer, which simulates the process in real time parallel to the true process by using the input and output vector of the closed loop system and corrects the control strategy. Bloesch et al. [39, p.5] have shown in their research, that the problem of sensors with non-negligible time delay can be solved to an adequate result by using a state-observer. The reason for that is that the state-observer allows to configure and to control the stability behaviour of the closed loop feedback architecture. If a process can be observed or furthermore controlled, is related to the possible states of the system, and furthermore to the measurements of the DOF [46, pp.632-636 Controllability and Observability]. In the other hand a state-observer architecture has a big impact to the calculation capacity of the UAV target because the real-time process simulation of a 6 DOF rigid-body becomes very complex.

### 3.3 CONTROL SYSTEM CHARACTERISTICS

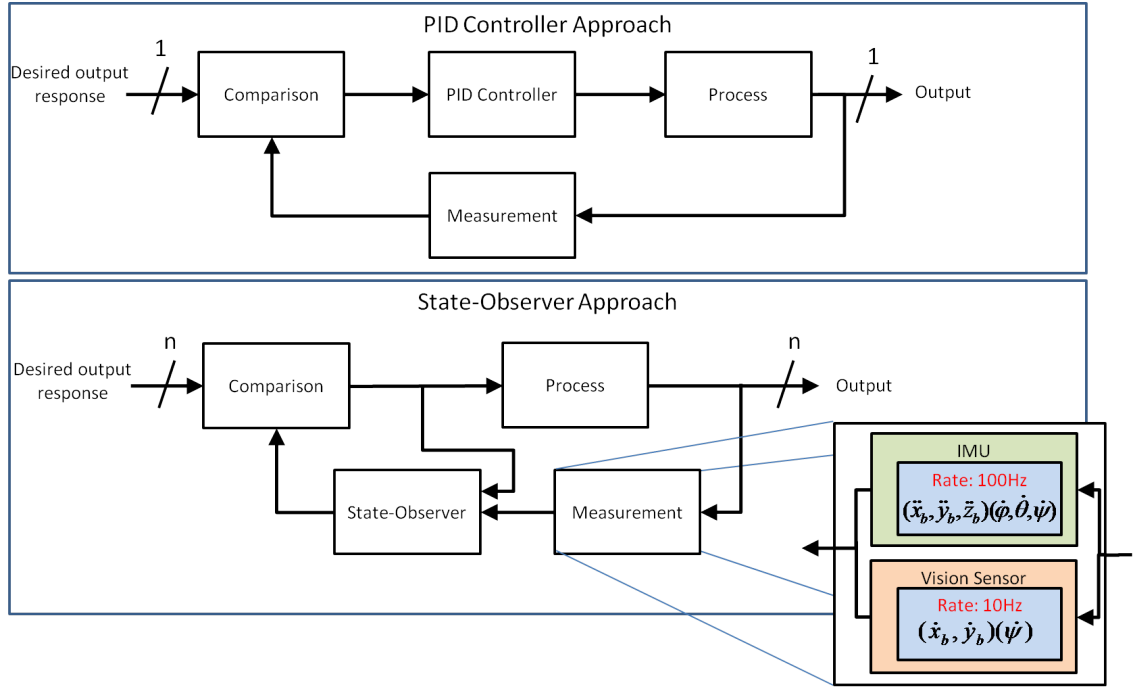


**Figure 3.10:** PID-Controller and State-Observer in closed loop system with variable sample sensor rates

#### 3.3.2 Performance Measures in the Time Domain

Control systems usual are designed and evaluated in different domains under consideration of the special behaviour of these. The closed loop feedback architecture can be described with a transfer function, which shows the behaviour of the closed loop feedback system in respect to the system boundaries. The time domain is used to visualize the time variant behaviour of the controlled value and allows definitions of performance measures. These measures are visualised in figure ??<sup>26</sup> and can be described with the following characteristics <sup>27</sup>.

<sup>26</sup>This picture extends the diagram presented in [?, Chapter 2, p.11 Characteristics of control systems]

<sup>27</sup>The content of the characteristics is derived from [?, Chapter 2, p.12 Requirements of control systems][46, Chapter 5, pp.228-230 The Performance of Feedback Control Systems]

### 3.3 CONTROL SYSTEM CHARACTERISTICS

---

- Stability: A control system is called stable, if the controlled value  $y(t)$  reaches a constant value and does not oscillate between a set of values.
- Precision: The precision describes the ability of steady state error minimization of a control system. The best case of precision is  $e(\infty) = y_{set}(\infty) - y(\infty) = 0$ .
- Transient oscillation: The oscillation process of a system is described with the needed time of the function is needed to reach the range of tolerance  $T_s$  and is called settling time. This time depends on the rise time which describes the first entrance point of the range of tolerance. A short rise time can bring the disadvantage of a big maximal overshoot  $y_{max}$ , which should be kept minimal.
- Robustness: A control system is characterized as robust, if it does not become unstable if system values change over time in scope of their tolerances. Such tolerances can occur from temperature variations or tribological reasons.
- Load of actuator: The load of the actuator(s) should be minimal. That means that the maximum actuator value should be equal to the needed value to prevent unnecessary work.

### 3.3 CONTROL SYSTEM CHARACTERISTICS

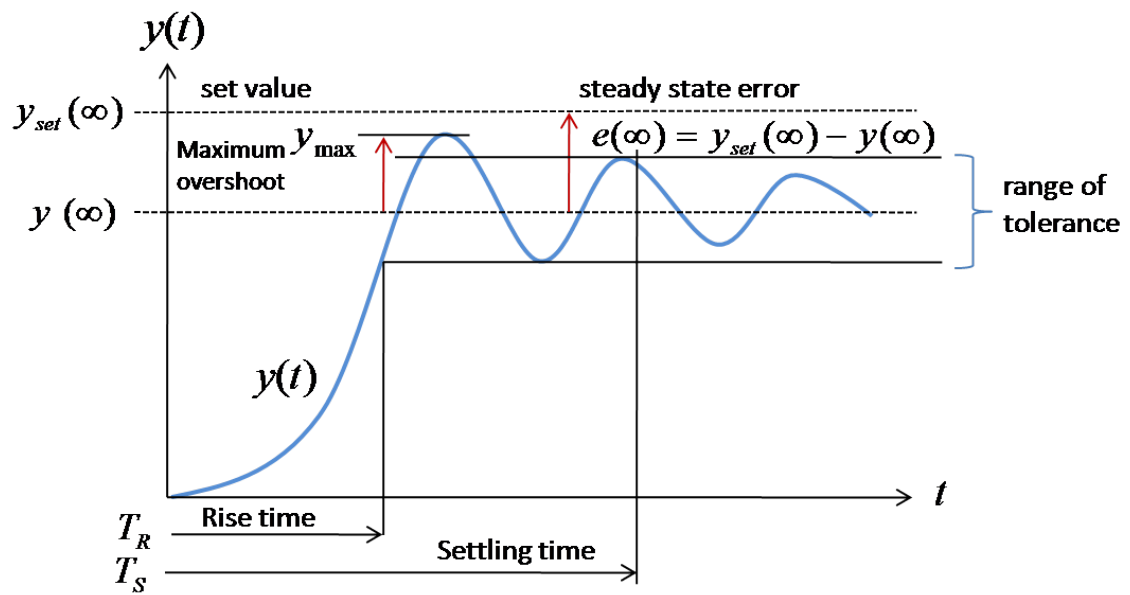


**Figure 3.11:** Performance measurement values of control systems

#### 3.3.3 Continuous and Discrete Time and Frequency Domains

The necessity of the linear approximation and the simplification of systems, led the analysts to the use of the Laplace transformation. This method transfers relative easily solved algebraic equations in the Laplace domain for the more differential equations in the time domain[46, pp.41-47 The Laplace Transform]. Combined with the fact that the sampling rate of a computing system can have a big impact to the stability of it, the z-transformation allows transferring functions from the continuous frequency domain to the discrete frequency domain [46, pp.749-754 The z-Transform]. These two transformations and the corresponding retransformations are visualized in the figure ??<sup>28</sup> and can be executed in a

<sup>28</sup>This figure bases on the theorems in [?, Chapter 4, p.17 Definitions and Rules of the z-Transform]

### 3.3 CONTROL SYSTEM CHARACTERISTICS

---

simple form by using transformation tables <sup>29</sup>.

---

<sup>29</sup>See Transformation tables in [46, pp.42 Important Laplace Transform Pairs] and [46, pp.751 z-Transforms]

### 3.3 CONTROL SYSTEM CHARACTERISTICS

The frequency domain equations are described as functions of the complex numbers. This continuous frequency parameter is discretized by using the following abbreviation  $z = e^{sT}$  where  $T$  is the sampling rate of the discrete system. The factor  $k$  in the discrete domain symbolizes the  $k^{\text{th}}$  sample value of the function and can be described as parameterization factor of the sample time  $T$  [?, Chapter 4, p.19 z-Domain set value transfer function of a closed loop control system].

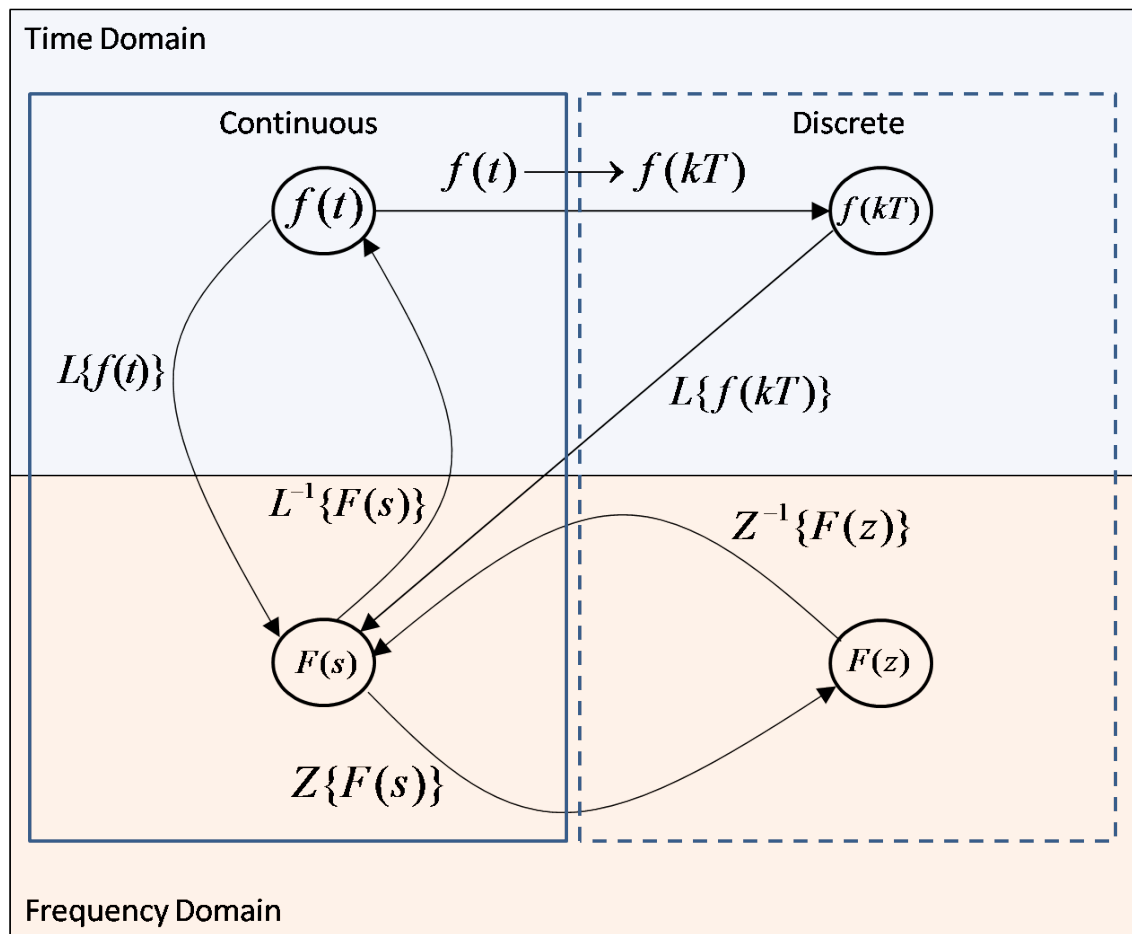


**Figure 3.12:** Transformation possibilities of continuous and discrete time and frequency domains

### 3.3 CONTROL SYSTEM CHARACTERISTICS

---

#### 3.3.4 Stability criteria of Transfer Functions

The mentioned simplification of Closed Loop Control System(s) (CLCS) in the following chapter can be shown by reducing the complete system to a quotient which contains polynomials for the numerator and denominator. This characteristically quotient is called Transfer Function (TF) and describes the behaviour of a system in relation to its boundaries. In the continuous domain the TF can be created as Set-Value-Transfer-Function (SVTF) (See formula ??) or as Error-Value-Transfer-Function (EVTF) (See ??) which allows investigations from two different input perspectives of the CLCS. The discrete closed loop control system can be used to describe the dynamic control behaviour of a discrete controller which controls a continuous process from the SVTF perspective (See formula ??). The interface between the process and the controller, is realised in this example with sample and hold components, which discretise the continuous process [46, p.747 Sampled-Data Systems]. The figure ??<sup>30</sup> visualizes the generic architecture of CLCS in the continuous and discrete domain. Thereby the figure shows that the components of a global TF of a CLCS also can be denoted as TF which describe the specific behaviour of the controller, the process <sup>31</sup> and measurement<sup>32</sup>.

---

<sup>30</sup>This picture extends diagrams presented in [?, Chapter 4, p.2 Generic linear Closed Loop Control System],[?, Chapter 4, p.19 z-Domain set value transfer function of a closed loop control system],[?, Chapter 4, p.21 Stability]

<sup>31</sup>In specific literature of control systems, sometimes the synonym plant is used for process

<sup>32</sup>The measurement component in the discrete domain is substituted with a sample component which holds the value of the process in the desired appearance

### 3.3 CONTROL SYSTEM CHARACTERISTICS

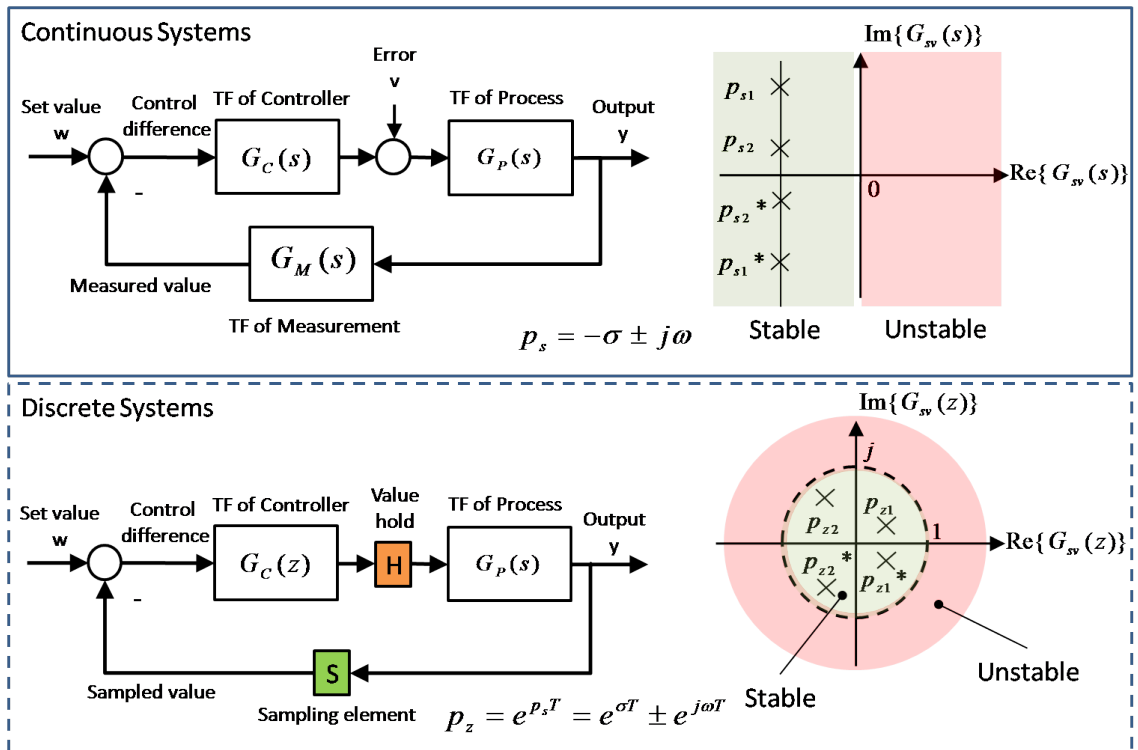


Figure 3.13: TF of continuous and discrete CLCS and their stability behaviour

The corresponding TF of the introduced domains are shown in the formulas ??, ??, ??<sup>33</sup>. Especially the SVTF contains important information of the stability behaviour. Continuous SVTF are stable, if the poles  $p_s$  of the quotient are located at the real negative section of the complex plane. Equivalent to that the stability of a discrete SVTF is given, if the poles  $p_z$  are located in the unit circle of the complex plane <sup>34 35</sup>.

<sup>33</sup>See [46, p.754 Closed-Loop Feedback Sampled-Data Systems]

<sup>34</sup>This causes the quantisation relation of the frequency  $z = e^{sT}$

<sup>35</sup>CLCS which have poles located on the edges of the stability sections are called semi-stable. Such CLCS are totally not robust and also assigned to the set of unstable systems

### 3.3 CONTROL SYSTEM CHARACTERISTICS

---

This stability behaviour in the complex plane is visualised in the figure ?? . Consequently the sample rate of digital systems and the corresponding sensors has a big impact to the stability of CLCS<sup>36</sup>.

$$G_W(s) = \frac{Y(s)}{W(s)} = \frac{G_C(s) * G_P(s)}{1 + G_C(s) * G_P(s) * G_M(s)} \quad (3.12)$$

$$G_V(s) = \frac{Y(s)}{V(s)} = \frac{G_S(s)}{1 + G_C(s) * G_P(s) * G_M(s)} \quad (3.13)$$

$$G_W(z) = \frac{Y(z)}{W(z)} = \frac{G_C(z) * G_P(z)}{1 + G_C(z) * G_P(z)} \quad (3.14)$$

---

<sup>36</sup>See [46, p.756 Stability Analysis in the z-Plane]

# Design and Implementation

## 4.1 Analysis of Existing Quadrocopter Architecture

Before the focus can be concentrated to the distributed error correction scheme of the HSE quadrocopter system, the overall existing architecture has to be introduced in this section. The importance of this introduction causes the necessity to understand and analyse the system which has to be simulated. An overview of the realized and pending components is visualized in figure ???. This overview includes the main systems of the general architecture which are Quadrocopter, Remote Control, Global Position System (GPS) and the Base Station. Thereby the Quadrocopter is controlled over a permanent unidirectional wireless communication to the remote control, which cyclic sends a pulse-width-sum-signal with the steering information. Thereby the RC-Receiver interfaces a microcontrollers' Enhanced Capture Timer (ECT) of in the CCU, which allows real-time decoding of the information. Further for observing and testing purposes, the architecture allows to observe and to configure parameter and state variables of the quadrocopter in mid-air.

## 4.1 ANALYSIS OF EXISTING QUADROCOPTER ARCHITECTURE

To fulfil this, the quadrocopter can send and receive data via a serial<sup>1</sup> ZigBee<sup>2</sup> communication to the base station, which runs a Java-Application that captures and visualizes the data and allows configurations in real-time<sup>3</sup>. By regarding the quadrocopter system, it can be considered as an architecture with CCU mounted and uncoupled components for detecting movements of the system. These components have special behaviour in aspects of resolution, quantisation etc. and bring a impact to the control and flying behaviour of the quadrocopter.

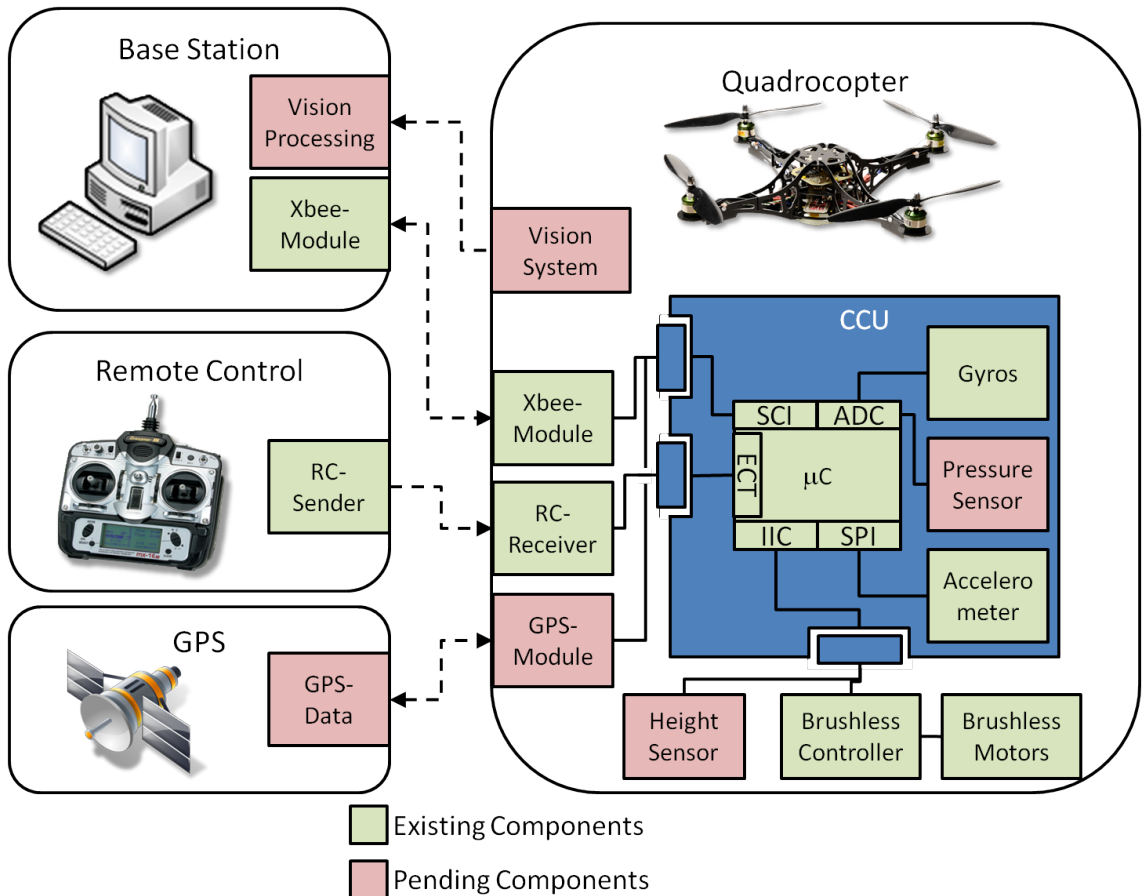


**Figure 4.1:** Existing quadrocopter architecture and future developments

<sup>1</sup>This wireless communication interfaces the Serial Communication Interface (SCI) of the CCU

<sup>2</sup>See [?]

<sup>3</sup>Real-time means in this case that the data is pre-buffered at the quadrocopter and asynchronous send to the base station. This allows a fine grained resolution of data capturing and evades time delays of synchronous sending data

## 4.1 ANALYSIS OF EXISTING QUADROCOPTER ARCHITECTURE

---

### 4.1.1 Central Control Unit

The CCU of the HSE Quadrocopter, which is one of the main interesting components in relation with a simulation, is a outcome of a interdisciplinary corporation of the HSE Faculty of Electronics and Mechatronics in Göppingen<sup>4</sup> and the HSE Faculty of Information Technology Esslingen<sup>5</sup>. The dedicated central unit of the CCU is a MC9S12XDT256<sup>6</sup> microcontroller from Freescale, used for the flight control task.

Additionally the sensors, which are used for the determination of the quadrocopter location in space, are also mounted on the PCB. The architecture includes an accelerometer,<sup>7</sup> that measures the acceleration in  $X_B$ -,  $Y_B$ - and  $Z_B$ -direction, three gyroscopes<sup>8</sup> for roll-, pitch- and yaw-velocity determination and an air pressure sensor to determine the height. Furthermore a battery sensor (voltage divider) on the board allows the calculation of the new set-points for the brushless controllers<sup>9</sup>, because the resulting RPM/thrust of the motors depends on the actual battery voltage. For communication with the base station, a XBee<sup>10</sup> module is used directly mounted on the flight control PCB.

Beside that, there are a couple of external interfaces available for remote control, an Inter-Integrated Circuit (IIC) bus to command the brushless controllers and a Background Debug Mode (BDM) as programming interface.

---

<sup>4</sup>See <http://www.hs-esslingen.de/hochschule/fakultaeten/mechatronik-und-elekrotechnik.html>

<sup>5</sup>See <http://www.hs-esslingen.de/hochschule/fakultaeten/informationstechnik.html>

<sup>6</sup>See [26, Data-sheet of HCS12X family]

<sup>7</sup>See [?, Data-sheet gyroscopes]

<sup>8</sup>See [7, Data-sheet gyroscopes]

<sup>9</sup>See [?, Wiki Brushless Controller BI-Cl V1.2]

<sup>10</sup>See [21, XBee Pro Module]

## 4.1 ANALYSIS OF EXISTING QUADROCOPTER ARCHITECTURE

---

The interfaces for a distance sensor, a GPS receiver and a servo (e.g. for a camera mounting) are available for future extensions (See pending components in figure ??)[32, p.57 Central Control Unit].

A closer look on the IMU, show that the locations of the sensors are designed WRT the velocity or acceleration, which has to be measured. So the sensor which measures the accelerations of the translation movements WRT the B-frame is mounted in the middle of the CCU to avoid the measuring of rotational components. Similar to that, the gyroscopes also mounted to positions, with the focus to zeroise measurements of unwanted values. So it is possible to describe with these combination of sensors the mathematical model presented in chapter ?. As described in chapter ?? another important point in digital systems is the quantisation behaviour. In case of the given CCU there two aspects which have to be considered. One aspect is the sample time of the control system and the other the resolution, sensitivity, noise etc. of the IMU.

The sample time of the system thereby depends on the load of the microcontroller. This load can be configured or changed by changing the embedded software with the focus to reduce the load. In contrast to that, the behaviour of the sensors cannot be changed, because these work autarchical and provide the specified performance defined in the data-sheet. Based on that, it is important to reflect the behaviour of these sensors in the simulation of the system. As visualised in figure ??, the translational sensors provides a different behaviour as the rotational sensors. This causes to the interface and the internal functionality of these sensors.

## 4.1 ANALYSIS OF EXISTING QUADROCOPTER ARCHITECTURE

---

The acceleration sensor provides a digital readout of the measures via Serial Peripheral Interface (SPI). Thereby the quantification is given with the quotient of the gravitational acceleration and the sensor sensitivity ( $g/340$ ) / LSb [ $(m/s^2)/bit$ ] and the limits, which are specified with  $6g$  in each direction.

Differently to the digital readout, the gyroscopes which build up the rotational part of the IMU provide an analog signal with maximal detection of  $5.23 rad/s$ , which is represented with a voltage level between ground and reference voltage of  $3.3V$  and need to be digitalized with the controllers' Analog to Digital Converter (ADC). This ADC provides a resolution of 10bit and combined with the gyroscope it results to a resolution of  $0.0142 (rad/s) / LSb$ <sup>11</sup>. So the IMU provides measures across the B-frame, which fulfil the rotational part of the GVV  $\nu$  and the translational part of the derivative GAV  $\dot{\nu}$ .

---

<sup>11</sup>The calculations of this chapter are derived from [47]

## 4.1 ANALYSIS OF EXISTING QUADROCOPTER ARCHITECTURE

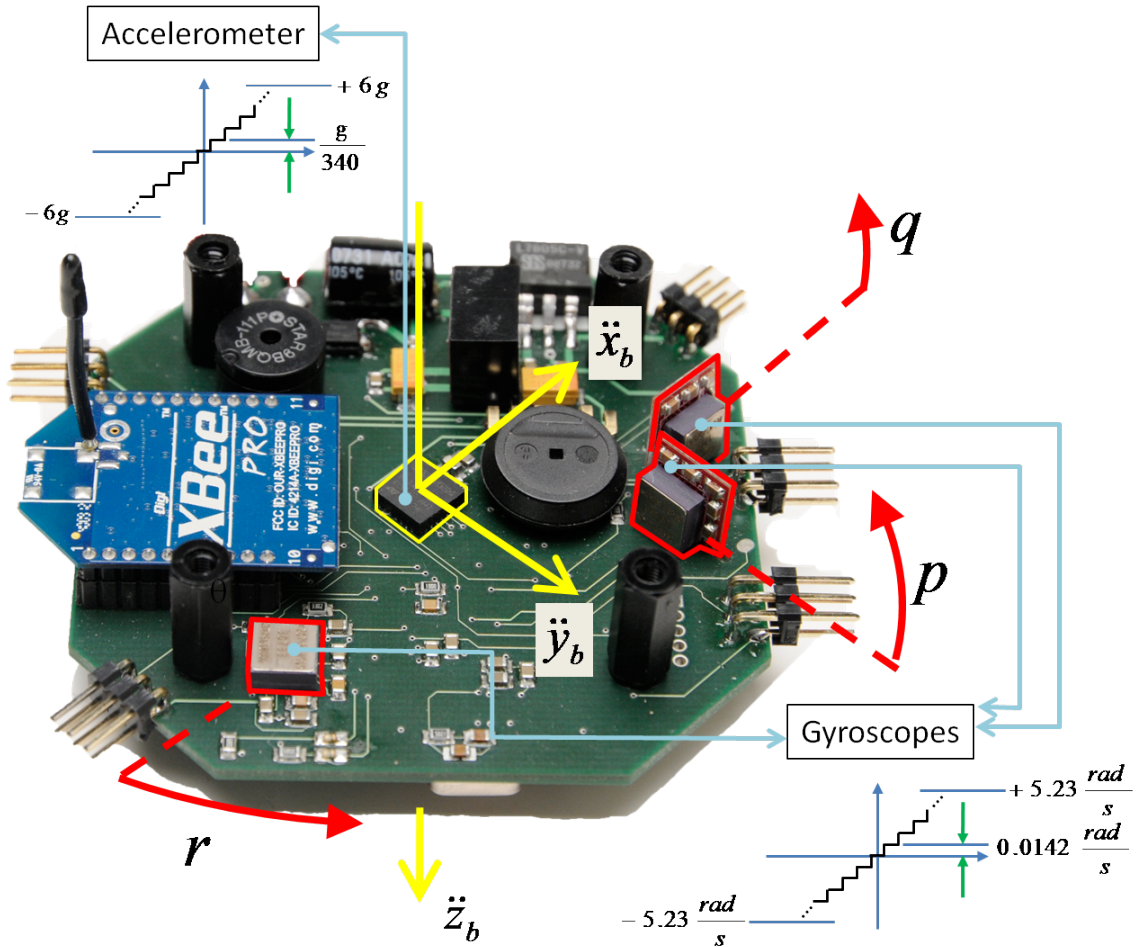


Figure 4.2: CCU and IMU

### 4.1.2 Characteristics of Sensors and Actuators

An important aspect in relation to the quality of control, and further the flight behaviour, is the characteristic of the IMU and actuators in view of precision. In the case of the CCU here, the noise sources are the noise of the Microcontroller (MC), the noise drift of the MEMS characteristic in relation to the temperature and the vibration of the motors. Because of this mix of noise sources, the determination of the average noise cannot be determined with investigating the data-sheets of the

## 4.1 ANALYSIS OF EXISTING QUADROCOPTER ARCHITECTURE

---

sensors.

A way of determination, which is executed here, is an experiment which includes the capturing and investigation of the real sensor readout in the preferred hovering state. Experiments with running engines and shut off engines, show that the biggest impact to the total noise originates from the imbalance of the rotors. This effect originates to the fact that small irregularities of the rotors have a big impact to the noise in case of the needed rotor speeds for the hovering state.

The results of the captured sensor data in a duration of 11 seconds are visualised in ?? with the corresponding variances  $S_{N-1}^2$ , presented in appendix ???. The  $S_{N-1}^2$  in this case is a measure which shows the dimension of noise influence and further the sensor values, which lost because they cannot be detected.

## 4.1 ANALYSIS OF EXISTING QUADROCOPTER ARCHITECTURE

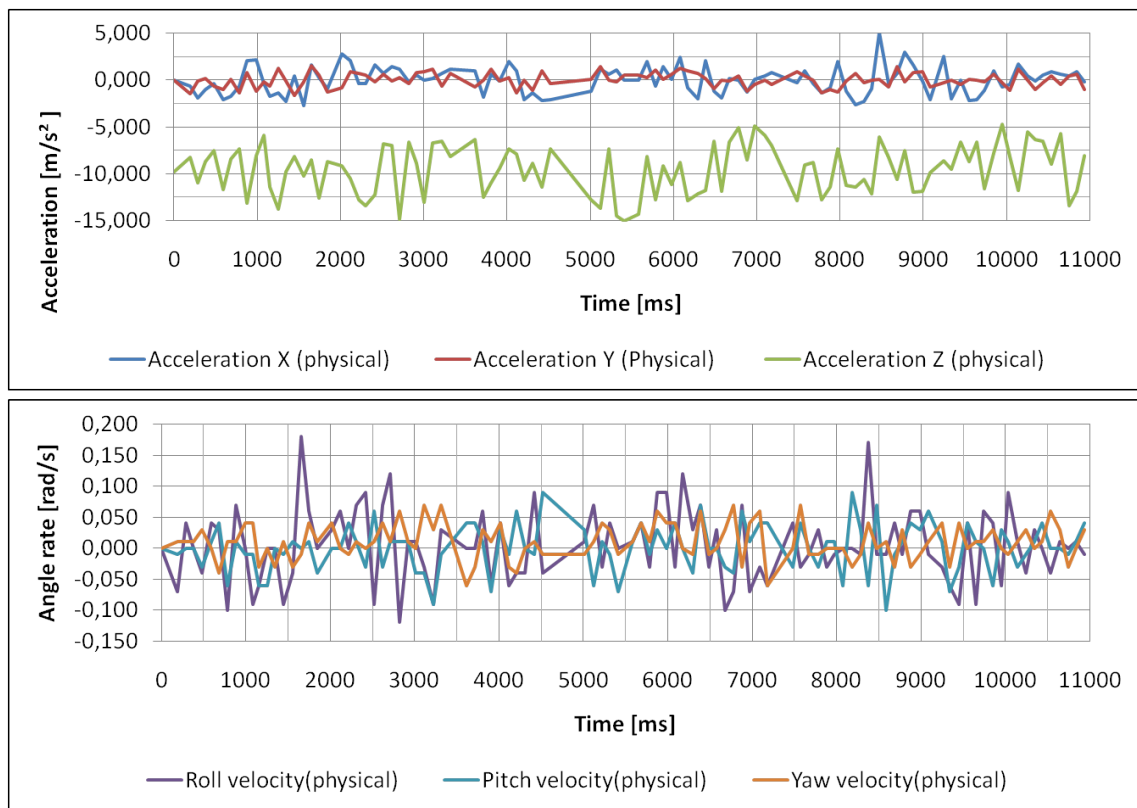


Figure 4.3: IMU noise analysis in the hovering state

## 4.1 ANALYSIS OF EXISTING QUADROCOPTER ARCHITECTURE

---

The investigation of the actuators can be executed by using a stroboscope with sufficient frequency resolution. This approach also was applied in this project here. The picture ?? visualizes the experiment, which was captured with a satisfactory exposure time of the camera. So the frequency of a rotor can be located, by vary the frequency of the stroboscope.

Finally the located rotor will optically stand still, and the other rotors will optically rotate in the original direction, or in the reverse direction. This behaviour demonstrates the engines, that run faster or slower as the located engine.



**Figure 4.4:** Experimental environment for set-point drift measurements

With the execution of the described experiment, it is possible to identify the set-point drift of the particular engines. The results of the different set-point drift are visualised in the figure ???. The mentioned set-point of the engines is a 8bit value, which is written to the control register of the brushless controller.

## 4.1 ANALYSIS OF EXISTING QUADROCOPTER ARCHITECTURE

---

Thereby the force, that is required to lift up the dead weight of the quadrocopter, is equivalent to the force needed for the hovering state. This force is nearby reached with the set-point of 100 on a scale from 0 to 255. As visualized in the curves in ??, the particular engines have a characteristic realization of the required set-point input, which can vary from ideal set-point.

These engine characteristics also depend to the mounted rotors and further environmental and physical behaviour which can varies over time. So the exact reconstruction of the engines' characteristics, can be unsuitable for a simulation. A better approach is to define an area different set-point drift are visualised in the figure ??.

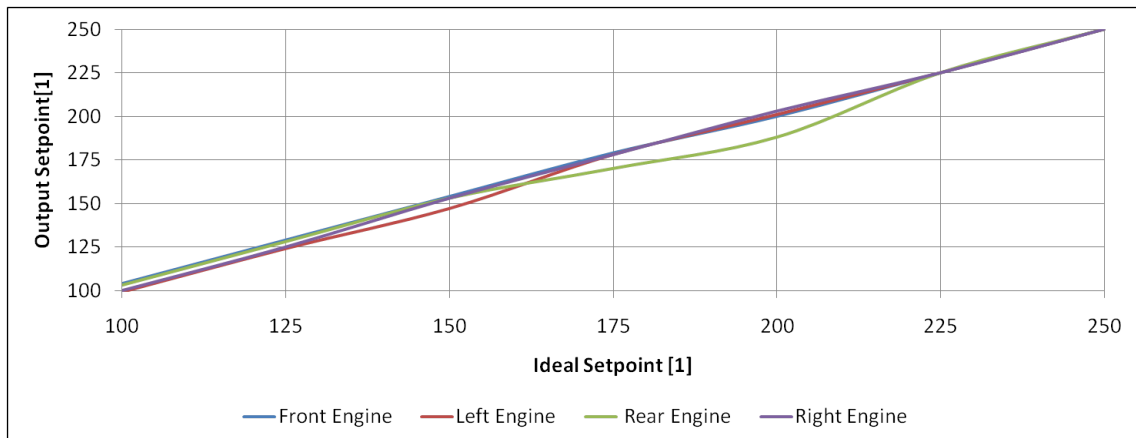


**Figure 4.5:** Set-point analysis of engines

## 4.1 ANALYSIS OF EXISTING QUADROCOPTER ARCHITECTURE

---

### 4.1.3 Embedded Software Architecture

Aspects like exchangeability, modular simulation, modular testing and dependency minimisation lead to an encapsulated modular layer design of the embedded software of the quadrocopter. The composition of the quadrocopters' embedded software, shown in the component diagram in ??<sup>12</sup>, is extended with the real-time behaviour of the call hierarchy.

Thereby modules, which use an asynchronous interrupt and a corresponding service routine to handle events are marked with a flash icon. Another important information is presented with a special dependency which contains the Cycle Time(s) (CT) of the component call. This value helps to understand and to research the sample behaviour of the sensors and further the control behaviour. Generally as well as in this project here, the Hardware Abstraction Layer (HAL) encapsulates the control registers, which are directly related to the peripherals and the MC, and allows a generic access to the functionality of the hardware.

The quadrocopter HAL contains generally five points of service access. These interfaces provide beside the service of initialisation and update of the quadrocopters' real-time image, an access to the communication with the base-station, an on board diagnosis system for noticeable visual and acoustic warnings and the access to the system timer to facilitate Time Triggered (TT) execution in the main routine.

---

<sup>12</sup>This diagram is derived from the architecture presented in [32, p.77 Embedded Software]

## 4.1 ANALYSIS OF EXISTING QUADROCOPTER ARCHITECTURE

---

Further the real-time image, located in the data layer, provides a protected access to the actual state and data of the quadrocopter. So the state of the quadrocopter is accessed by the application layer uncoupled from the HAL and at a central data pool which allow only one state of each value. At the top level of the layer architecture, the application layer contain the control, filter and base-station communication logic of the system. Thereby the main routine uses a TT call strategy to realise Deadline Monotonic Scheduling (DMS) with specific CT of the components.

Two important points of this scheduling architecture, also described by Audsley et. al [10], are the fact that the sum of the execution times of every routine (including Interrupt Service Routine (ISR)) has to be smaller as the smallest deadline, which is in this case 5ms, and further the biggest deadline has to be smaller as the repeating period of execution. This constraints limit the calculation complexity of filter, control or further on-Board algorithms drastically and have to be considered in further developments and simulations.

## 4.2 ADOPTED APPROACH

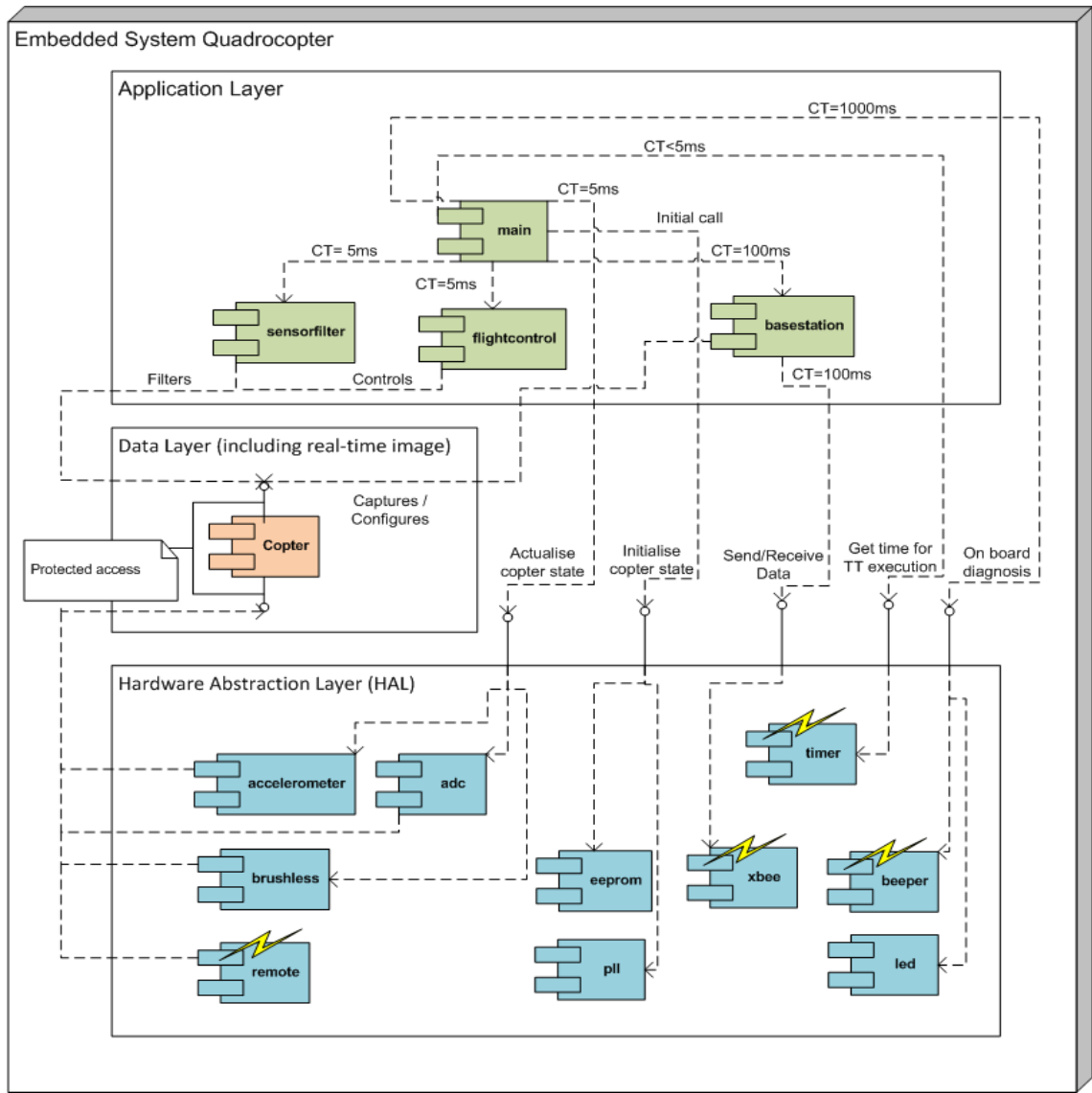


**Figure 4.6:** Software components and their relationship of the Embedded System Quadrocopter

## 4.2 Adopted Approach

After the introduction of the existing quadrocopter architecture and the analysis about the relevant characteristics of the soft- and hardware-modules, the adopted

## **4.2 ADOPTED APPROACH**

---

approach which will be researched here is presented in this chapter.

## 4.2 ADOPTED APPROACH

---

Based on the introduction of the distribution approaches, presented in chapter ??, the ONCA in combination with OFIP and SWBIP approach will be researched here. As mentioned in the comparison of these approaches, the advantages and disadvantages are related to the aspects of interesting. So the aspects of simulation prototyping and behaviour investigation of the image processing, as well as the delay tolerances in relation to the control behaviour lead to the mentioned approach decision. As shown in figure ?? the adopted architecture is composed of the simulation of the base station with the corresponding image processing and the simulation of the quadrocopter components which are in focus of interest. Beginning with the set values of the embedded system, the remote control component provides time variant signals of the angular set values for roll and pitch, the angular velocity value of yaw WRT the B-frame and the thrust value. These set values are the primary input for the body related control, which interfaces the physical model simulation with the same input values, which are provided from the CCU and the output values. Withal the input values are transformed to a desired form, which is used for PID control. Beside the IMU values of the CCU, the physical model provides an image sequence related to the position values of the quadrocopter WRT the B-frame. Thereby the image capturing process is simulated with a high resolution underground image and the projection of the desired image resolution on it. These image sequence is provided to the simulated on-board vision system according to the ONCA architecture. Further the vision system includes a send process with an output image-buffer to provide the images to the base-station, and an receive process with an input correction-value-buffer. At the other side of this wireless correspondence the base-stations' process also uses a buffered *I/O*, and determines the translation (*u* and *v*) and rotational values ( $r_{of}$ ) from the calculated OF field.

## 4.2 ADOPTED APPROACH

Finally the additional controller, which realises the drift elimination in the hovering state, is located in the quadrocopter system and observes the set values of the remote control. The idea thereby is to find a value state of the set and sensor values, which symbolises that the hovering state is desired by the pilot and further the quadrocopter body is ready to reach that state. To realise that behaviour a state machine, which is located in the module "Check Hovering State", decides in real-time the activation of the visual system. So the set values of a second controller, that is located in the separate position control module, are switched from zero to the received correction values. This has the effect that the body controller is delegated by the second position controller and corrects the position with a correction flight manoeuvre. If the pilot sends new set values, after the quadrocopter has reached the hovering state, the position controller is deactivated and allows the pilot and further the body controller an uninterrupted flight and batch-processing of set values.

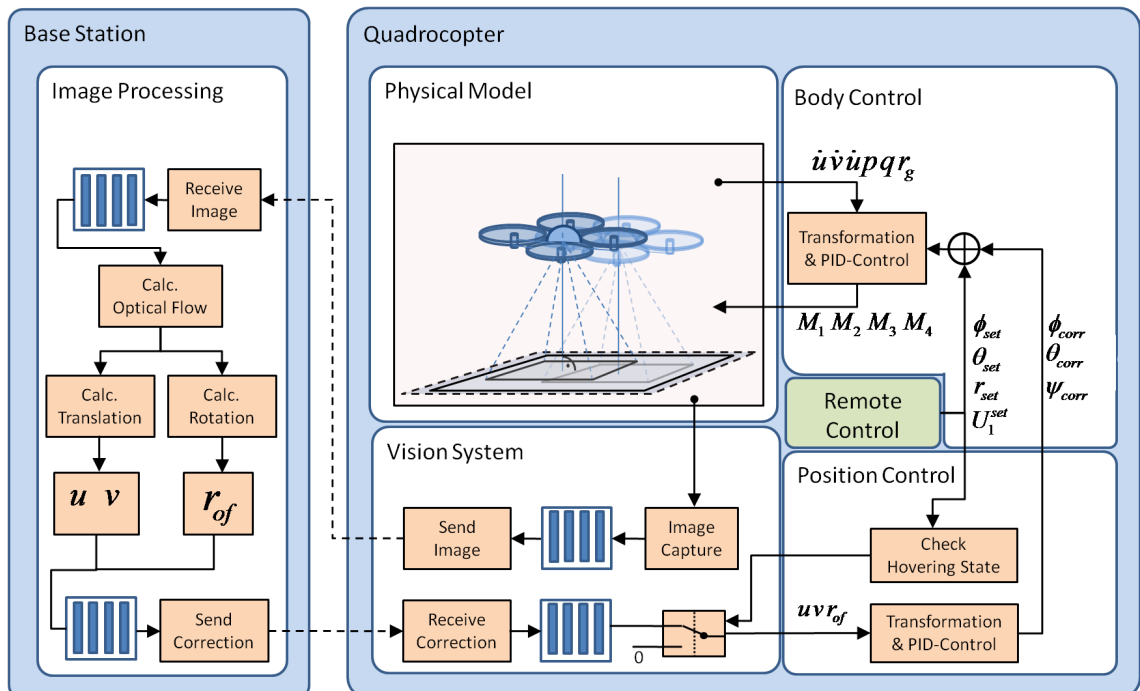


Figure 4.7: Adopted approaches' architecture

### 4.2.1 Control Approach

Before starting the design of the quadrocopter controller, it is helpful to understand and analyse the abstract behaviour of the separated, physical processes and to proof the correct function of the approach. This strategy lead in this project here to the construction of a simulation which shows the behaviour of realising an angular set-point value to one axis of the quadrocopter, which include two engines as actuators. As visualised in figure ??, two opposing engines realise the angle movements in the specific pitch- or roll-axis. These engines can realise an individual gain to the given set-point and influence the precision of the control system. Another point which is problematically in this case is the fact that the feedback angle acceleration of the CLCS, has to be integrated two times.

The combination of the unprecise gain of the engines and the two integrations influences the stability of the CLCS enormous. To simulate this behaviour and to impart the expected effects, a abstract simulation is build up and executed in Simulink with two configurations. As visualised in ?? the plant includes two engines, simulated as a sequence of a direction and individual gain. Furthermore two integrators transform the angular acceleration to a angular velocity and position which is used for feedback for the cascaded PID-Controllers. This feedback is designed as switch which can be interrupted, to fulfil a tests scenarios with single and cascaded PID control approaches.

## 4.2 ADOPTED APPROACH

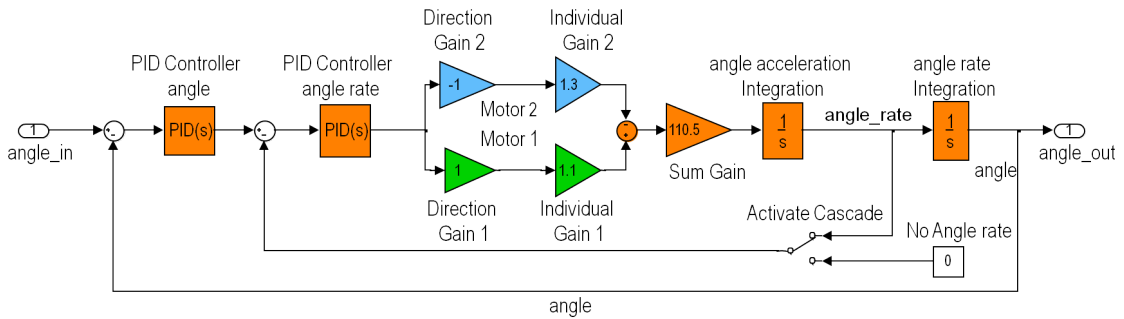


**Figure 4.8:** Abstract CLCS of one angle

As introduced in chapter ??, the stability behaviour of CLCS can be shown with a pole diagram and the investigation of the location of the poles (See Pole Map ??). Another method, to proof the stability in the frequency domain, is given with the Nyquist Criterion [46, pp. 487-493, Relative stability and Nyquist Criterion] and describes that each integration in a system affect a shift of  $90^\circ$  of the frequency phase. The criterion describes that the phase at the x-axis' point of 0dB of the corresponding gain has to be bigger as  $-180^\circ$ . So also this theorem proofs, that the determination of a value which passes two integrators, must have a PID-cascade to ensure that the feedback prevents a critical frequency phase shift.

These relations are visualised as bode diagram in figure ?? with logarithmic axis of the gain, frequency and phase. Furthermore the step response of the PID-cascade and the single feedback PID-controller (See Step Response ??) shows the stable and the oscillating unstable behaviour of these configurations.

## 4.2 ADOPTED APPROACH

---

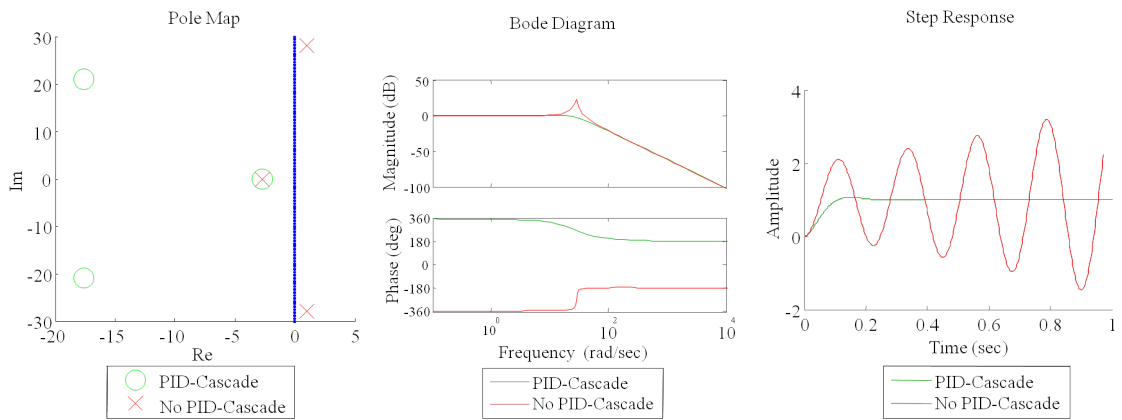


**Figure 4.9:** Pole Diagram, Bode Diagram and Step Response of one angle system

### 4.2.2 Problems, Limitations and Assumptions

This chapter focus the existing problems in the real implementation of a distributed, visual drift correction scheme of UAV, and shows abstractions and assumptions that are made for the structure and implementation of this projects' simulation. Such characteristics can be separated into domains, which provide the basis of problem and limitation analysis and allow to define a abstraction level. This abstraction level can be used to focus and analyse, just the characteristics of a specific part of a solution. This allows to concretise and locate problematic behaviour before searching for a solution at a wrong section. A concrete example for this argumentation can be given by regarding the camera domain.

Characteristics like the focal length influences the sharpness of the image and influences the image processing algorithm to calculate the OF. But this characteristic can be classified as problem, that has to be solved after the characteristics of more basic problems has been investigated.

## 4.2 ADOPTED APPROACH

---

The focal length  $f$  can be abstracted with setting the height  $Z$ , between the image plane of an ideal projection model and the underground, equal to  $f$  and to assign both values the fixed value of one meter. This allows to project the values of the ground points  $P = (X, Y, 1)^T$  directly to points on the image plane  $p = (x, y, 1)^T$ <sup>13</sup>. Further assumptions of the camera domain are, the camera does not create distortions<sup>14</sup>, the optical axis is projected rectangular to the underground<sup>15</sup> and the exposure of the environment is constant over time<sup>16</sup>. So the assumption in relation of the DOF of the camera system can be described as same as the DOF of the quadrocopter body, but reduced in the rotational movements around the axis which originates in the middle of the image plane. The quadrocopter body domain defines the behaviour of the movements of the hovering state, which can be assumed as a 5 DOF by reducing the movements across the axis  $Z_B$ . The realization of these two different DOF system can be realized with a real-time image correction process as described in ?? or with a hinge mechanism which keeps the image plane planar to the ground.

In the simulation this assumed state of the camera domain is realised with a state machine and the orthogonal projection of a simulated camera image on a underground image, as mentioned in chapter ?? . Another domain, which includes limitations and has to be defined here, is given with the underground domain. The related assumptions to this domain, are that no objects exist, which moving relative to the quadrocopter e.g. no moving light reflections, and the underground image contains points and contrast,

---

<sup>13</sup>A detailed mathematical deviation of this abstraction presented in [37, Chapter 2, pp.15-16 instructions of transformation]

<sup>14</sup>This fact also is implicated with the usage of the ideal projection model

<sup>15</sup>This implicates that the camera movement is planar to the ground and the camera is mounted correctly on the UAV. This assumption is adopted from [?, p.78 Motion Model Deduction]

<sup>16</sup>Experiments with a real camera involve a correct camera calibration (see appendix ??), and a environment preparation of the exposure to realise these characteristics

### 4.3 SIMULATION OF EMBEDDED SYSTEM QUADROCOPTER

which can be evaluated in the OF algorithm. For example, an underground image of a snow-covered landscape which contains segments with no contrast is not usable for this approach. Finally the communication between the base-station and the quadrocopter is abstracted as delay. This abstraction excludes communication fail, synchronisation or segmentation problems and assumes a smooth operation of the image and correction value transmission and reception. This behaviour is also symbolised with synchronous buffering systems in figure ??.

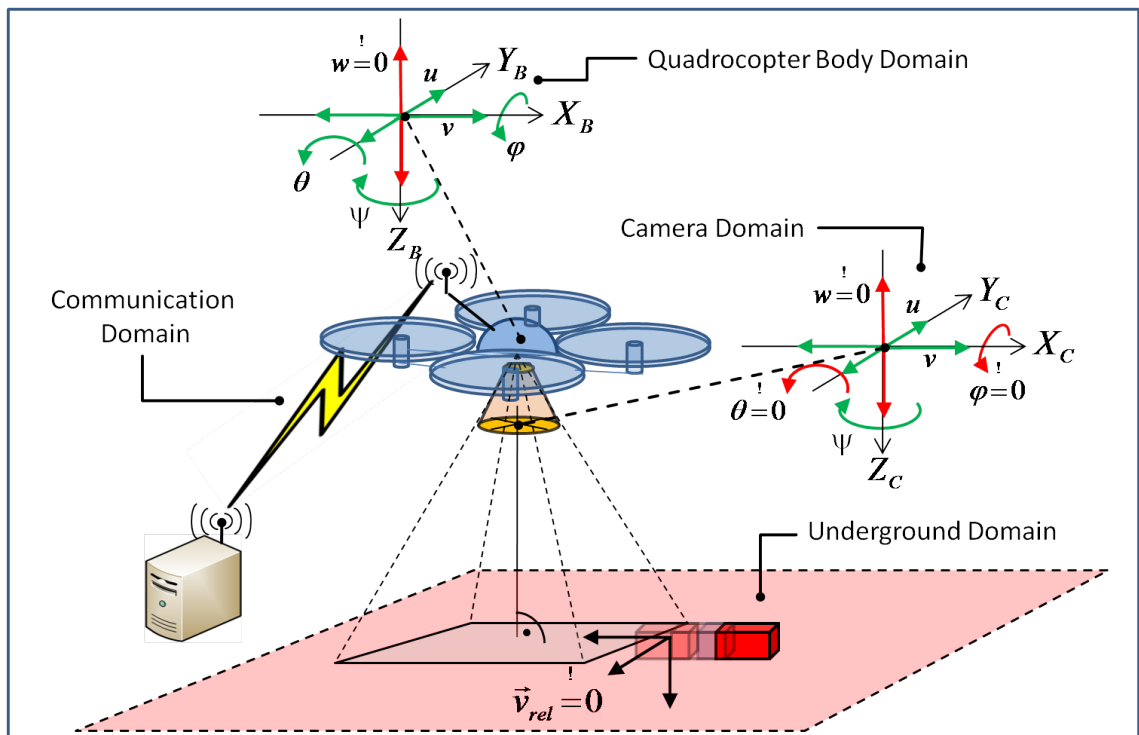


Figure 4.10: Problems and limitations separated in domains

### 4.3 Simulation of Embedded System Quadrocopter

The architecture of the embedded system simulation is constructed by following the modular design.

### 4.3 SIMULATION OF EMBEDDED SYSTEM QUADROCOPTER

---

The focus of this execution was to full-fill the aim of an exchangeable and flexible simulation architecture, which can be changed and reconfigured with minimal effort. This design criteria results to the architecture of Simulink modules as visualised in ??, and allows a hierarchical realisation of the quadrocopters' system simulation. The separation of modules contains a control library which allows to use several control modules in relation to the development state. As shown, the first development is executed as prototype in a native Simulink model without having complexity or resource limitations. This model is refined to an embedded MATLAB model, which contains only Matlab code which is cyclic executed. This refinement allows to simulate the quantisation and limitation behaviour of an embedded controller and further to evaluate if the implementation algorithm works correctly. The last step is to implement or to generate the embedded controller to the quadrocopters' embedded system target language C, and to evaluate this with the HIL module over a serial interface. This last step includes aspects like resource limitation analysis, algorithmic calculation complexity etc.

Based on this method, this project here focus the development of a Simulink controller in the abstract level by using the IMU and Optical Correction (OC), which can be implemented and realised in the same way as the existing control algorithm which controls only by using the IMU. The sensors and actuators are grouped in a own library and allow generic customisation of a sensor and actuator model and can be exchanged if the real hardware is changed. This exchange behaviour is also given in other components of the embedded quadrocopter system simulation and can be extended with implementation of new modules WRT the interface architecture.

### 4.3 SIMULATION OF EMBEDDED SYSTEM QUADROCOPTER

The optical-sensor has a special function in this project. It allows running tests and simulations of the quadrocopter system with a reduced simulation complexity. This is fulfilled because this module can generate the behaviour of the image processing signal with mathematical functions and can so reduce the simulations' execution time. Finally the utility library contains tools for analysis, visualisation and steering of the quadrocopter simulation, which have an important function in the performance test process of this project.

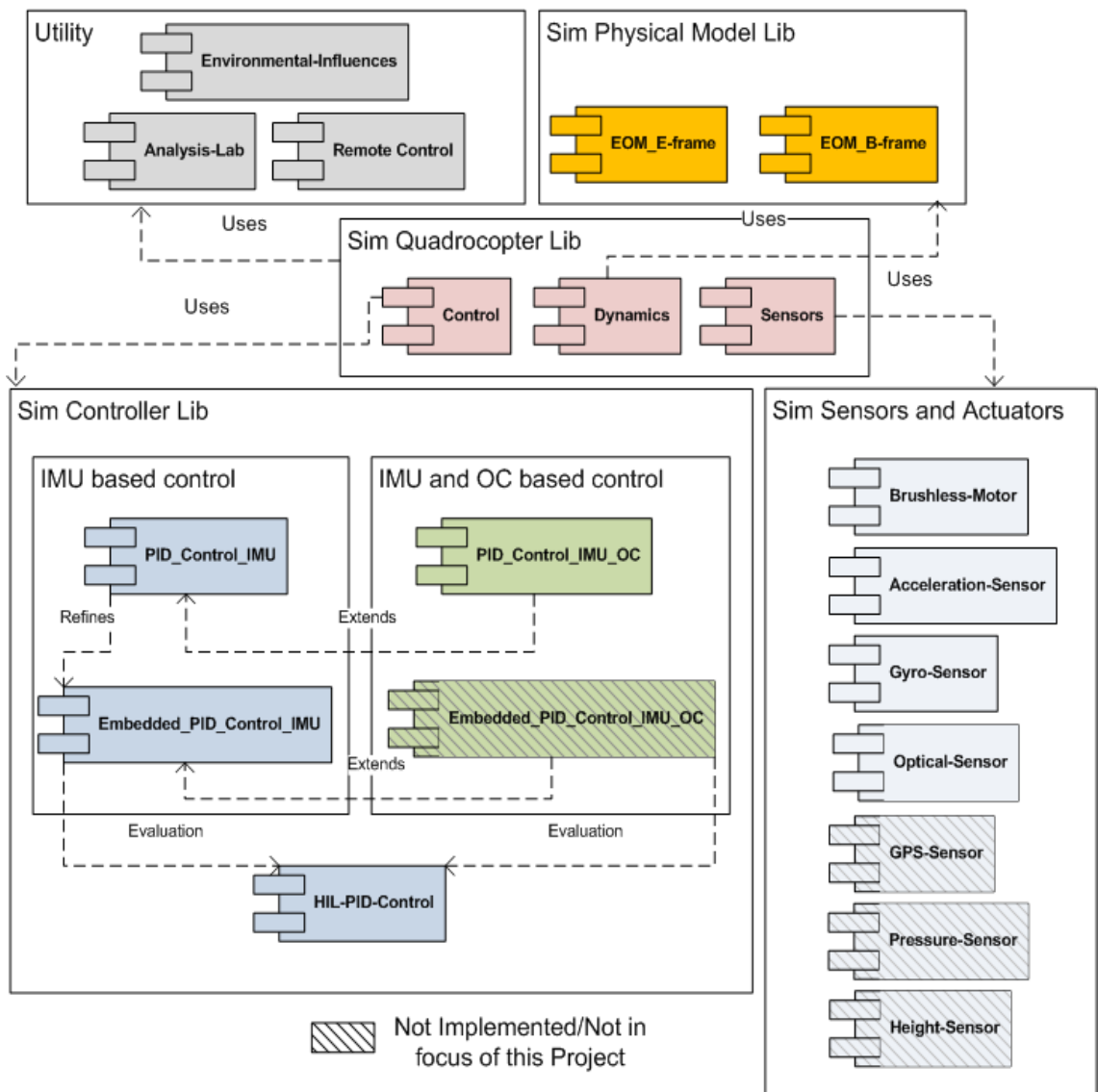


**Figure 4.11:** Modular overview of the Embedded Quadrocopter System Simulation

### 4.3 SIMULATION OF EMBEDDED SYSTEM QUADROCOPTER

---

The customised embedded quadrocopter system architecture is shown in figure ?? as Simulink model, which contains a CLCS architecture. The set-values from the remote control can be generated in different ways and support a virtual flight with a 3D-mouse or further a flight manoeuvre constellation of steering values. This signal is a composition of pulses defined with the Heaviside-function<sup>17</sup> and multiplied with ramp-signals and can be accessed for batch-simulation.

These set values are realized in motor values by the control component. This component executes, with respect to the mentioned development state, a controller simulation till a HIL communication. In each case the controller knowledge of the quadrocopter movements are provided by the sensors. In this special customisation the input signals of the sensors are provided by the Dynamics block and can be assumed as optimal.

Thereby the sensor block provides the signal with disturbances like noise and quantisation as in reality. Further the correction values for the drift elimination are already known by the sensor block and can be also disturbed by regarding the signal quality of the optical movement detection. Another way to determine these correction values is to send these via the output of this model to the base station and to receive the corresponding correction.

The signal pos-vel-acc includes all signals, produced by the Dynamics block, and provides a generic interface between the related collaborative blocks. Another strategy to test the stability of the control algorithm is the generation of environmental influences. This can be executed similar to the remote control with the generation of a velocity vector signal stimuli, which is add as error to the actual

---

<sup>17</sup>See [?]

### **4.3 SIMULATION OF EMBEDDED SYSTEM QUADROCOPTER**

---

optimal velocity value calculated by the EOM.

## 4.3 SIMULATION OF EMBEDDED SYSTEM QUADROCOPTER

To provide the opportunity of batch-processing-simulation, the error signals can also be accessed outside the model.

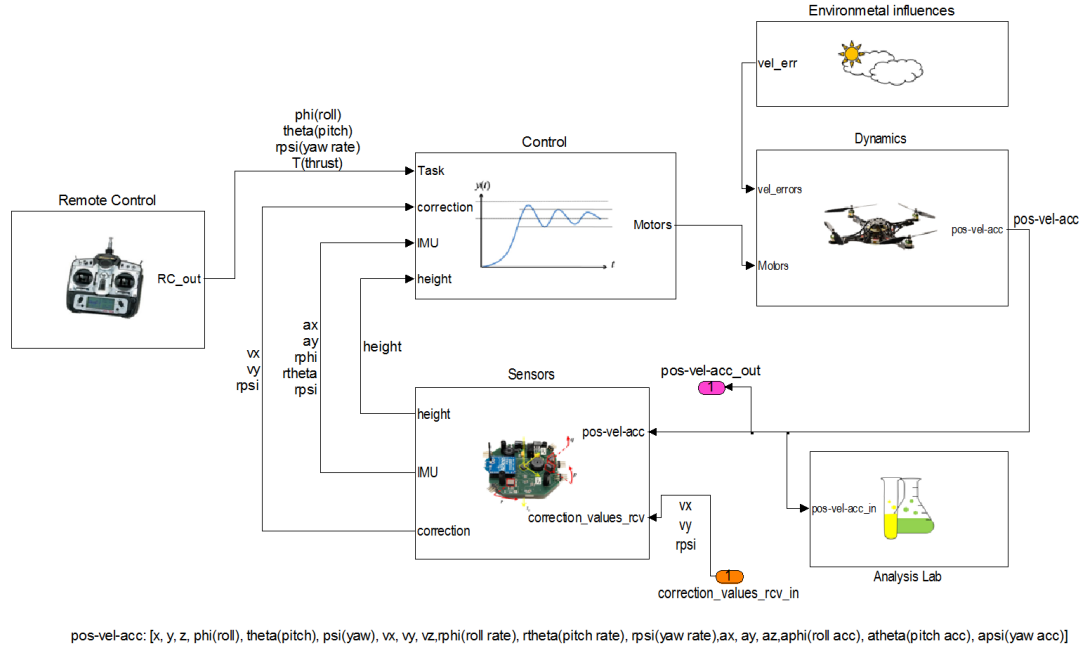


**Figure 4.12:** The customised CLCS architecture in Simulink

### 4.3.1 Flight Dynamics

The realisation of the dynamics block in Simulink is based on the researches presented in chapter ?? and on the EOM presented in chapter ???. First the derived GAV  $\dot{\zeta}$  WRT the H-frame was analysed to determine the dependencies of the ODE. Based on that, the physical model was build up with the aim to ascertain all positions, velocities and accelerations of the quadrocopter body, that is required for this project. The result is presented in a schematic view in the figure ???. Thereby this module gets the register set-values, corresponding to the brushless controllers in the reality (See??), and passes the mentioned pos-vel-acc vector to the next block.

### 4.3 SIMULATION OF EMBEDDED SYSTEM QUADROCOPTER

In this process the actuators engine blocks transform the set-point to a corresponding force  $F_n$ <sup>18</sup> and Revolutions per Minute (RPM) value  $\Omega_n$  (See ??).

These values of the different motors are composed to the movements  $U_n$ , by executing the calculations presented in equation ?? and further to the resulting RPM value  $\Omega$ . Furthermore, these output values are passed to the calculations, which based on the component  $\dot{\omega}^B$  WRT the B-frame of the equation ???. To determine the velocity and the angle, this vector is integrated two times. A special behaviour of this block is that the calculation of the  $\dot{\omega}^B$  needs also its own values. So the start values have to be initialised in this case for the initial execution with the values zero. Equivalent to the B-frame component of  $\dot{\zeta}$ , the E-frame component  $\ddot{\Gamma}^E$  from the equation ?? is used to calculate the translation acceleration, velocity and position vectors. Thereby the translations also passed through two integration processes.

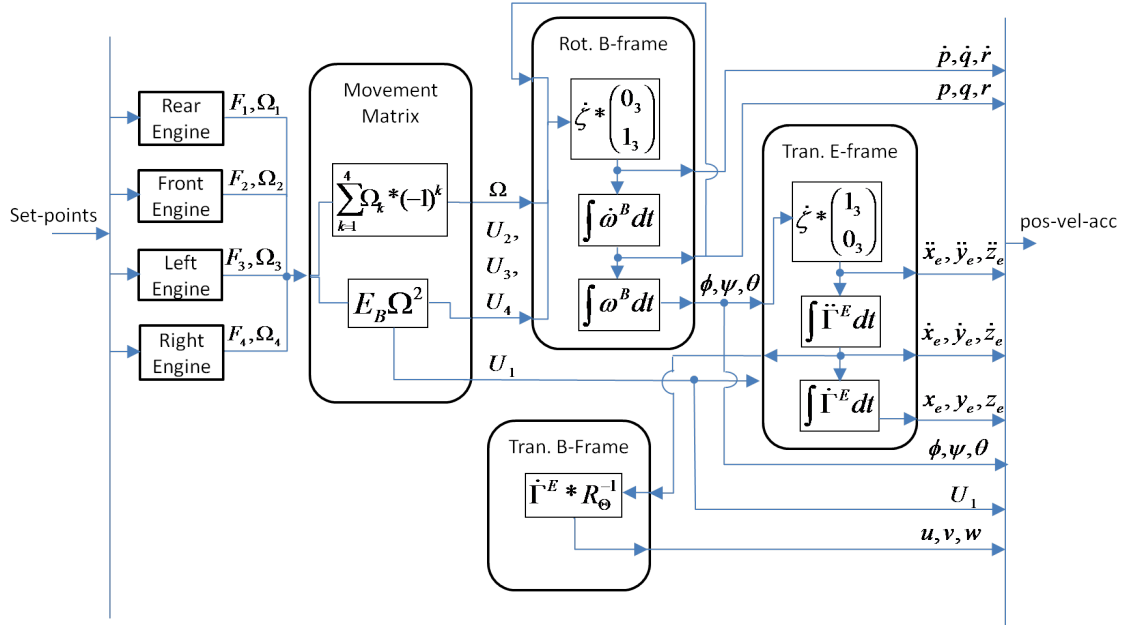


Figure 4.13: Schematic realisation of Dynamics Module

<sup>18</sup>The index n stands for the number of engine and ranges from 1 to 4

## 4.3 SIMULATION OF EMBEDDED SYSTEM QUADROCOPTER

---

These calculated values are combined to the output vector and provided as output. The GVV  $V^B$ , which is needed to simulate the on-board behaviour of the acceleration sensor, is determined with the inverse rotational matrix multiplied with translation GVV  $\Gamma^E$ . The generic aspect of this approach is that a generally EOM dynamics model also will have the same output values and will be compatible to the same interface, if it has 6 or less DOF. Furthermore the determination of all movement values allows the simulation of future developments with each kind of movement detection sensor.

### 4.3.2 Control

Observing the analysed control behaviour, presented in chapter ??, the final quadrocopter controller is a MIMO controller, which includes several cascaded PID SISO controllers. The figure ?? visualises the detailed controller architecture. Starting at the input values of the control module the angular velocities, the translational acceleration values and the set values are combined for control usage. Thereby the different sources of the values are symbolised with superscript symbols like "Gyr" for gyroscope, "Opt" for optical sensor, "Acc" for acceleration sensor and "Set" for set-value. These input values run first through a process of transformation, which converts the raw sensor values to usable physical values for the control process. In this case the angles for pitch and roll are not determined with an integration but are calculated using the translational accelerations of the corresponding rotation axis.

### 4.3 SIMULATION OF EMBEDDED SYSTEM QUADROCOPTER

This is possible because the gravitational orthogonal force is related to these rotations and can be used to determine the angles without an integration process. The conversion of raw- to physical-values, presented in chapter ??, allows an easier control realisation and processing.

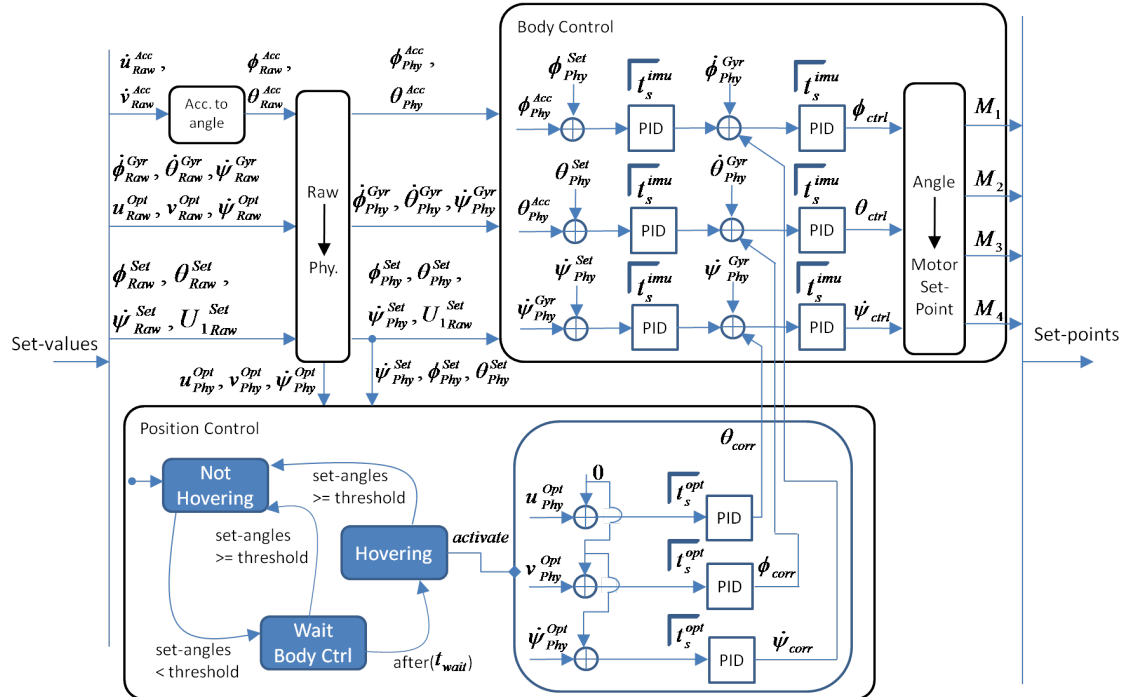


Figure 4.14: Quadrocopter Control Architecture

The converted physical values are passed to the position-correction and body-control-process. Thereby the position-correction-process passes the set-values to an internal state-machine which detects the hovering state and activates the position-correction-controllers. For realising this, the state-machine checks the set-values of the angles and checks if these are smaller as a defined threshold, which symbolises that there is no activity of the remote control. After reaching this threshold the state-machine switches to a state which delays the activation of the position-correction-controller for the duration of  $t_{wait}$ .

## 4.3 SIMULATION OF EMBEDDED SYSTEM QUADROCOPTER

---

This delay is needed for the body controller and the related cascaded PID controllers to reach the steady-state of the hovering position. The activation of the position-controllers, which try to minimise the input values of the optical sensor, affects that the output values of these controllers are integrated to the first stage of the cascaded PID controller in the body control. The result is that this collaboration of the controllers affect the needed behaviour for position correction of the hovering state, because the error value of one controller architecture is passed as set-value to the other architecture. Finally the cascaded PID control realises movements given from remote control, or manoeuvres needed for position correction, and passes the angular values to a conversion block for the motor set-points. This block realises the variations of the particular motors by realising the desired thrust set-value  $U_1$ . Another important characteristic in the design of this simulation is the option to run the body and position-control PID controllers with different sample times ( $t_s^{opt}$  and  $t_s^{imu}$ ). This behaviour originates from the facts, that the IMU sensors can provide a higher sample rate as the optical sensor, and the sample rate can influence the characteristics of a CLCS (See ??).

### 4.3.3 Sensors and Actuators

A simulated dynamic model, as introduced in chapter ??, provides as mentioned optimal movement signals, which does not reflect the reality. So an artificial process which creates a disturbing signal fused with the optimal signal, can be used to investigate and simulate the realistic behaviour of the sensors and actuators. These characteristics are also regarded in this project here with the result to transform the optimal signals with the experienced knowledge of chapter ??.

### 4.3 SIMULATION OF EMBEDDED SYSTEM QUADROCOPTER

The results are presented as Simulink models in ???. Both components, sensor and actuator, contain similar functions to limit and amplify (Saturation and Gain) the incoming signal. Gyroscope and acceleration-Sensors further contain a quantification, offset and noise process to fulfil these typical effects. The sensor model can so be customised individually by configuring these mentioned characteristics, and provides a model close to reality. In the other hand, the actuator model provides only one configurable characteristic, the motor gain, which is used to simulate the error characteristic of the engines presented in chapter ???. Beside this the brushless motors access the same, experimental determined tables for the set-point to thrust and thrust to RPM conversion. Important thereby is that these conversion tables realise a non-linear relation between the set-point and thrust, like in the reality. Further the important behaviour of the actuator delay is simulated as a delay process in the frequency domain. The presented generic blocks in this chapter, are customised once for the simulation of the existing hardware of the quadrocopter and integrated in the sensor module CLCS shown in figure ???. So in focus of this project here, the characteristics of these blocks are not varied for further investigations.

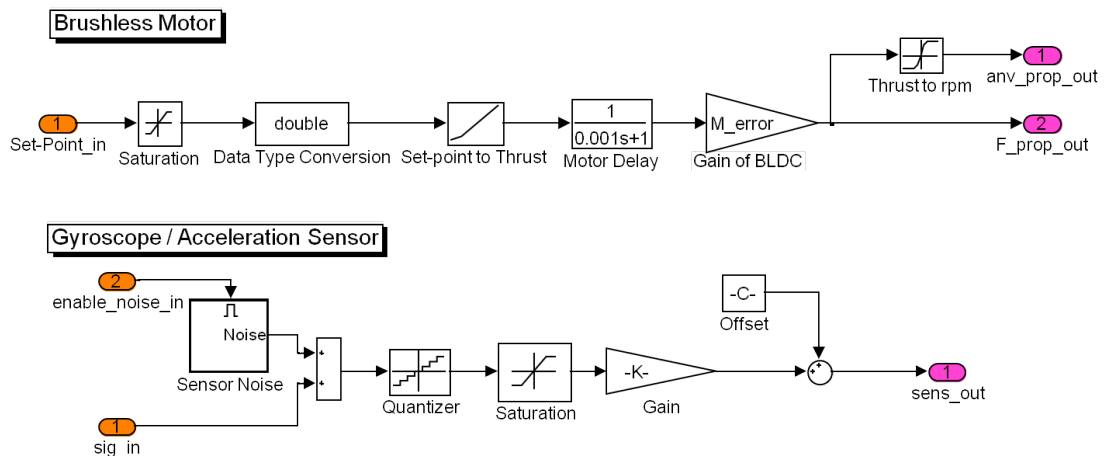


Figure 4.15: Sensors and Actuators

### 4.4 Simulation of Base Station

The aims considered in the base stations' simulation are the exchangeability of image processing algorithms and modules and further the ability to vary characteristics of the captured images. The aspect of algorithm exchangeability is realised with an architecture, which separates the image processing from interpretation of the derived values. Regarding this aspect, different image processing modules provide different form of values. As shown in figure ?? the OF algorithms are also logically separated in high and low level algorithms. This hierarchy architecture aspect provides the ability to mix high and low level algorithms from different frameworks.

Beside the algorithm architecture, the simulation of the base station provides several variations of source and sink of the processed video. The source thereby can be an synthetic video, which is generated with the assumptions mentioned in chapter ??, or a real captured video. Thereby the synthetic video provides the ability to vary the image size and frame rate, which can not be executed in real videos. Similar to the simulation of the embedded system quadrocopter, the movements of the camera view can be steered with the remote control module or with the environmental influences.

Thereby the environmental influences can provide a desired trajectory with variable velocity or acceleration, which can be used as reference to evaluate the quality of optical movement detection. Finally the analysis lab, as mentioned in the embedded system quadrocopter simulation, also provides the option to observe and analyse customised models, build up with the modules of this simulation.

## 4.4 SIMULATION OF BASE STATION

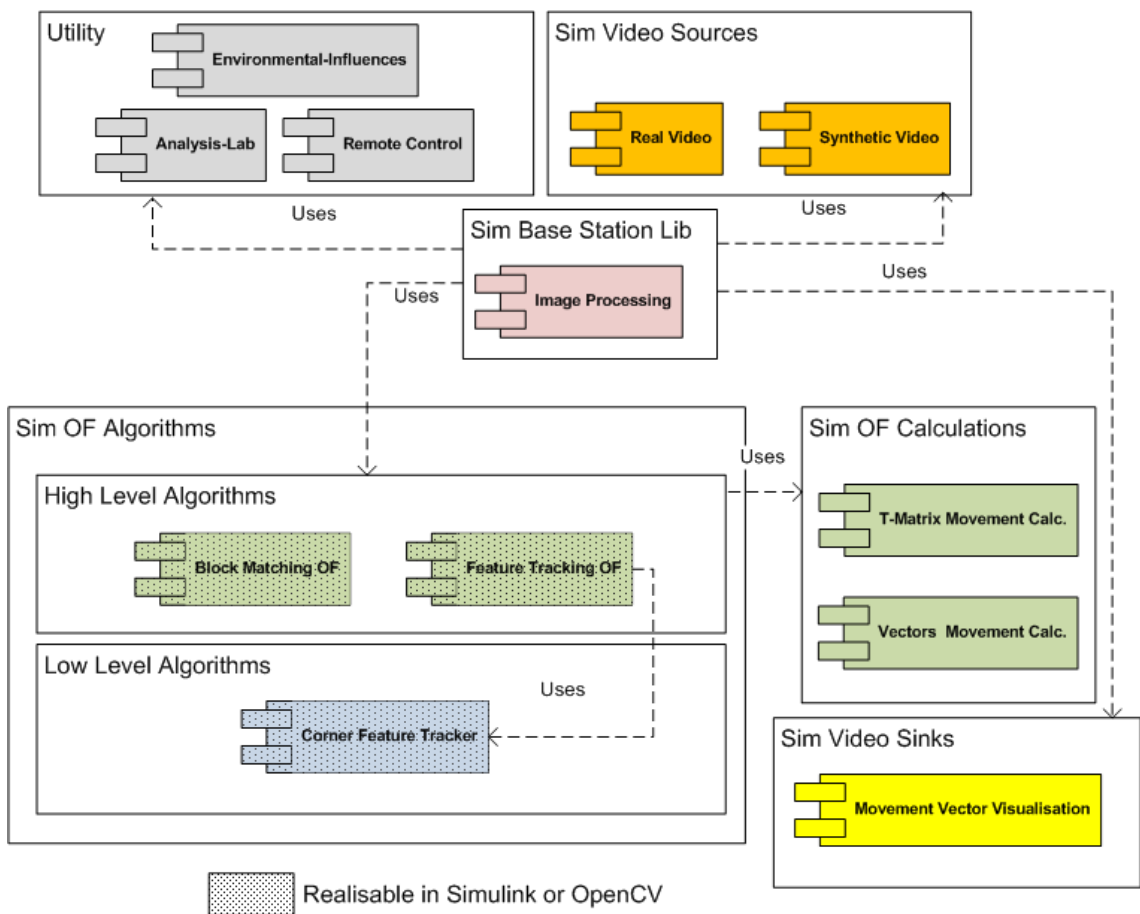


Figure 4.16: Simulation of Base Station

### 4.4.1 Video Sources: Synthetic Video vs. Real Video

As mentioned, the video input of the optical movement detection process can be created synthetic, or a real captured video can be used. Regarding the synthetic video, the frame rate and image size can be configured because the generation of the image stream is created with a transformation of the image window executed on the ground image.

## 4.4 SIMULATION OF BASE STATION

---

This transformation is executed using a transformation matrix, which describes the translation and rotation of the next image. The sample-rate configuration thereby is realised in the integral, which contains the sample time  $t_s^{Opt}$  of the image capture. In contrast to that, the real video source process, can just decrease the sample rate by selecting and forwarding each  $n^{th}$  image. Further it is not possible to determine the trajectory of the image movement, because the video caption was executed with the relation to the physical movement of the camera<sup>19</sup>.

It can be summarised that the synthetic video can be used for prototyping and executing test cases. The benefit thereby is that the possibility to capture measures, influenced by unexpected effects, is very low and the input-data of the test cases is created and realised exactly. So the experimental results can be regarded as isolated from unexpected influences and can provide the essential behaviour of the tested components. In the other hand the real video provides a realistic trajectory scenario, which contains a lot of influences like distortions, light effects, noise and so far. So the real video approach can help to fine tune filters and to optimise the image processing, but should not be used for the initial prototyping steps of development. Another important aspect in the real video approach is that the trajectory should be measured in real world, with a reliable measurement configuration. This has to be a great deal more precise as the expected precision of the image processing, to prevent misjudgements of the evaluated results.

All in one, the synthetic video approach is suitable for the first prototyping simulations and the real video for the final fine tuning. The challenge thereby is the

---

<sup>19</sup>The synthetic video architecture is derived from video mosaicking memo, presented at <http://www.mathworks.com/help/toolbox/vision/>

#### **4.4 SIMULATION OF BASE STATION**

---

crossing level from synthetic to real video.

## 4.4 SIMULATION OF BASE STATION

That means the synthetic video simulation has to reach as much as possible the real video, before the exchange of the video sources can be executed.

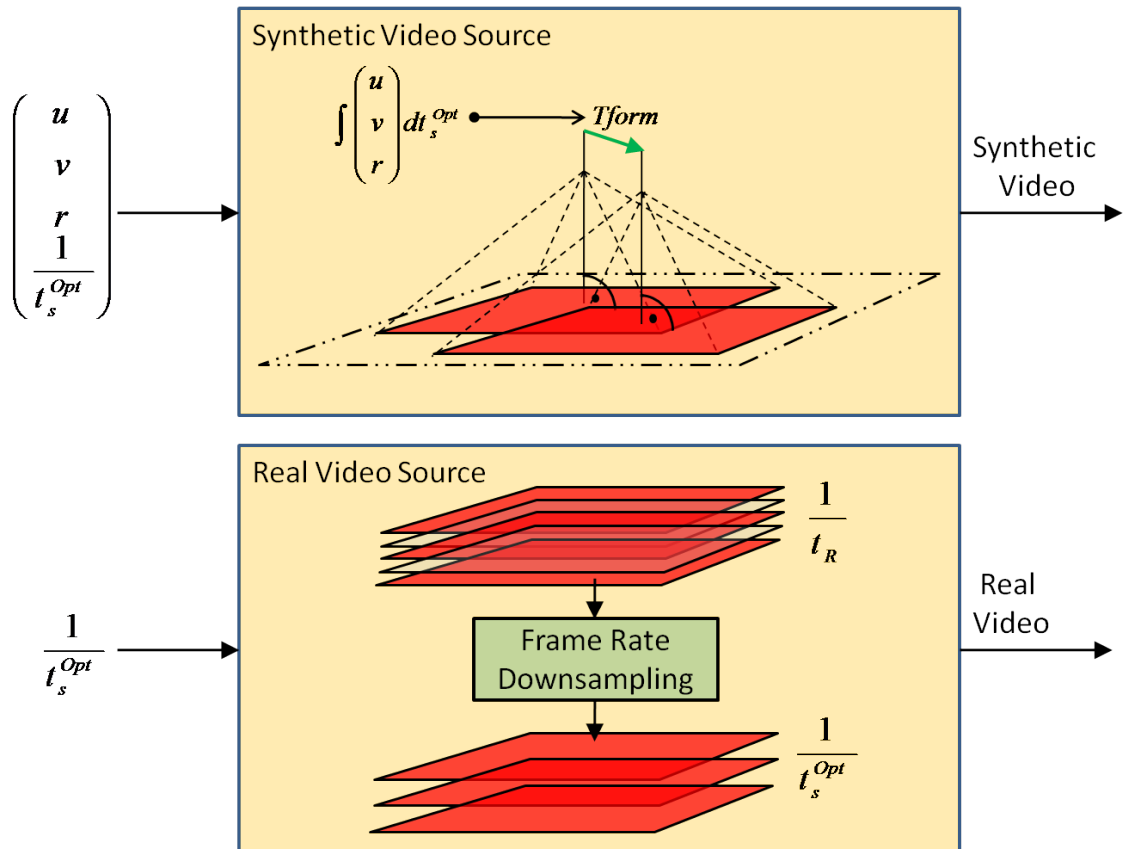


**Figure 4.17:** Synthetic Video generation and Real Video

### 4.4.2 Calculations

The interpretation of the optical flow is executed in two different ways in this project here. These approaches, mentioned in the architecture overview ?? as calculations, provide the same output with different input representations.

## 4.4 SIMULATION OF BASE STATION

The first approach, presented by Termtanasombat [41], is called Flow Number Calculation (FNC)<sup>20</sup> and determines the quantity of the optical flow by calculating the average of optical flow over the magnitude of the velocity vectors. A similar calculation is visualised in figure ??, with the difference that the velocity vectors of the raw optical flow are represented as complex numbers. Further the average calculation is executed with the accumulation of the average of the imaginary and real part in each direction. This resulting vectors are symbolised with  $\omega_i$  with the index corresponding to the direction and axis. Thereby, the assumptions presented in chapter ?? allow the mentioned movement set, which does not contain the movements in  $Z_B$  direction and a corresponding Focus Of Expansion (FOE) <sup>21</sup>.

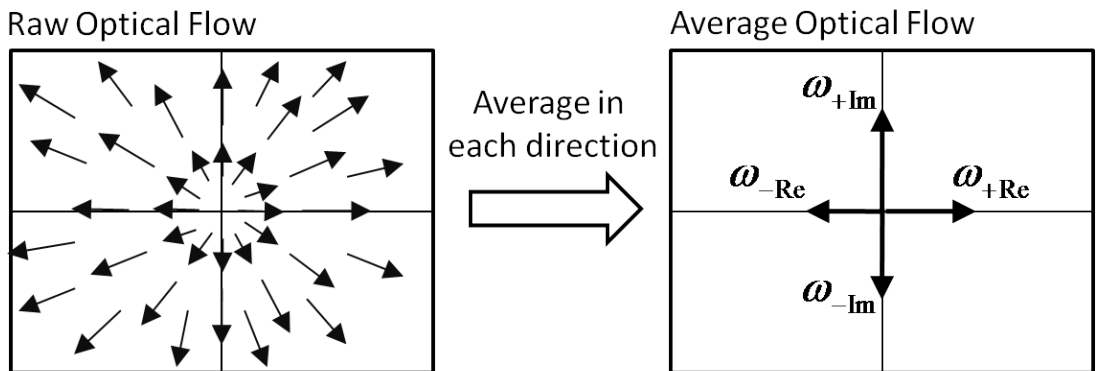


**Figure 4.18:** Averaging process of Raw Optical Flow Field

The defined DOF allow to calculate the desired velocity values of movement from the average optical flow. This procedure is shown in figure ???. There we can see a combination of rotational and translational movement as average optical flow. First, to determine the rotational movement, the smallest magnitude of the velocity vectors is the used as indicator.

<sup>20</sup>This approach is presented in figure ?? as Vectors Movement Calc.

<sup>21</sup>Such a FOE is shown e.g. in the middle of the raw optical flow in figure ??

## 4.4 SIMULATION OF BASE STATION

The idea behind that is, that the rotation around the centre of the image is represented in each average velocity vector. Additionally, just a rotational movement can influence in parallel all four average velocity vectors. So the separation of the translational and rotational movements can be executed with subtract the constant rotational offset, represented in the circle, from each average velocity vector. The complement results a translational combination of the vectors in  $X_B$  and  $Y_B$  direction. A problem of this described interpretation of the rotational component is the missing information of the rotation direction. Consequently the direction of rotation has to be adopted from the yaw gyroscope sensor.

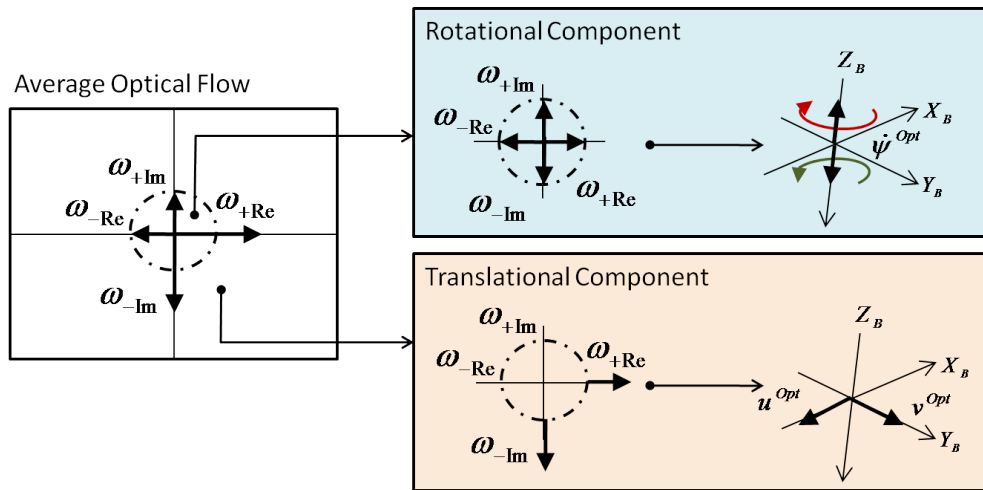


Figure 4.19: Determination of rotational and translational component with the Flow Number Calculation approach

Another approach to determine the desired translation and rotation velocities is to determine the Transformation Matrix (Tform)<sup>22</sup> between two images in an image sequence. In this project here, the tracked features of both images are represented as two dimensional points. An algorithm, which estimates the movement of the points , called Random Sample Consensus (RANSAC), provides the determination of the Tform in each sample step.

<sup>22</sup>This approach is presented in figure ?? as T-Matrix Movement Calc.

## 4.5 OPTICAL MOVEMENT DETECTION ARCHITECTURES

Furthermore, this matrix contain information of rotation and translation which allows the determination of these values with a reverse calculation shown in figure ???. Combined with the known sample time of the image sequence, the determined angle and translation positions can be transformed to velocities. The important characteristic of the Tform calculation is given with the determinable direction of the rotation movement.

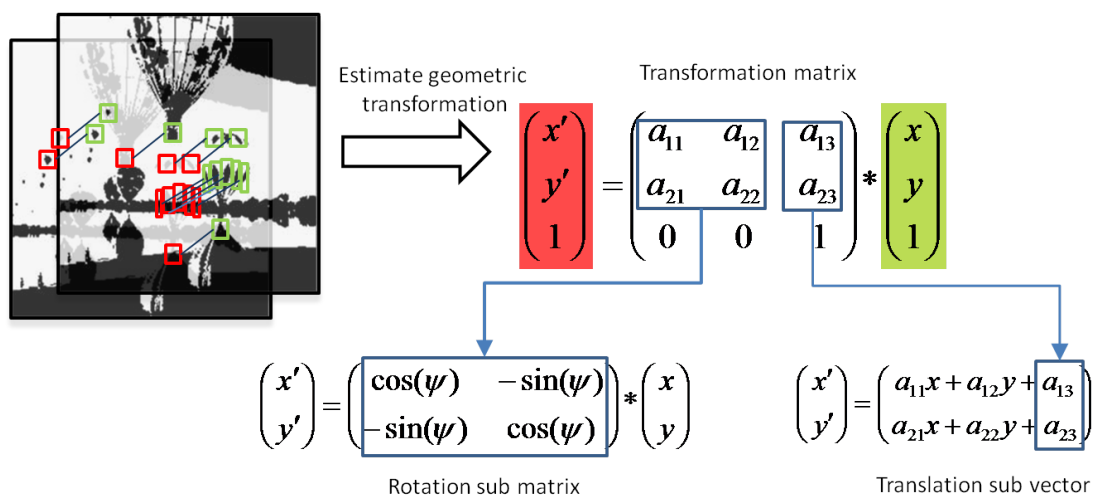


**Figure 4.20:** Determination of rotational and translational component with the Transformation Matrix approach

## 4.5 Optical Movement Detection Architectures

The presented optical movement detection algorithms and calculations can be realised in several ways of implementation. Two of these approaches are introduced and described in this chapter. One approach is given with the Video-and-Image-Processing-toolkit © of MATLAB/Simulink. This toolkit provides an easy and fast way to realise image and video algorithms, using the MBD approach. This way of development brings a lot of advantages, but also disadvantages.

## 4.5 OPTICAL MOVEMENT DETECTION ARCHITECTURES

---

Another possibility to realise image and video processing algorithms is given with OpenCV (See chapter ??). This framework allows, as mentioned, the usage of a huge amount of optical algorithms and provides further very detailed configurations of these. But why it is not possible to use just one of these two optical movement detection architectures? The problem is that each of these architectures has strengths and weaknesses. In the development of the base stations' image processing, the realisation was executed in MATLAB/Simulink. Regarding the necessity of spiral model to present with less effort a first running prototype, the MATLAB/Simulink-Native Video and Image Processing (VIP) is better suited. As presented in chapter ?? the limited amount of algorithms of the MBD framework can become a drawback for extensions and refinements of the realised VIP architecture. So it is important to have the ability to extend manually the VIP algorithms of the MBD tool. Such extension can be executed with MATLAB/Simulinks' Mex-Architecture (See chapter ??). The following table ?? introduces some important characteristics of both frameworks, and shows the advantages and deficits of these.

## 4.5 OPTICAL MOVEMENT DETECTION ARCHITECTURES

---

graphic/ComparisionOpenCVSimulink.pdf

**Figure 4.21:** A comparison between MATLAB/Simulink-Native VIP and OpenCV VIP

# Experimental Results and Analysis

The following chapters present the examined results and analysed aspects. First the image processing characteristics are analysed with test scenarios, which focus the interesting aspects of investigation. Each test scenario contains beside the description of the investigated domains, also the expected results of the experiments. These expectations are compared, with the results of the experiments and discussed. After the analysis of the image processing, the chapter ?? shows the characteristics and optimisation of the control architecture and the analysis and tune strategy of the control system. Finally the analysis of the position correction scheme in chapter ??, focus the complete position correction system and combines the previous analysed results together. Thereby different scenarios are executed with different configurations and disturbances. Furthermore a final analysis also demonstrate the hovering state characteristics of the focused configurations.

## 5.1 Analysis of Image Processing

This section introduces the specifically configured test environment and the corresponding results of the analysed topics, related to the motion detection. Furthermore, the testing analysis is separated in three domains of variation, pre-

## 5.1 ANALYSIS OF IMAGE PROCESSING

sented in figure ???. The basic idea thereby is to create a 2D-trajectory by using a stimulus as evaluation source of the results. This stimulus can be executed in three types of motion, presented in the stimuli domain. Basically, the stimulus is given as rotational or translational velocity type, which also provides an output value from the image processing. Additionally, to test the reaction behaviour of the a image processing configuration, it is important to use velocity steps, or further, acceleration inputs. Such tests show how fast the changed value can be reached by image processing, and give a measure for the time impact. Another domain that can be separated for the tests here is the algorithm and calculation domain. As visualised, this segmentation can be structured as a tree with n nodes which contain the image processing algorithms and calculations as leaf nodes. As mentioned, in this project here the algorithm and calculation constellation is reduced to the two visualised combinations, for reasons of algorithm support of the used simulation framework.

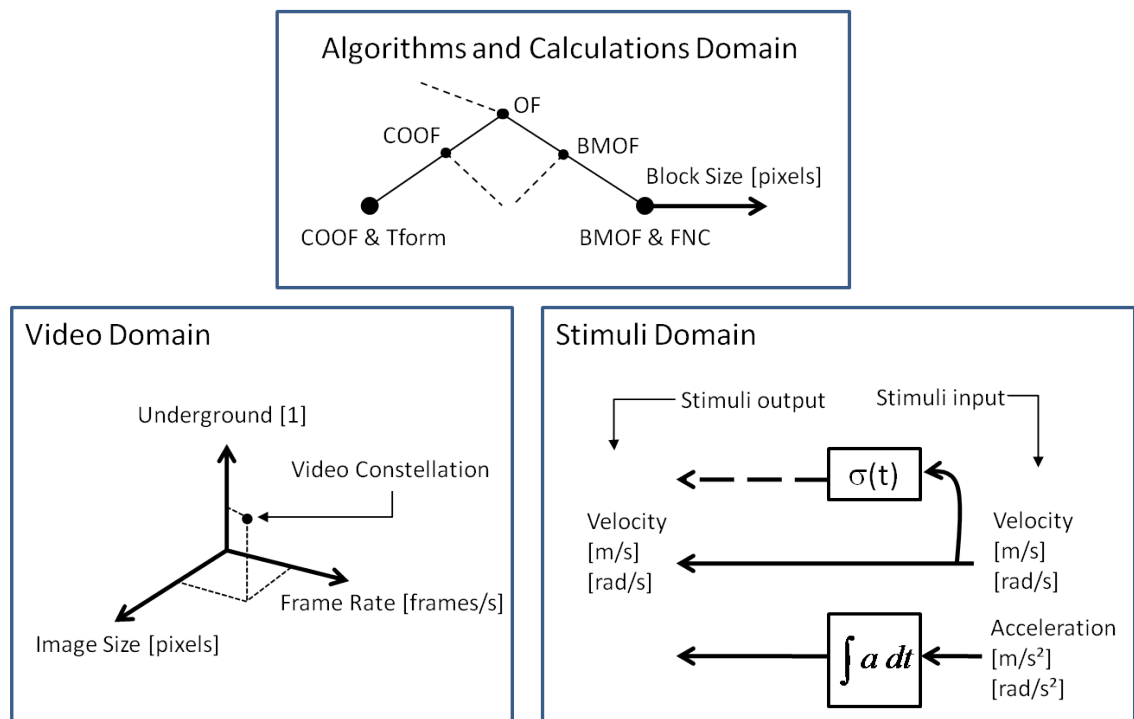
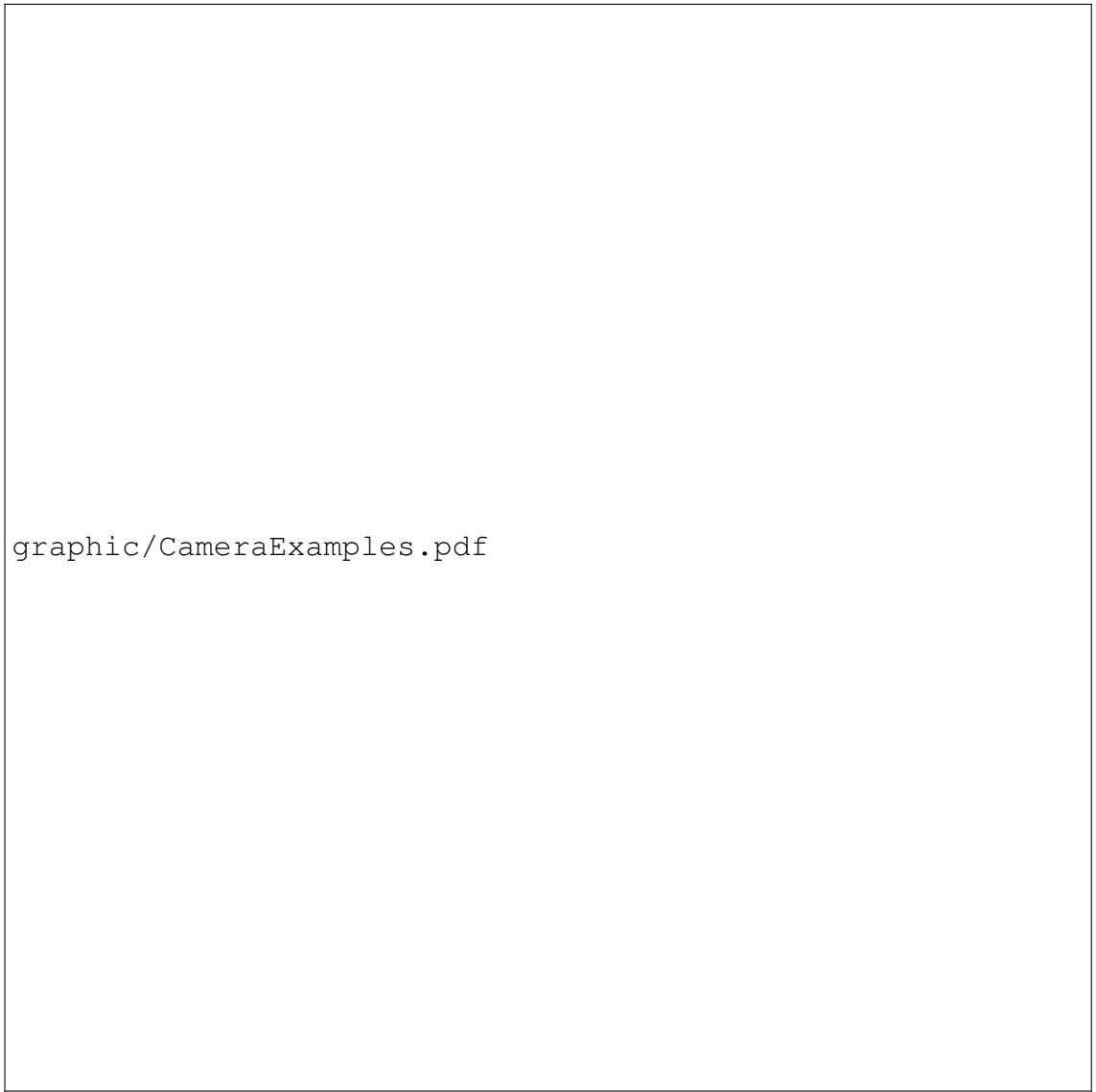


Figure 5.1: Image processing analysis domains in focus of this project

## 5.1 ANALYSIS OF IMAGE PROCESSING

---

Finally, the regarded aspects in relation to this project of the video source behaviour are summarised in the video domain. To provide a realistic environment, the chosen ranges of experimental analysis are derived from the data-sheets and publications <sup>1</sup>, presented in ???. Afterwards, the components and their corresponding decision criteria of the video domain are presented and discussed in the following points.



graphic/CameraExamples.pdf

**Figure 5.2:** Examples of camera configurations derived from literature

---

<sup>1</sup>See [54, p.35], [39, p.6], [12, p.22], [40], [34, p.4]

## 5.1 ANALYSIS OF IMAGE PROCESSING

---

- **Frame Rate:**

The frame rate is related to the maximum velocity in the regarded DOF, which can be detected by the camera system. In relation to the image size, algorithm and calculation and the stimulus, it can be determined which constellation to the Frames per Second (FPS) can provide satisfactory results. Generally, the ideal constellation is, regarding the frame rate, to reduce the processed images per second as far as possible. By doing this, the calculations, as well as the transmission complexity from quadrocopter to base-station, are reduced. The variations which will be executed here in the experimental analysis are 10, 20, 40, 60, 80 FPS.

- **Image Size:**

Similar to the frame rate, the image size can also influence the maximum velocity that can be detected by the camera system. Important thereby is the behaviour of the objects, moving relative to the camera system. Similarly, a big image window size allows to observe a bigger amount of points similarly. Furthermore, in a constellation of similar conditions, points are projected to a big image window for a longer period. In contrast to that, points stay into the focus of a small image for a short-time interval. Therefore, in such cases a higher image processing sample rate is desired to provide the same quality of results. On the other hand, if we also assume the same conditions of image composition, a bigger image window size requires a higher data size which also influences the transmission and the calculation of the image processing. Based on the camera examples presented in ??, the following image size variations in the corresponding experiments are 320x240,

## 5.1 ANALYSIS OF IMAGE PROCESSING

---

640x480, 768x576, 800x600, 1024x768 [height x width].

- **Underground:**

The underground variation is a special behaviour of the experimental analysis related to this project. Based on the fact that the presented algorithms of optical movement detection focus different aspects of the image, it can be assumed that the motion detection behaviour will be alternating by varying undergrounds. So the undergrounds presented here focus two characteristics. As visualised in ??, the first underground (amorphous) provides amorphous groups of different contrasts. In contrast to that the second (segmented amorphous) provides additionally segmentations like edges and corners. Finally, the third (cornered) has mainly a cornered and edged structure. This variation of amorphous and corned structures provides a challenge to the algorithms that work with corner detection and block matching.

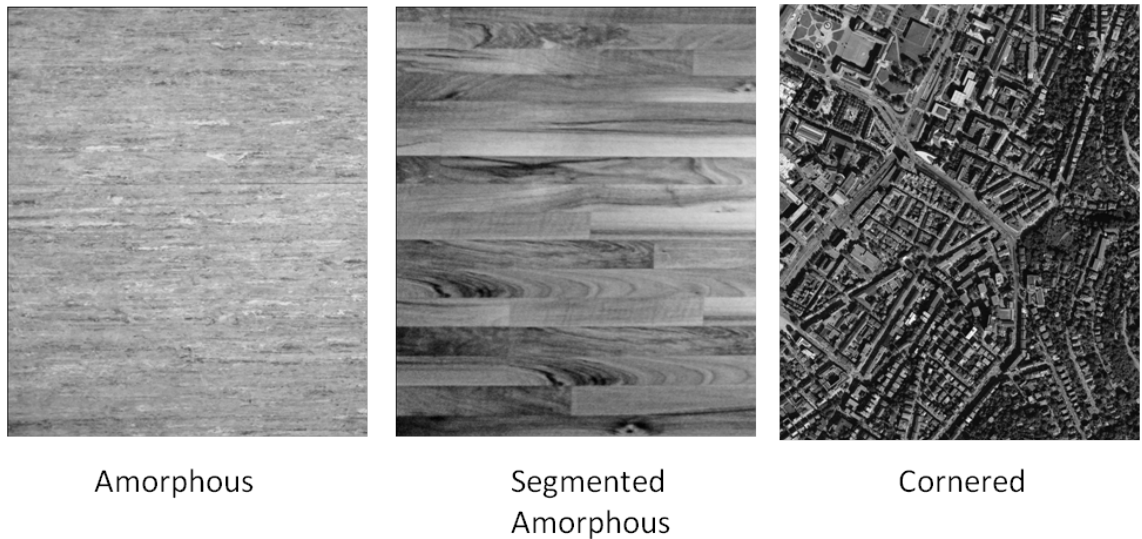


**Figure 5.3:** Different undergrounds with amorphous, segmented amorphous and cornered structure

## 5.1 ANALYSIS OF IMAGE PROCESSING

---

### 5.1.1 Aspects of Reproducibility and Reliability

This chapter introduces the methods executed to proof the correct function of the image processing simulation. First, the sources which influence the test scenarios were analysed and evaluated. Thereby, it is important to clarify if there are any elements inside these that generate noisy or randomly values. In case of the real and synthetic video source, this is not the case, because the real video never changes in the course of execution, and the synthetic video generates the same output with the corresponding same input. To verify this reproducibility, and further the correctness of the synthetic video, two experiments were executed several times. These experiments are visualised in figure ???. As shown, a special underground for measuring the movement is installed for the rotational and translational test. Furthermore, the movements  $\Delta\psi$ ,  $\Delta x$  and  $\Delta y$  are tested versus the corresponding simulation time  $\Delta t$ . The result can be compared with the configured stimulus, and it can also be evaluated whether the velocity input was realised correctly. These test case executions show that the synthetic video environment is reliable and reproducible.

## 5.1 ANALYSIS OF IMAGE PROCESSING

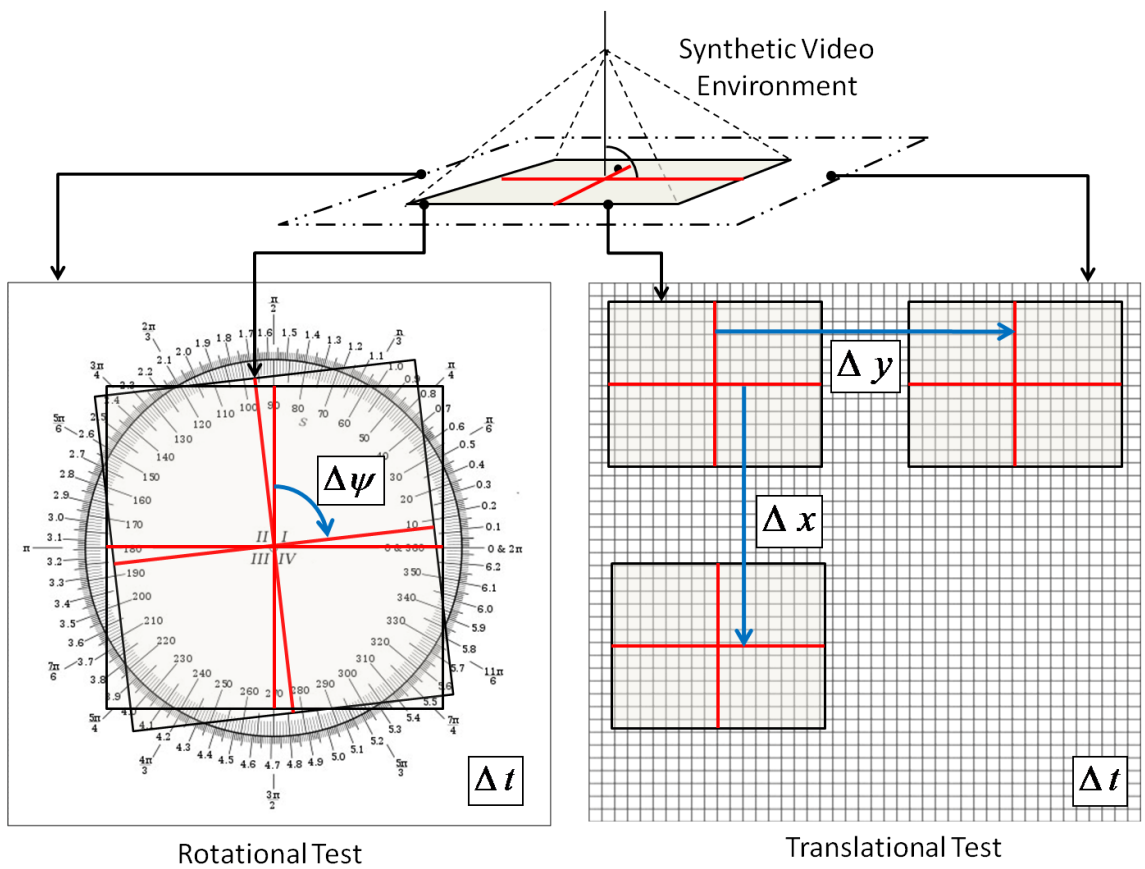


**Figure 5.4:** Evaluation of Synthetic Video

### 5.1.2 Test Scenarios, Expectations and Results

As presented in figure ??, the variance rate is enormous. So the optical movement detection algorithms and corresponding calculations are tested in several scenarios which focus a specific behaviour with a corresponding expectation of the result. The goal thereby is to provoke expected characteristics, or to demonstrate that the expectations are not fulfilled by the result of the corresponding test scenario. For a better overview, the test plan ?? shows the relations between the domains of variation. Each scenario is driven by a stimulus data which contains

## 5.1 ANALYSIS OF IMAGE PROCESSING

the three mentioned components of the stimuli domain, presented in ???. Beside this, each test scenario separately focuses on the rotational and translational behaviour.

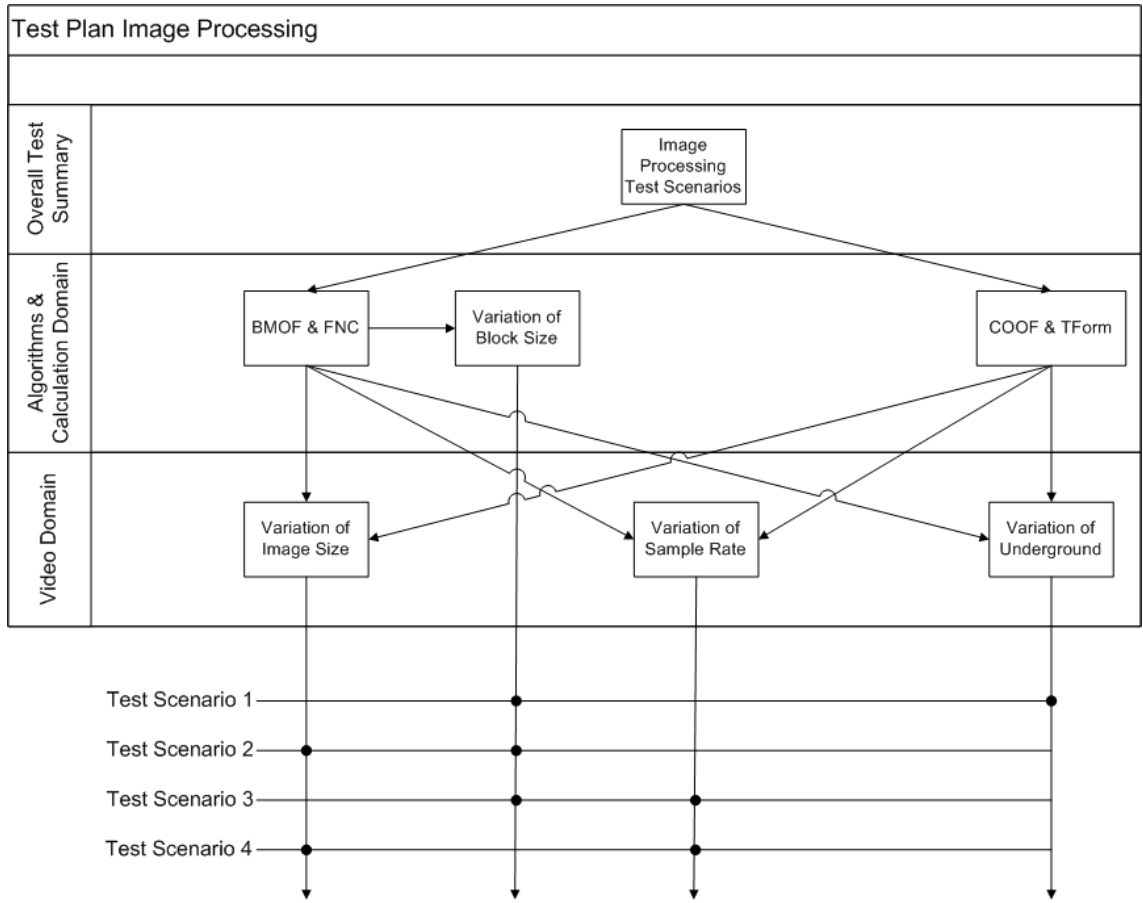


**Figure 5.5:** Image Processing Test Plan

### **Image Processing Test Scenario 1: Variation of Underground**

As mentioned in the description of the underground item, a flight scenario can be influenced by the underlying underground image. So this test scenario focused on the behaviour of the different algorithms in relation to the underground. To provide suitable results for investigation, the configurations of the used algo-

## 5.1 ANALYSIS OF IMAGE PROCESSING

---

rithms must also been varied. In this case, it is interesting to vary the Block Matching Optical Flow (BMOF) algorithm's block size, which can have an impact on the result. This scenario bases on the expectation that the structure of the underground influences the quality of movement detection in relation to the used algorithm. Furthermore, as expected, the Corner Detection Optical Flow (COOF) algorithm should show the best results on the cornered underground, because the built-in corner tracker can find a bigger amount of features. On the other hand, the BMOF should operate satisfactory in the amorphous structure. The reason for this expectation is that the similarity measure of blocks is not as high as in the corned structure, because of the amorphous behaviour. This measure should influence the rate of exactly matching blocks. Finally, the segmented amorphous structure should expectably demonstrate that both algorithms work moderate on this structure, but not as good as in the expected more advantageous structure.

### Image Processing Results of Test Scenario 1

Starting with the translational analysis of test scenario 1, the result presented in ?? shows the characteristic of the COOF algorithm. The expected best case behaviour for this algorithm is proved to be as expected, the cornered structure. Interesting to see is that the segmented amorphous underground nearly shows the same results as the best case. The amorphous underground affects, as expected, some outlines (See ?? arrow No.2), probably because the found feature amount is not high enough, or some features raise errors because of the same structure. On the other hand, this assumption could be the reason for the apparent better detection ability of the acceleration stimulus part with the cornered structure (See ?? arrow No.4). Another unexpected behaviour, which is probably related to the

## 5.1 ANALYSIS OF IMAGE PROCESSING

sample time, is that the complete output curves react with a delay of 100ms (See ?? arrow Nr.1 and Nr.3).

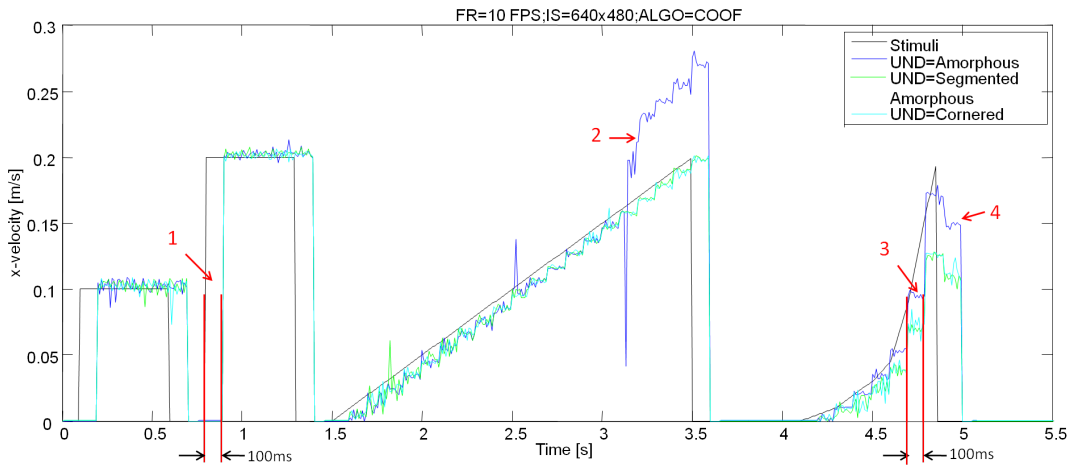


**Figure 5.6:** Image Processing Result of Test Scenario 1: Translational analysis of COOF

The results of the BMOF algorithm are visualised in figure ???. Thereby the unexpected but interesting behaviour was found that the BMOF algorithm reaches the limit of maximum velocity, in this special case  $0.1m/s$ , faster as the COOF algorithm under equal conditions. Furthermore, the expected best suited underground is the amorphous structure, but just on the aspect of precision (See arrows No.1, ??). But this noise behaviour could also be a limitation of the simulation, caused by multiple calculations of the same sampled image sequence (See arrow No.2 and No.3). Another unexpected behaviour is that the BMOF algorithm has a better offset behaviour, in relation to its block size, with the cornered structure. This means that the BMOF algorithm does not normalise the detected velocities in relation to the blocks, to a relative level that affects the problem that a coarse-grained block segmentation has a lower offset in the equal environment as a fine-grained segmentation.

## 5.1 ANALYSIS OF IMAGE PROCESSING

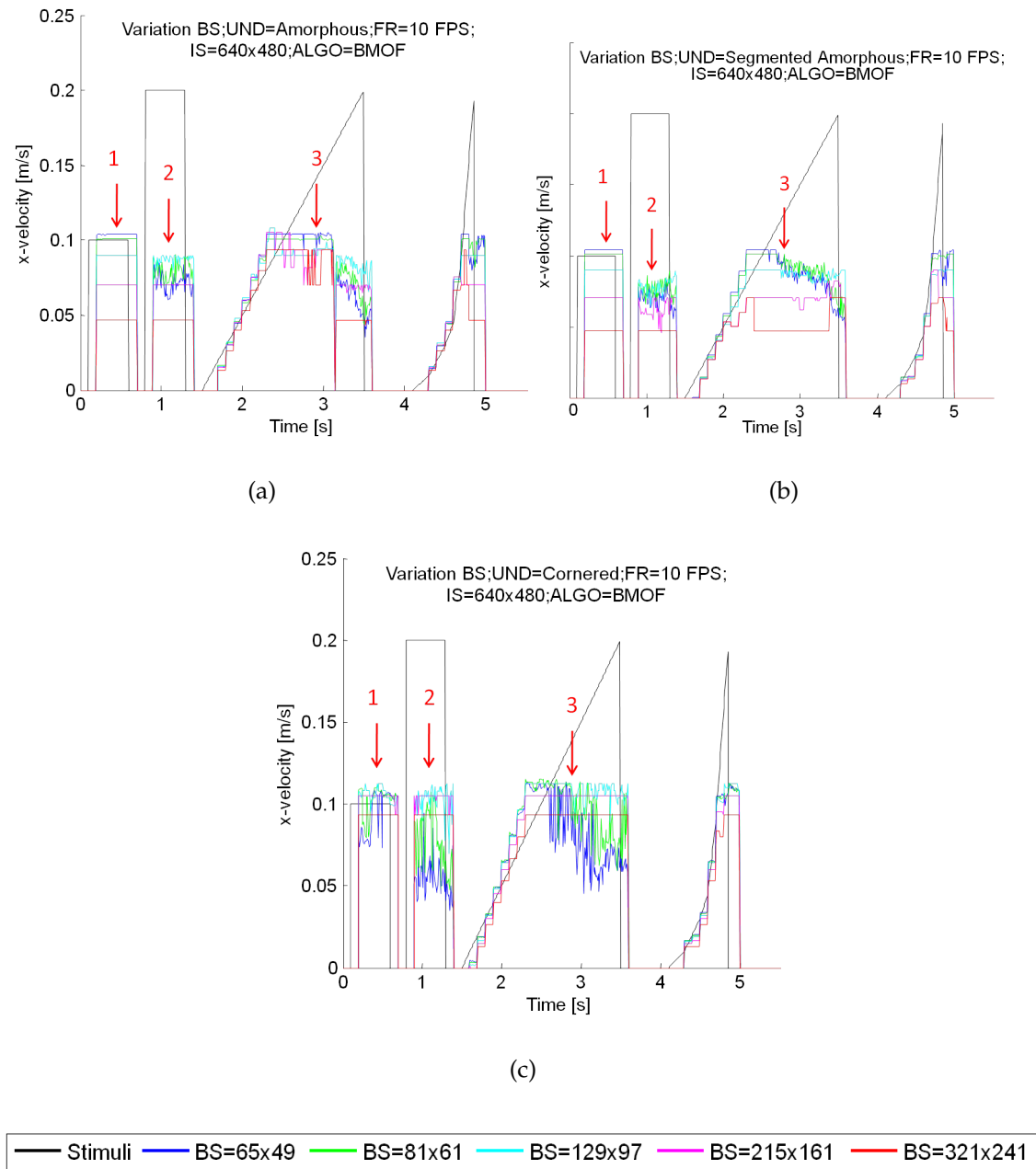


**Figure 5.7:** Image Processing Result of Test Scenario 1: Translational analysis of BMOF

Afterwards, the experimental results of the rotational behaviours show enormous differences in several aspects. First, the diagram (a) in figure ?? visualises the rotational COOF algorithm behaviour in a test with a maximum gain of  $2 * \pi/s$ . As

## 5.1 ANALYSIS OF IMAGE PROCESSING

---

mentioned, the COOF algorithm can detect the rotational direction. This information is reflected in the sign of the detected velocity. As visualised, the negative direction of the rotational behaviour shows a counter-clockwise rotation. As we can see, the first pulse, with a gain of  $\pi$  is nearly error-free detected (See ?? arrow No.1). In contrast to that, the COOF algorithm shows problems with reaching the gain of  $2 * \pi$ , (See ?? arrows No.2 and No.3). These errors are possibly based on the combination of a rotational movement and the low sample rate. Such an effect is also discussed and presented in the stroboscopic torque measurement in chapter ???. Unexpected was in this case that the COOF algorithm also showed errors with the amorphous and cornered structure, but provides the best matches with the segmented amorphous structure. The reason could be a big amount of dissimilar forms, based on the amorphous and cornered structure. The diagram (b) shows the result of the BMOF algorithm, which is under no circumstances useful. In this case, it is obvious that the low sample rate along with the corresponding high rotational velocity affects a big amount of error matchings.

## 5.1 ANALYSIS OF IMAGE PROCESSING

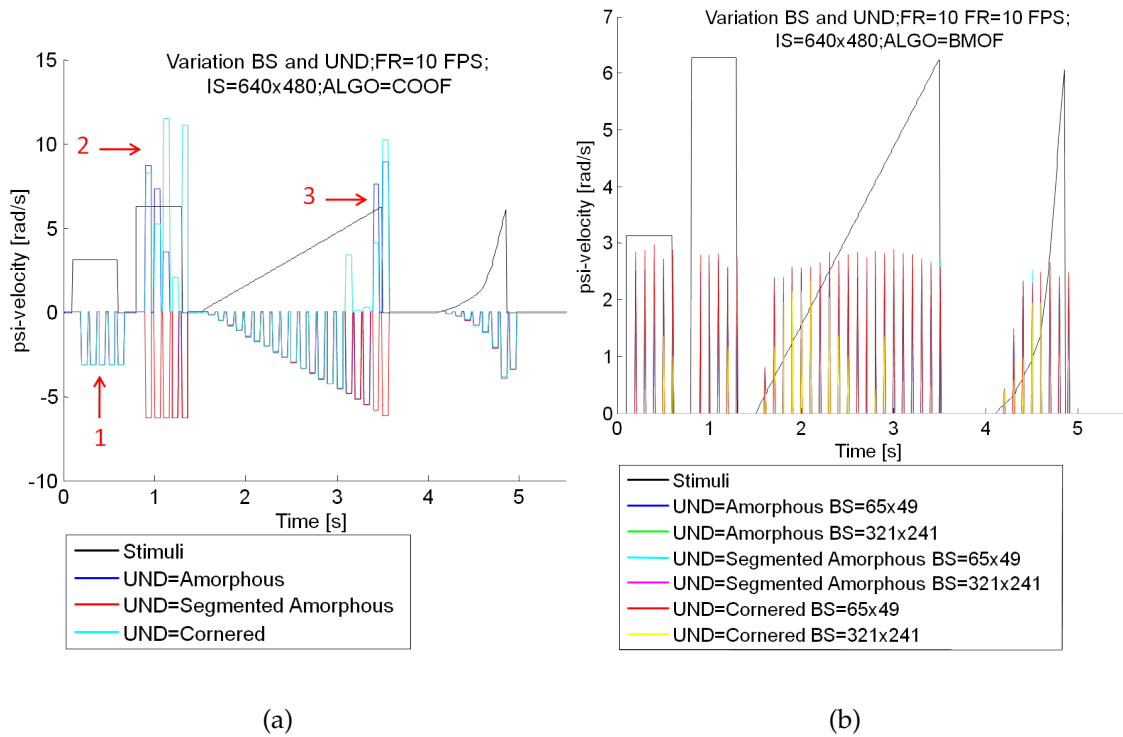


**Figure 5.8:** Image Processing Result of Test Scenario 1: Rotational analysis of BMOF and COOF

Because of the poor rotational behaviour of the BMOF, the rotational experiment of this algorithm was executed with a sample rate of 80 FPS. The result is the first satisfactory configuration for the rotational behaviour of this algorithm. Returning to the original focus of this test scenario, the underground structure that showed the best results is the segmented amorphous with the fine-grained configuration of blocks (See ?? arrow No.1). This behaviour is argumentative, because it acts like the COOF algorithm. Possibly the mentioned reason of the highest dissimilarity of forms can also lie in the characteristic of best matches.

## 5.1 ANALYSIS OF IMAGE PROCESSING

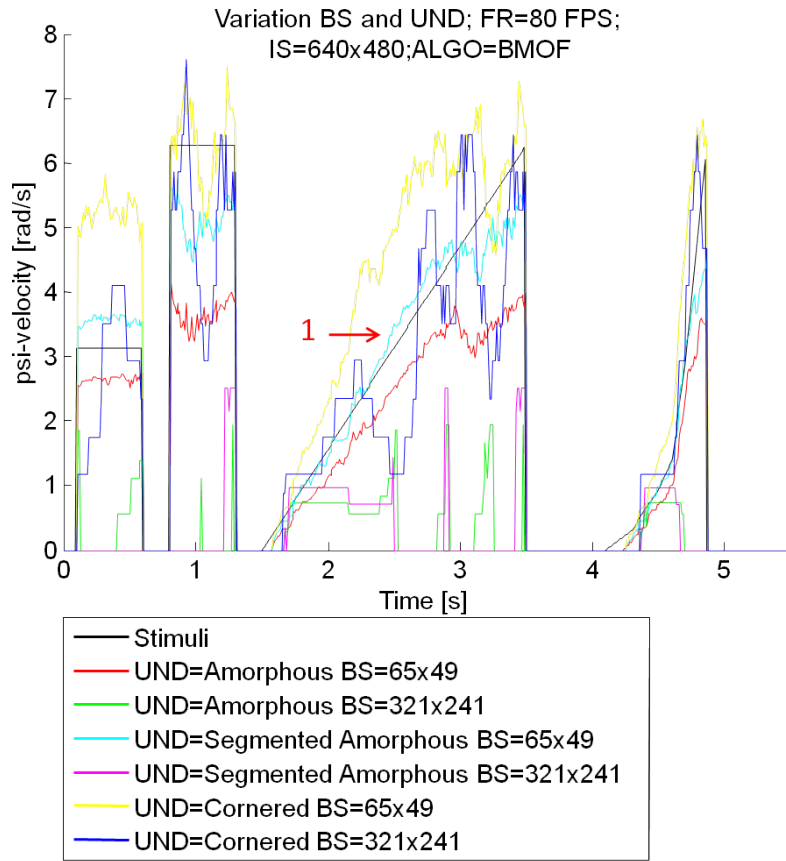


**Figure 5.9:** Image Processing Result of Test Scenario 1: Rotational analysis of BMOF with conformed frame rate

### Image Processing Test Scenario 2: Variation of Image Size

The image size of the captured images is related to this data size, and further to the transmission time to the base station. So this test sequence focuses on the variation of usual image sizes, presented in the introduction of this chapter and based on the presented camera examples in ???. As is well known from the first test scenario, the block size of the BMOF is also being varied in this test case to analyse the corresponding relation of block and image size. The underground which was chosen in this scenario is the segmented amorphous structure, which was not

## 5.1 ANALYSIS OF IMAGE PROCESSING

---

changed over the test execution. The goal and expectation of this test case is to demonstrate the relation of image size and maximum translational or rotational speed that can be detected. Also interesting is to investigate whether the precision of movement detection is related to the image size. This expectation is based on the assumption that more points can be captured in a bigger image and this leads to a more exact determination of movement. Another interesting characteristic is the question which algorithm can provide a better performance in aspects of precision and maximum speed with the same image size. The expectation is that the COOF algorithm will show better results and will not be as dependant on the image size, as the BMOF algorithm. This assumption bases on the fact that COOF takes all tracked features similarly into account in each step, and is not dependent on a limited search area as is the case with the BMOF algorithm.

### **Image Processing Results of Test Scenario 2**

The unsatisfactory result of the rotational behaviour of the BMOF, presented in ?? (b), lead to the decision to change the frame rate for test scenario 2. So the frame rate of this test scenario was increased from 10 FPS to 80 FPS for feasibility reasons. Starting with the BMOF algorithm, the executed tests are visualised in ?. Thereby, diagram (a) contains the executed test scenario with the smallest block size (fine-grained), and diagram (b) presents the output of the algorithm with the biggest block size (coarse-grained). Generally, the drawback of the fine-grained configuration can be seen in the second pulse. In contrast to the coarse-grained configuration, the fine-grained output shows a noisy gain behaviour(?? (a) arrow No.1 ). Additionally, the fine-grained configuration shows the unexpected behaviour of more exactly reaching the stimulus signal in the ramp phase (?? (a)

## 5.1 ANALYSIS OF IMAGE PROCESSING

---

and (b) arrow No.2). Combined with the result that the fine-grained configuration is more noisy, it is logical that it reacts faster as the coarse-grained configuration. Regarding the small velocities of the ramp and exponential part of the stimulus, it is noticeable that all image size configurations have a small dead zone before they react to the stimulus ?? (a) and (b) arrow No.4). So because this characteristic exists in all configurations, and was not detected in test scenario 1, it is possible that it is related to the increased frame rate of this scenario. Furthermore, we can see that the maximum speed limit is not as much related to the image size in the configuration of this scenario as expected. This can be assumed because the difference in the output error between the biggest and smallest image size, with the best block size configuration, is less than 10% ?? (a) and (b) arrow No.3). A better visualisation of all test errors, executed in each constellation of block and image size, is visualised in diagram ?? (d). As expected, the smallest image size corresponds to the biggest errors. Further, it is interesting to see that least errors are reached diagonal to the block and image size axis. This means that the optimal configuration is related to the optimal segmentation of the image with the corresponding block size ?? (d) blue concave area). The translational behaviour of the COOF in relation to the image size is visualised in diagram ?? (c). As anticipated, this algorithm shows nearly the same behaviour in each configuration of the image size. The unexpected behaviour is that the output signals' noise is bigger than in a similar test with a sample rate of 80 FPS. So it can be assumed that the sample rate has a bigger impact on the noise and precision of the COOF algorithm as the image size.

## 5.1 ANALYSIS OF IMAGE PROCESSING

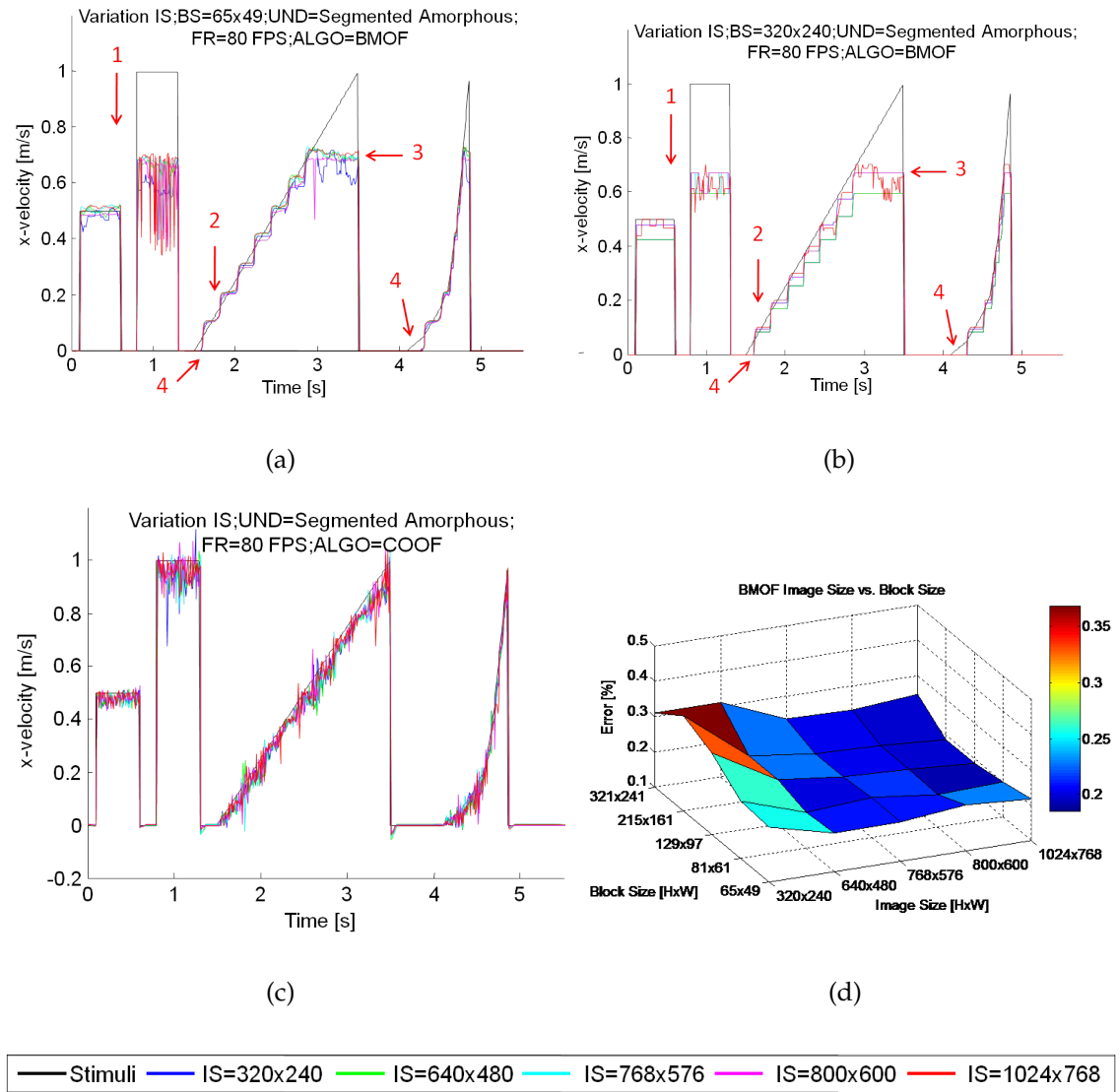


**Figure 5.10:** Image Processing Result of Test Scenario 2: Translational analysis of BMOF and COOF

On closer consideration of the rotational result in relation to the image size, as expected the COOF operates nearly perfectly in contrast to the BMOF. As visualised in diagram ??(c), the test scenario with a maximum limit of  $2\pi/s$  rotational velocity could not utilise the maximum limit of the algorithm. So this experiment was executed again with a higher gain, to reach and investigate the limitation of

## 5.1 ANALYSIS OF IMAGE PROCESSING

---

COOF. The result is that the rotational velocity limits of the COOF are nearly two times and the translational even five times higher than the best-suited configuration of BMOF. By regarding the fine-grained (a) and coarse-grained (b) block size rational behaviour of the BMOF, it is interesting to see that the fine-grained configuration is superior to the coarse-grained. The unexpected behaviour thereby is that the best error value is reached with corresponding middle or small image sizes (blue area in figure ??(d)) and not with the biggest image sizes. Thereby, this deviation is not that big, so it is possible that this phenomenon originates from the Gaussian distribution off errors, related to the underground. On the other hand, it is possible, as mentioned in the investigations of the translational behaviour, that an ideal configuration of image size and block size results in average from an error minimum.

## 5.1 ANALYSIS OF IMAGE PROCESSING

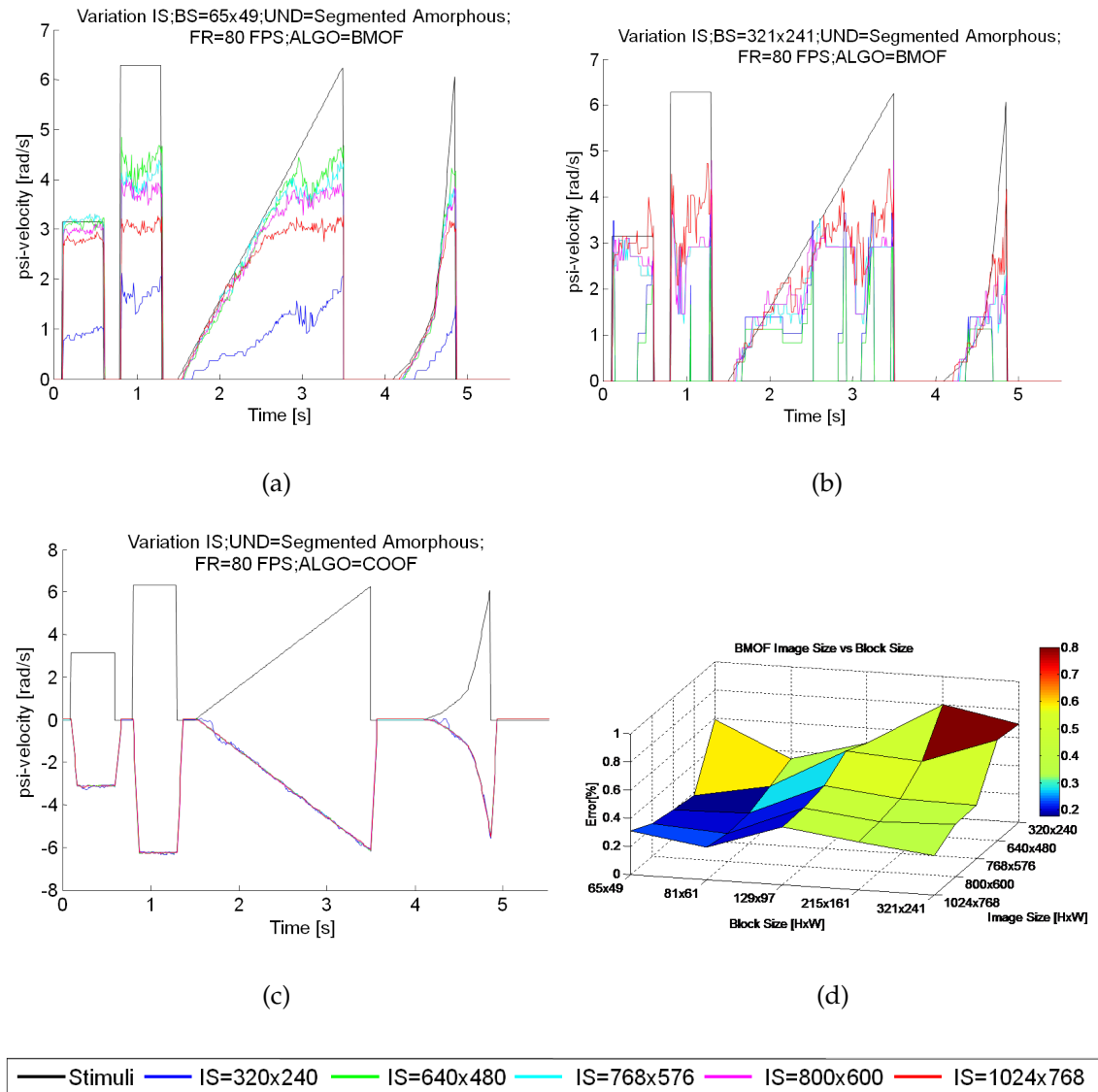


**Figure 5.11:** Image Processing Result of Test Scenario 2: Rotational analysis of BMOF and COOF

### Image Processing Test Scenario 3: Variation of Sample Rate

The Sample Rate variation test scenario, based on MATLAB/Simulink's time variant simulation of dynamic systems, and provides the perspective to analyse

## 5.1 ANALYSIS OF IMAGE PROCESSING

---

the algorithm behaviour in relation to the presented rates in the introduction. As mentioned, similar to the image size, the frame rate also has an impact on the load factor of the image processing and transmission spectrum. So in this scenario, the introduced algorithms should be investigated with the intention to determine the limits of maximum speed operation, and to figure out which algorithm, with corresponding configuration, provides the best result related to the same frame rate. The expected result of this scenario is that both algorithms will reach a limit, but the COOF will work with higher velocity conditions. Based on the mentioned expectation in test scenario 2, the limited search region of the BMOF will increase the error possibility with ascending speed. On the other hand, the BMOF algorithm should show a more precise processing at lower speed and frame rate, because with increasing successful block matches, the possibility of error matches is decreased. This expected characteristic could be demonstrated with a jigsaw puzzle example, in which also the possibility to find the right piece in a region increases in relation to the amount of already located pieces.

### **Image Processing Results of Test Scenario 3**

In the previous test scenarios, the rotational and translational speed limitation of BMOF, related to the highest sample rate, was determined and presented in ?? (a) (b) and ?? (a) (b). As expected, the COOF algorithm shows better results in the aspect of speed limitation as BMOF. The expected behaviour of higher precision in the region of a low sample rate of the BMOF algorithm is shown in diagrams ?? (a) and (b). As we can see, the fine-grained configuration shows a smoother characteristic of the output signal, in contrast to the coarse-grained block segmentation, which reacts step-wise to the stimulus. Unexpected thereby was that the

## 5.1 ANALYSIS OF IMAGE PROCESSING

---

highest sample rate has the biggest delays and reacts very quantitative in relation to stimulus change (?? (a) (b) arrow No. 2 and No.4). These delays, related to the ascending sample rate, could occur because the changes between the captured images are very small and could not be detected by the algorithm. That means velocity changes in the dead zone could remain undetected in a trajectory. On the other hand, sample rates over 20 FPS can detect the stimulus signal up to the biggest velocity value. In contrast to that, the small sample rates 10 FPS and 20 FPS reach their limits in the presented diagrams (?? (a) (b) arrow No.3). As mentioned, the COOF algorithm shows, with ascending sample rate, an ascending noise characteristic which could also originate from the small changes between the images, which rise to error localisations of the features (?? (c)). This noise error behaviour of the COOF was compared with the error of the BMOF algorithm. The 3D-diagram (?? (d)) shows that the BMOF has the biggest errors in the region of a small sample rate and block size. The COOF algorithm, which is unattached from block size variation in this diagram, shows the best results at sample rate values of 40 and 60 FPS. In the other sample rate regions, the error is influenced by the quantisation or by the noise. The comparison shows that generally, the error variation and average error of COOF are smaller than the the values of the BMOF algorithm. On the other hand, the BMOF algorithm shows a better error behaviour at the highest sample rate than the COOF algorithm (surface slice in blue region).

## 5.1 ANALYSIS OF IMAGE PROCESSING

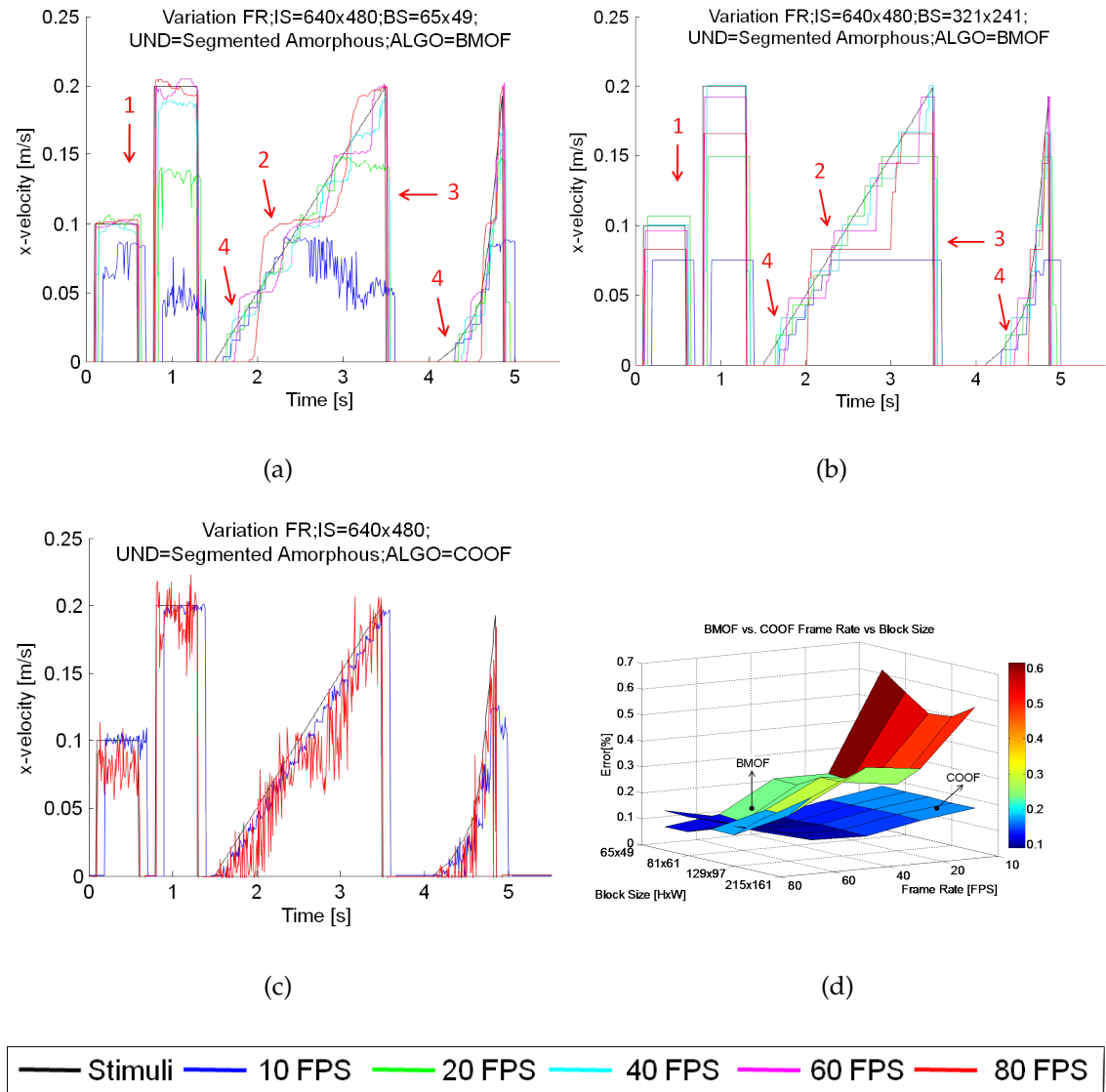


**Figure 5.12:** Image Processing Result of Test Scenario 3: Translational analysis of BMOF and COOF

The rotational behaviours of the two algorithms show many unexpected characteristics. By comparison to the coarse-grained block segmentation, the fine-grained segmentation of the BMOF shows relatively satisfactory results. As we can see in diagramm ?? (a), the highest frame rate provides the best results and

## 5.1 ANALYSIS OF IMAGE PROCESSING

---

the highest rotational speed detection. The lowest frame rate, as also presented in test scenario 1 (See ?? (b), can not detect any movements satisfactorily and shows just a noisy signal. As expected, the COOF algorithm also shows, in this scenario, a better rotational determination. On the other hand, it shows an unexpected behaviour related to the increase of the frame rate. As we can see in ?? (c), the best results are captured with the highest frame rate. This result has almost no noise. With descending frame rate, the noise of the output signal is amplified, with the worst case visualised at the lowest frame rate. This effect could be based on the mentioned optical effects of the sample rate and the confusion of the tracked features, or could originate from an unexpected time variant limitation behaviour of the simulation. Finally, a descriptive figure of the error characteristics of both algorithms is presented in ?? (d). As we can see in the results of the COOF surface, this algorithm improves the error characteristic with ascending frame rate. This is based on the fact that noise is reduced with ascending frame rate. In the result surface of the BMOF, it can be seen that both variation values, frame rate and block size, have nearly equal influence on the error characteristic of the algorithm. This assumption is derived from the diagonally descending surface of this algorithm.

## 5.1 ANALYSIS OF IMAGE PROCESSING

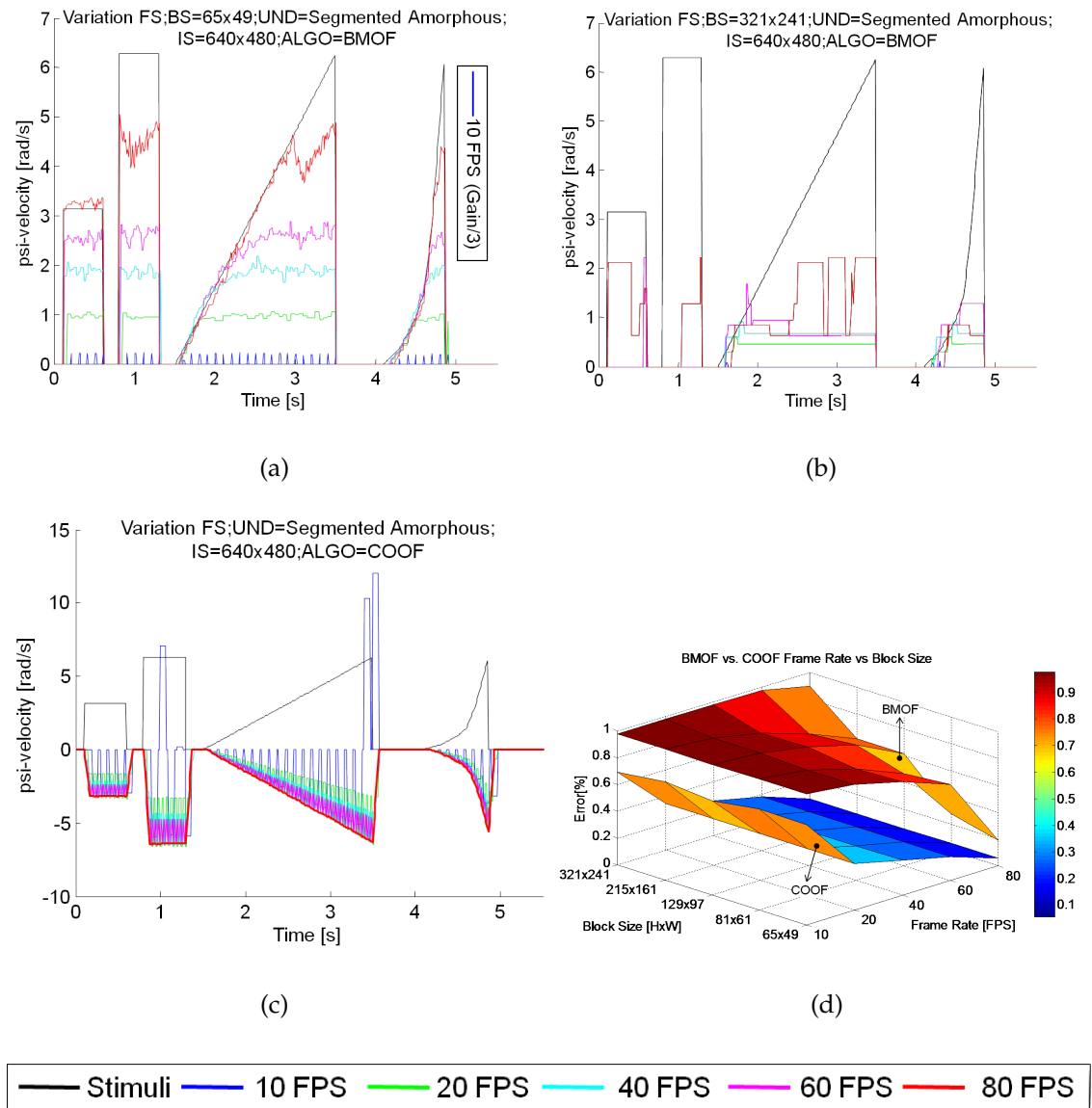


**Figure 5.13:** Image Processing Result of Test Scenario 3: Rotational analysis of BMOF and COOF

## 5.1 ANALYSIS OF IMAGE PROCESSING

---

### Image Processing Test Scenario 4: Variation of Image Size reciprocal to the Sample Rate

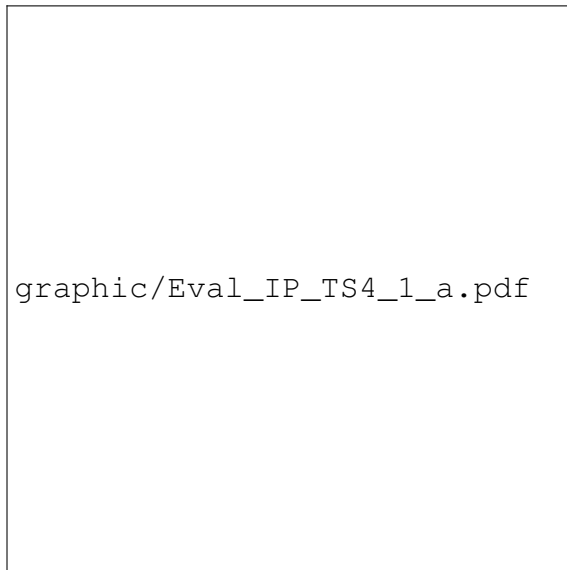
In this test scenario, the two parameters, image size and sample rate, are varied simultaneously. The aim thereby is to show the relation between the two parameters and the impact on the error amount of both algorithms BMOF and COOF. Additionally, it has to be analysed which parameter has the biggest influence on the error behaviour. The expected result of the comparison of the error characteristics of the two algorithms is that the COOF algorithm will generally have a lower error surface in the analysis in rotational and translational behaviour, and will show a better best-case error-characteristic than the BMOF algorithm. These assumptions base on the mentioned prospected characteristics, described in the previous test scenarios.

### Image Processing Results of Test Scenario 4

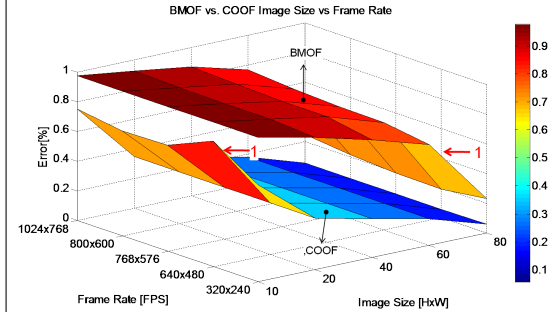
A comparison of the focused algorithms, including the translational (a) and rotational (b) analysis, is shown in figure ???. Regarding the error rate of the translational behaviour of both algorithms, we can see that the expected error surface of the COOF algorithm is truly lower than the error surface of the BMOF. Also correctly expected in this case was the best case behaviour (?? (a) arrow No. 2) of the BMOF. The pointed corner in the diagram shows that the best-case error value of the COOF is lower than the corresponding best-case error-value of the BMOF algorithm. An unexpected behaviour is that the error behaviours of both algorithms show an interesting response in the section of 40FPS. In this case, BMOF

## 5.1 ANALYSIS OF IMAGE PROCESSING

shows a better error characteristic in comparison to the COOF algorithm, which contains one of the biggest error values in this section. The rotational behaviour, shown in ?? (b), shows that both algorithms have the worst error characteristic in the section of the lowest sample rate. The BMOF algorithm shows, especially in this section, an error of nearly 100%. Furthermore, we can see that the BMOF algorithm can only provide a satisfactory result between the sample rates of 60FPS and 80FPS. In contrast to that, the COOF algorithm shows the first acceptable error behaviour at less than 20FPS. So the COOF algorithm could be the correct one to realise a distributed error correction scheme with a sample rate of 20 FPS. Both diagrams show the relation to the two parameters, varied in this scenario. As we can see, the frame rate has a bigger impact to the error characteristic than the image size. This fact can be determined because the biggest variations of the output is shown in direction of the frame rate axis.



graphic/Eval\_IP\_TS4\_1\_a.pdf



(a)

(b)

**Figure 5.14:** Image Processing Result of Test Scenario 4: Translational and Rotational analysis of BMOF and COOF

### 5.1.3 Summary

This chapter showed several interesting characteristics of the realised image processing simulations. Starting with the results of the first test case, it can be said that the error and precision characteristic was nearly the same for all tests. Some unexpected effects were found in these test cases which can be explained with the internal algorithm characteristics. Finally the variation of undergrounds shows that undergrounds with nearly the same contrast distribution have nearly the same results. Regarding the second test scenario, the variation of image sizes shows, unexpected an impact on the translational noise behaviour of the COOF algorithm and the rotational speed limitation of the BMOF algorithm. The translational behaviour of BMOF and the rotational behaviour of COOF show an insensitive attitude in relation to the image size variation. The variation of the frame rates shows a dramatically increasing impact of noise behaviour of the COOF with increasing frame rate, and a limitation behaviour of maximum speed detection of the BMOF. Furthermore, the results of the experiments of the frame rate variation show the unexpected behaviour of output signals' delay. Finally, the fourth test scenario demonstrated that the impact of the frame rate, in relation to the error of the output and input signal, is much higher than the error impact related to the image size.

### 5.2 Analysis of Control behaviour

This chapter focuses on the analysis of the body and position control behaviour. The aim thereby is to demonstrate the ideal control configuration for the final test analysis. So influences of the disturbances of the image processing are not regarded in this case. Therefore the analysis and optimisation of control is executed in this chapter with the sensor disturbances of the IMU existing in reality only. Regarding the mentioned theory of control systems in chapter ??, the criteria of stability and performance measurement can be executed systematically in linear systems. Systems which include non-linearities can be linearised in one operating point of the non-linear component. In case of the quadrocopter plant, the set-point of the brushless controllers and the corresponding thrust are non-linear (See ??). So a strategy to fine tune the PID controller parameters by regarding the non-linearity behaviour is presented in ??<sup>2</sup>. As we can see in the presented state chart, the first separation for further analysis steps is to determine if the plant is linear or not. In case of a linear plant, the methods presented in the figure and discussed in ?? can be executed. If the plant is non-linear, a linearisation at an operating point can be helpful to linearise the model and to execute the linear analysis systematically. In case of the quadrocopter, the linearisation at several operating points show the same unstable results (See ?? (a) and (b)).

---

<sup>2</sup>This strategy was established in an interview with Prof. Dr. Kull and bases on the theory presented in [30]

## 5.2 ANALYSIS OF CONTROL BEHAVIOUR

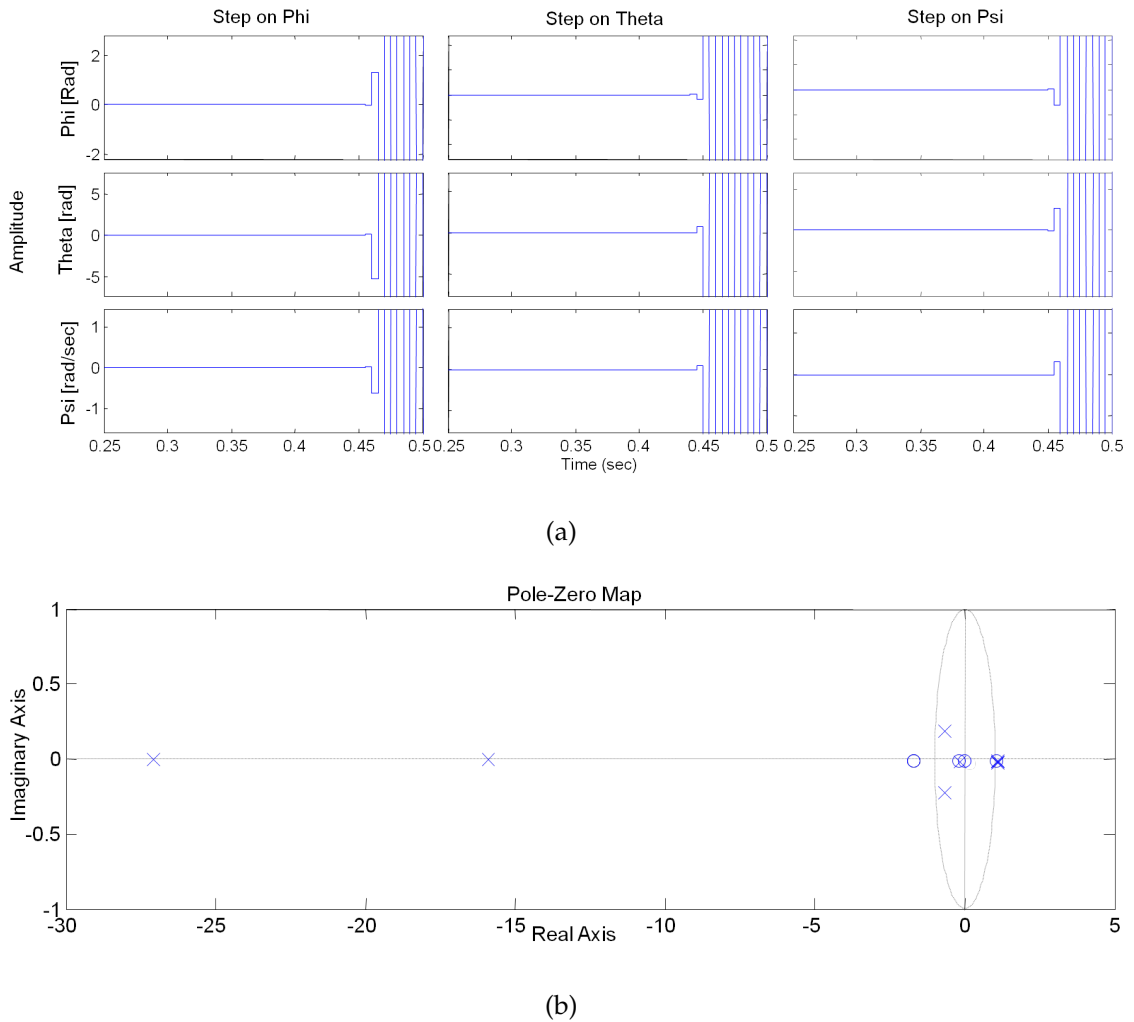


**Figure 5.15:** Step response and Pole-Zero map of linearised model

After the results of the linearised plant, the possibility to determine the optimal control parameters is the empirical method. This method presumes that the output values are independent from each other. In case of the quadrocopter model, the input values, which have an impact to the stability of the system, are the angles. These are independent from each other and do not need an uncoupling system. Such a system is a module integrated into the CLCS that eliminates the influences of related output values. The further analysis and determination of the

## 5.2 ANALYSIS OF CONTROL BEHAVIOUR

optimal PID values for each controller was executed with the Simulink-Design-Optimization-toolbox ©<sup>3</sup>, which uses several optimisation and minimization algorithms to find the best suited configuration of the controller parameters.



graphic/AnalysisOfControlStrategy.pdf

**Figure 5.16:** Control tuning strategy for linear and non-linear CLCS

The following figure visualises the optimal tuned step response behaviour of the body PID controllers. Thereby, the optimisation algorithm shows two possible

---

<sup>3</sup>See [38]

## 5.2 ANALYSIS OF CONTROL BEHAVIOUR

---

stable configurations, which differ in aspects of rise time, maximum overshoot and range of tolerance. The first stable configuration (?? (a) and (b)) shows a stable behaviour until the step of 1.2 [rad] for body angles  $\phi$  and  $\psi$ . Compared with the second configuration (?? (c) and (d)), which can only show a stable behaviour until the step value of 0.9 [rad], the first solution can be used to reach higher pitch and roll angles in flight. A possible drawback of the first configuration is the rise time, which is very high compared to the second configuration. A further cost of the high angle detection possibility is the oscillating behaviour of the first configuration. The second configuration thereby shows an increasing overshoot related to the increasing step stimulus. Regarding the yaw behaviour of both configurations, we can see that the performance values are nearly the same, and show a very good rise time behaviour. The first configuration shows a high frequency oscillation behaviour. This could originate from the small motor invariances of the quadrocopter. An evidence for that could also be the fact that this behaviour also exists in the second configuration, but not with the same frequency. Finally, the second configuration will be used for further experiments and analysis because of the better steady state behaviour. These configurations' steady state behaviour will have a small influence to the optical position control performance. So this aspect is very important, and therefore the justification for this decision. Further, the second configuration can be improved with limiting the maximum angles of pitch and roll to 0.75 [rad]. This limitation guarantees an acceptable overshoot and prevents instabilities of the system.

## 5.2 ANALYSIS OF CONTROL BEHAVIOUR

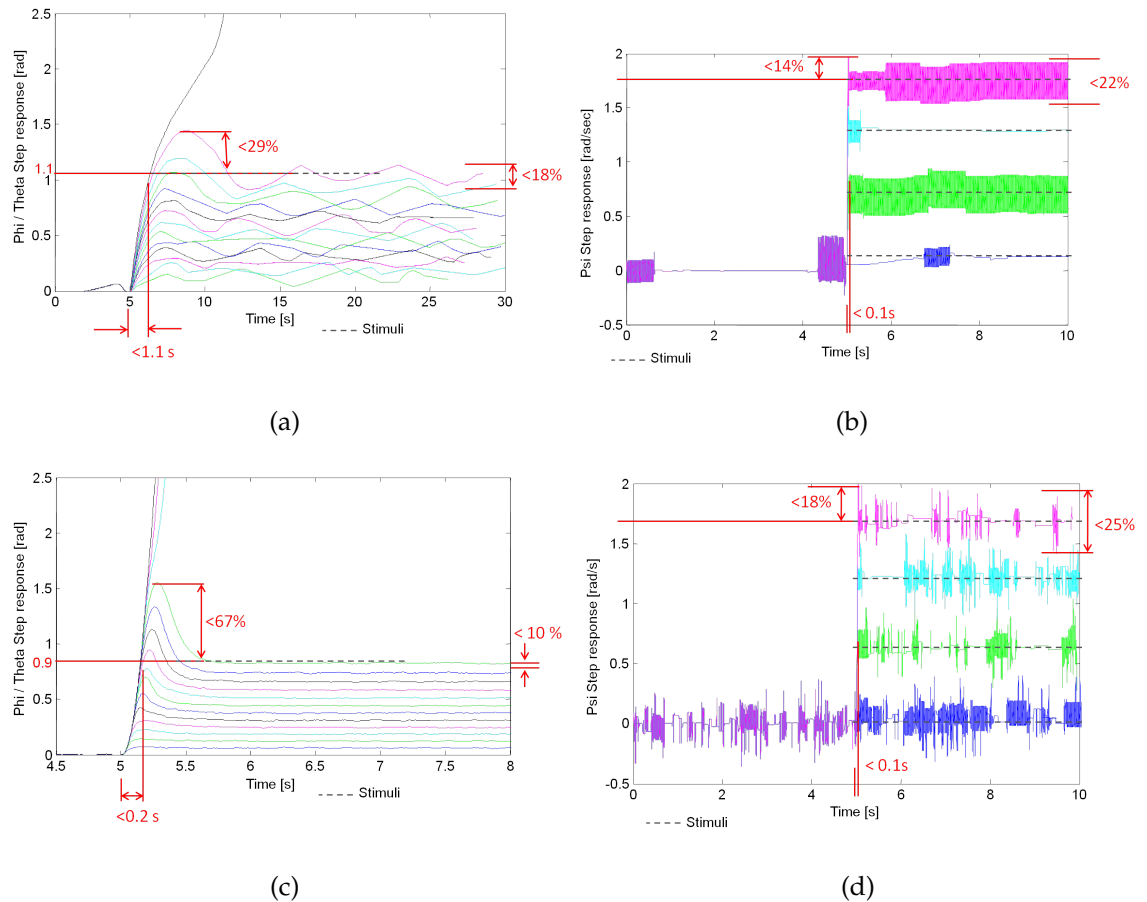


**Figure 5.17:** Results of Body PID Controller optimisation

The corresponding optimisation processing of the position PID controllers is shown in ???. Regarding the optimisation of the symmetrical axis angles  $\phi$  and  $\theta$ , we can see that the optimisation algorithms traverse some unstable configurations (See ?? (a)). Furthermore, several stable configurations were found by the optimiser, and the most suitable of these was chosen to realise the velocity position control for these axes. An interesting behaviour was found during the optimisation process of the optical  $\psi$  PID controller. As visualised in diagram ?? (b) the optimisation for psi was executed with a step disturbance. The aim of the controller is to equalise this movement to zero as fast as possible. As we can see, the predica-

### 5.3 ANALYSIS OF POSITION CORRECTION SCHEME

ment of this optimisation is that the steady state error grows with the precision of the output signal. An example is demonstrated with the green (?? (b) arrow No.1) and red (?? (b) arrow No.2) regression lines, which show this behaviour. This phenomenon can be an important argument against an optical position correction of the  $\psi$  angle if the shown noise characteristic influences the position controller. Generally it can be assumed that the gyroscope sensor value and the corresponding control circle should work vastly better than the optical solution for this angle.

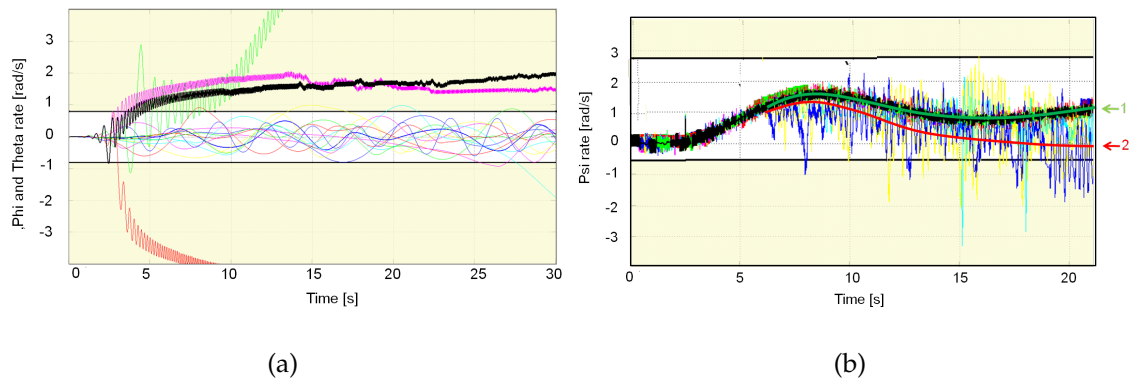


**Figure 5.18:** Results of Position PID Controller optimisation

### 5.3 Analysis of Position Correction Scheme

This section focuses on the collaboration between optimised controller system and image processing. These consolidated components will be called "position correction scheme" within the scope of this project. Furthermore, the position correction scheme will be analysed under the execution of the following test scenarios presented in figure ?? (a). As visualised, the test plan in this context is designed similar to the test plan of the image processing presented in ???. The

### 5.3 ANALYSIS OF POSITION CORRECTION SCHEME

difference here is that the test scenarios only focus on image size and frame rate variation, combined with a different model of 3D-trajectory stimulus. The decision in favour of these test scenarios is based on the results of the image processing analysis (See ?? and ??). These results show that the biggest influence and the most interesting behaviour of the image processing originates from the variation of frame rate and image size. Additionally, the stimulus is classified here in three segments. All test scenarios executed with the rotational and translational configuration, presented in ?? (b), and with an uplift stimulus that elevates the quadrocopter to a hovering state. For visualisation reasons, the rotational test is executed as a mixture of a translational and rotational part. Otherwise the 3D-Trajectory would be just a point, and so unsuitable for demonstration. The goal of these test stimuli is to show how the position correction scheme reacts under different conditions. Another aspect of segmentation is the different performance of regarded algorithms in case of rotation, translation and hovering tests.

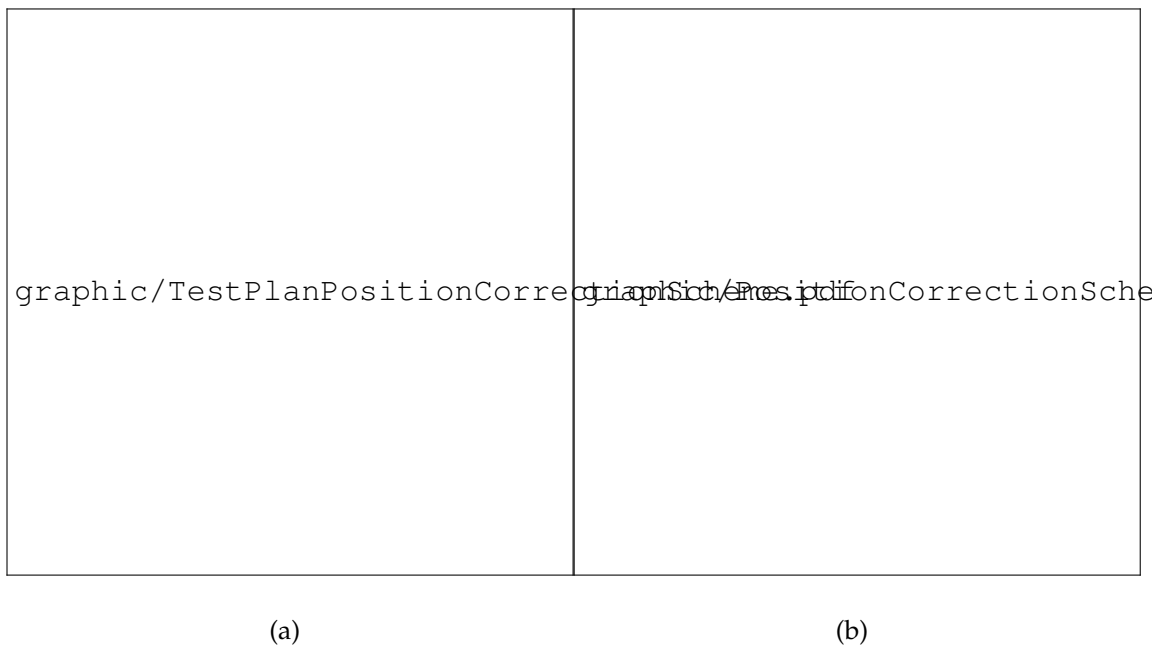


**Figure 5.19:** Test facility for hovering, rotational and translational position correction tests

## 5.3 ANALYSIS OF POSITION CORRECTION SCHEME

---

### 5.3.1 Test Scenarios, Expectations and Results

#### Position Correction Scheme Test Scenario 1: Variation of Sample Rate

One of the aims of this test scenario is to show the influence of the sample rate in relation to the introduced testing facility. To achieve this, the mentioned stimuli are executed with the introduced sample rates of 10, 20, 40, 60, 80 FPS, introduced in chapter ???. The expected quality of the position correction scheme will be strongly related to the results presented in ???. As mentioned, the variation of frame rate show a big impact to the noise behaviour of the COOF and the limitation behaviour of the BMOF algorithm. Furthermore, signals of both algorithms show a delay characteristic, especially in the area of low sample rates. So these algorithms will show their mentioned strengths and weaknesses in the following 3D-Trajectories.

#### Position Correction Scheme Results of Test Scenario 1

As expected, the impact of the maximum speed limitation of the BMOF algorithm is enormous. As we can see in figure ?? (a), the 3D-Trajectories are deformed with decreasing sample rate to the direction of the  $X_E$  and  $Y_E$  axis. So this test shows, in a very suitable example, how the speed limitation of an image processing algorithm can influence the position correction scheme (See corresponding 2D-Trajectory in ?? (a)). In contrast to the speed limited BMOF algorithm, the COOF algorithms' 3D-Trajectories are very precise (See ?? (b)). Also correctly expected was the disturbance of the noise behaviour of this algorithm. As visu-

### 5.3 ANALYSIS OF POSITION CORRECTION SCHEME

alised in figure ?? (b), the best results are not executed at the highest sample rate, but with a sample rate of middle image sizes. So it is demonstrated that the COOF algorithm shows the most suitable results with an average signal delay, and also an average noise behaviour, in the translational position correction tests.

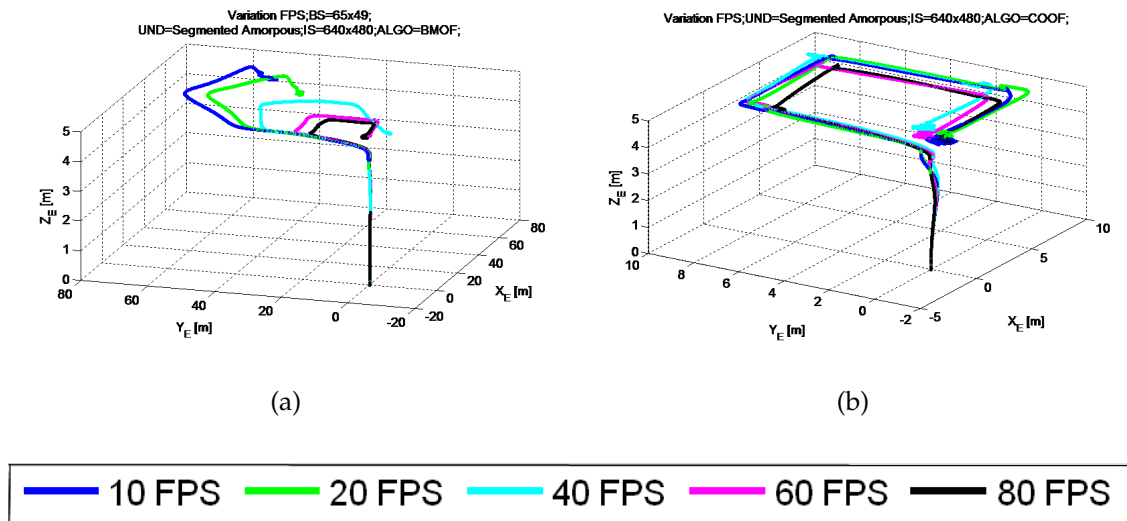


**Figure 5.20:** Position Correction Scheme Results of Test Scenario 1: Translational Test 3D-Trajectory of BMOF and COOF

The rotational tests of this scenario show some interesting characteristics. Starting with the BMOF algorithm, we can see an unstable behaviour which is visualised as diverging spiral that climbs in higher and higher orbits. This instability is based on the unsuitable image processing rotational performance of the BMOF algorithm at the lowest sample rate (See ??(a)). The further sample rates show a suitable result and visualise the S-form curve which is executed by the control system to stabilise the yaw-rotation and is coincident with the translational drift. Opposed to the characteristics of the COOF translational behaviour, the rotational 3D-Trajectories of this algorithm show a stable but different from expected behaviour. The best-suited configuration in this case is the highest sample

### 5.3 ANALYSIS OF POSITION CORRECTION SCHEME

rate, because it shows the shortest 3D-Trajectory. But compared to the other 3D-Trajectories, the difference is not as big as the impact of a 80 FPS sample rate in relation to the transmission or the image processing costs of the complete system.

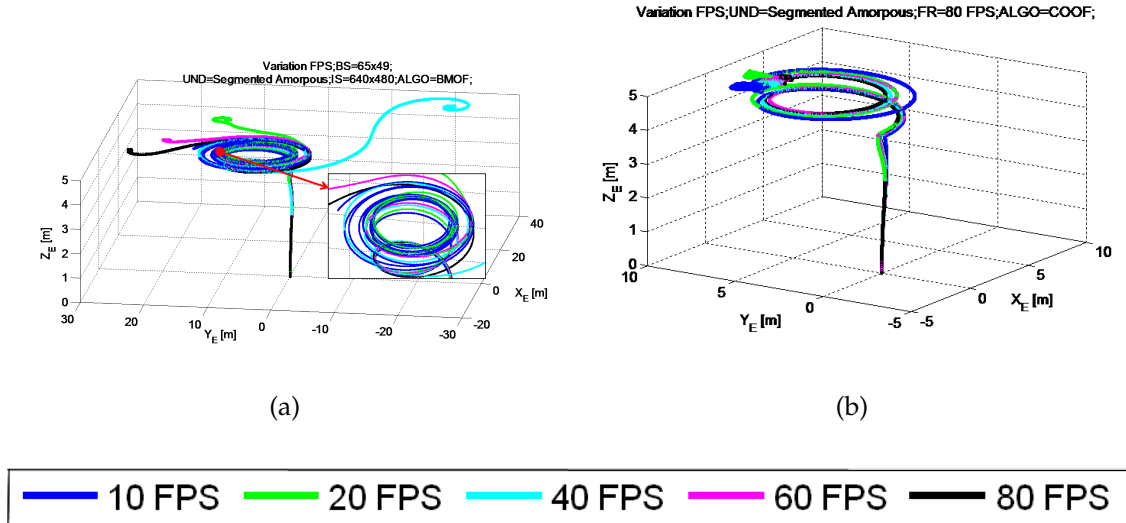


**Figure 5.21:** Position Correction Scheme Results of Test Scenario 1: Rotational Test 3D-Trajectory of BMOF and COOF

The next graphics visualise the hovering state behaviour of both algorithms for a time period of 60 seconds. Starting with the BMOF algorithm, visualised in ?? (a) and (b), we can see the same unsatisfactory behaviour for a sample rate of 10 FPS as demonstrated in the translational tests. As obviously visualised in ?? (b), the blue 3D-Trajectory hovers over a concrete closed area, but drifts arbitrary. Beside this, all other hovering tests are satisfactory, even the hovering state with 20 FPS. Regarding the hovering state behaviour of the COOF algorithm, we can see that the frame rate of 10 FPS shows a better result, due to the smaller area of hovering, than the maximum frame rate of 80 FPS (See ?? (d)). This characteristic is also visualised in graphic ?? (c), and could be the expected impact of noise

### 5.3 ANALYSIS OF POSITION CORRECTION SCHEME

which increases with increasing frame rate in context of the COOF algorithm. Furthermore, this noise behaviour of the COOF algorithm is also related to the image size and will be focused on in the second test scenario.

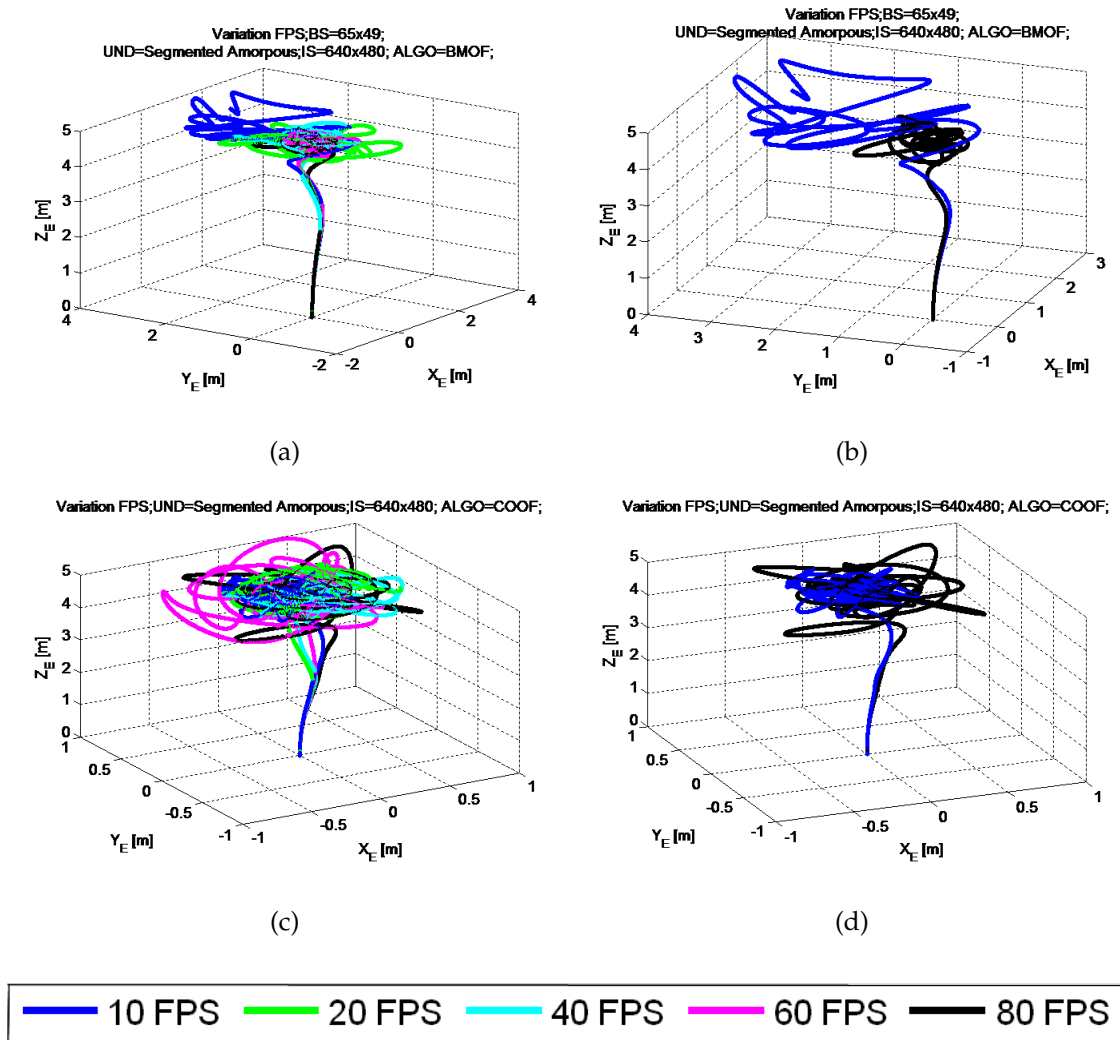


**Figure 5.22:** Position Correction Scheme Results of Test Scenario 1: Hovering State Test 3D-Trajectory of BMOF and COOF

## 5.3 ANALYSIS OF POSITION CORRECTION SCHEME

---

### Position Correction Scheme Test Scenario 2: Variation of Image Size

This test scenario is supposed to show the influence of the image size variation, combined with the mentioned test 3D-trajectories. Similar to the first test scenario, the focus here is on identifying how the presented characteristics (See ??) of the image size variation influence the quality of the position correction scheme. The point of interest thereby is the remarkable noise characteristic, with increasing image size, of the translational behaviour of COOF. Furthermore, the rotational characteristic of BMOF could also show an interesting performance, due to the angular speed limitation, which is notably special in the area of small image sizes. Equal to the previous test scenario, the expectation here also is that the quality of the position correction scheme will show weaknesses and strengths related to the image processing results of corresponding configurations. In comparison to the influences of the first test scenario, the influences of this scenario should show, as expected, less impact on the error characteristic of the position correction scheme.

### Position Correction Scheme Results of Test Scenario 2

The results of the translational behaviour of both algorithms are presented in ?. By focusing on the 3D-Trajectory of the BMOF algorithm, we can see an unexpected drift behaviour of the different image sizes (See ?? (a)). This behaviour could be based on the noise that occurs in the translational movements of BMOF, especially with small image sizes and high translational speeds (See ??). Compared to the long reaction distance of deceleration of the BMOF, the COOF re-

### 5.3 ANALYSIS OF POSITION CORRECTION SCHEME

acts very fast and reliable (See ?? (b)). This characteristic is based on the higher speed limitation behaviour of COOF. Another characteristic is that the noise of the COOF, with increasing image size does not show the expected influence, because all 3D-Trajectories are nearly equal. Finally, we can see that all the image size test 3D-Trajectories, combined with each algorithm, have a stable behaviour and end with a hovering state at one position point.

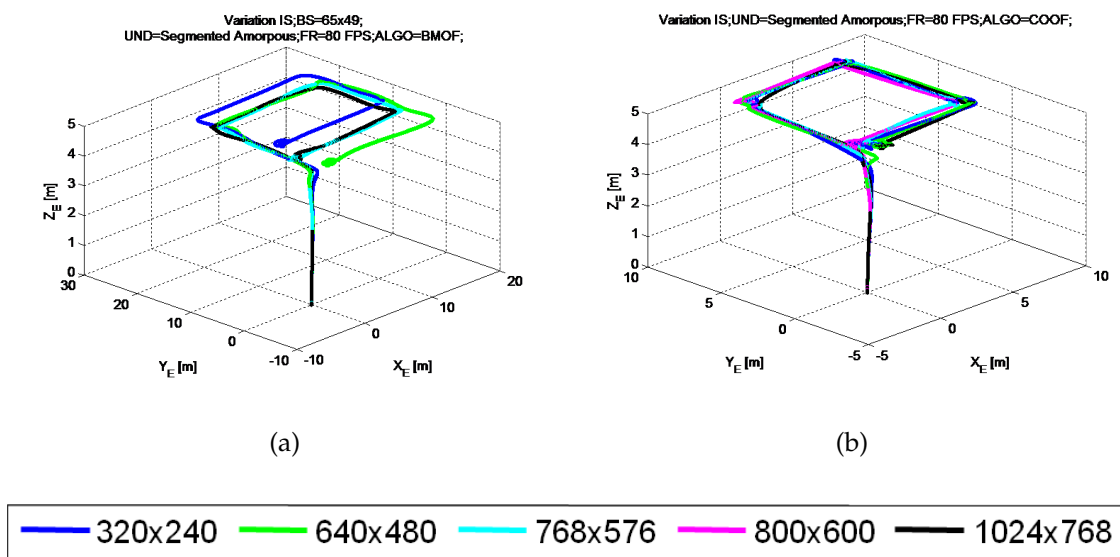


**Figure 5.23:** Position Correction Scheme Results of Test Scenario 2: Translational Test 3D-Trajectory of BMOF and COOF

The rotational behaviour of both algorithms can be measured with the length of the trajectory, which shows the relation to the stability of the position correction scheme. A suitable example for a nearly semi-stable configuration of the position correction scheme is shown in figure ?? (a). The smallest image size of BMOF shows a spiral which converges, with several rounds, to a spot in the middle. A truly semi-stable configuration would spin in one orbit around the stable point. With increasing sample rate, the stability increases and the corresponding length

### 5.3 ANALYSIS OF POSITION CORRECTION SCHEME

of the 3D-Trajectory decreases. Regarding the COOF algorithm 3D-Trajectories in figure ?? (b), the different variations of the orbits show an unexpected behaviour. As demonstrated and visualised in ?? (c), the image size variation showed nearly no influence to the 2D-Trajectory of the image processing. So it is possible that very small changes in the image processing domain influence the control architecture enormously. This could be a possible explanation for these variances of the rotational test 3D-Trajectories together with the COOF algorithm.

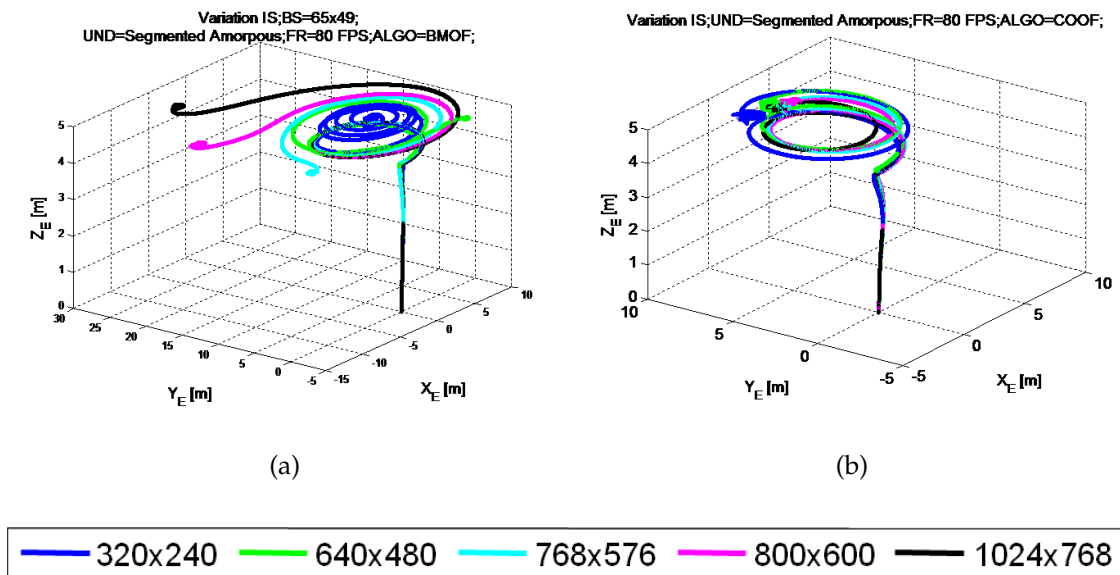


**Figure 5.24:** Position Correction Scheme Results of Test Scenario 2: Rotational Test 3D-Trajectory of BMOF and COOF

Next, the diagrams visualised in figure ?? show the hovering state test results of both algorithms. Starting with the BMOF, we can see that the image size does not show a big impact, as could be expected, and the 3D-Trajectories (See ?? (a)) have nearly the same area, spanned in  $X_E$  and  $Y_E$  direction. Especially the comparison between the biggest and smallest image size test 3D-Trajectories (See ?? (b)) shows that the BMOF algorithm is, notwithstanding the maximum speed

### 5.3 ANALYSIS OF POSITION CORRECTION SCHEME

---

limitation, robust in the area of small velocities. Compared to that, the COOF algorithm shows differences between maximal and minimal image size tests. As we can see in diagram ?? (d), the maximal image size configuration span a bigger area of correction to hover compared to the minimal image size configuration. Surprisingly, this unexpected behaviour could occur due to the characteristic of the COOF, which shows increasing noise with increasing image size (See ?? (c)). This assumption could be underlined, regarding the figure ?? (c), which shows that the next smaller image sizes after the maximum image size also perform worse, compared to smaller image sizes.

### 5.3 ANALYSIS OF POSITION CORRECTION SCHEME

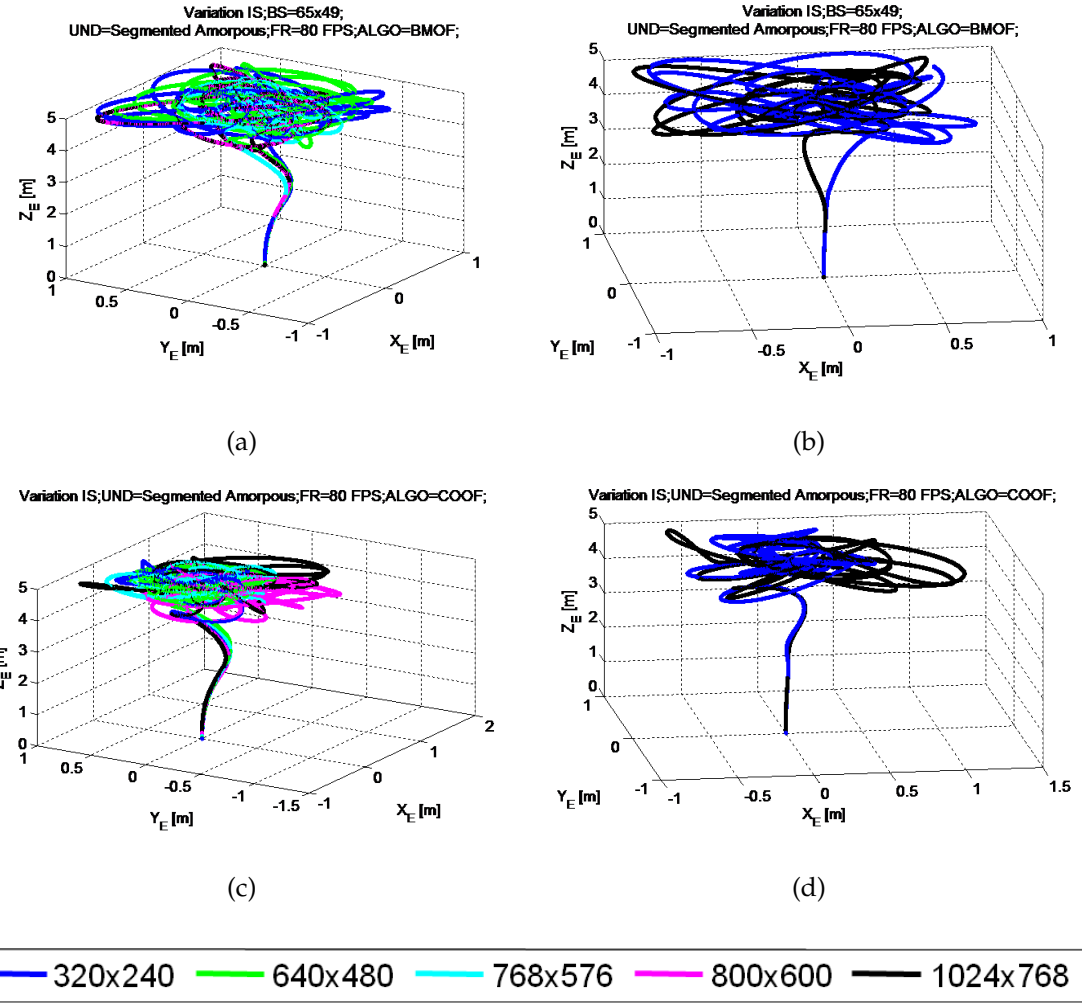


**Figure 5.25:** Position Correction Scheme Results of Test Scenario 2: Hovering State Test 3D-Trajectory of BMOF and COOF

#### 5.3.2 Summary

The position correction scheme test scenarios show that the image processing characteristic enormously affects the precision and quality of the 3D-Trajectories. The results show that the BMOF algorithm can perform suitable results with

### 5.3 ANALYSIS OF POSITION CORRECTION SCHEME

---

small movements, regarding the hovering state tests, but needs to be configured with, at least, a sample rate of 20 FPS. Otherwise, the results are not satisfactory, especially because the rotational behaviour reacts unstable in case of disturbances. Furthermore, the COOF algorithm shows a satisfactory performance in nearly every configuration. But in the hovering state, the COOF algorithm generated unexpected results in the area of big image size and high sample rates. This behaviour could be very suitable for a distributed error correction scheme. The benefits thereby could be that the resources of transmission are not utilised due to a high sample rate or big data packages accrued from big image sizes. Summarised, it can be said that the benefits of the COOF algorithm are more suitable, compared to the BMOF and its corresponding limitations and weaknesses. On the other hand, this simulation did not show the algorithm complexity of BMOF and COOF. The BMOF algorithm could probably show a low algorithm complexity, if it is executed in an embedded environment. In this case, these algorithms should be reconsidered, because an unexpected algorithm complexity of COOF could raise to an unstable position correction scheme, irrespective of the discussed benefits of this algorithm.

## Conclusions and Further Work

The analysis of the distributed optical position correction scheme in this Master's Thesis was executed with a new simulation concept for this special case, and showed the relations between the different configurations of control and image processing. The idea of this concept came up in a preceding intensive investigation of actual researches related to UAV realisation, stabilisation and control, and further investigations of optical possibilities of ego-motion. This review shows the necessity of automated simulation and test of marker-free visual feedback systems for the domain of UAV.

Additionally, investigations present a time-variant physical model for simulating each movement of the quadrocopter body. A further analysis showed how the real electronic components, like the IMU and the actuators, provide and realise the detected and desired signals. Based on these informations, a simulation was designed and implemented using the method of MBD and the MATLAB/Simulink tool-packages. Based on the examined results of optical models and image processing movement detection algorithms, an additionally simulation architecture was implemented, providing a flexible way to simulate different optical system behaviours.

## CHAPTER 6 CONCLUSIONS AND FURTHER WORK

---

Beside this, the simulation was designed modular, with the aim for each component to be exchangeable, and the interface design between the modules to allow extensions for future developments. Using this simulation equipment, several camera and image processing models derived from experiments executed in similar scientific projects, used to derive test scenarios for the demonstration of the impact of different image processing parameters. These image processing test scenarios focus on the variation of different undergrounds, sample rates, image sizes and image processing algorithm specific parameters. Under consideration of different speed stimulus, the results of these test scenarios show the rotational and translational behaviour of two algorithm movement detection abilities, and their limitations related to the characteristics of the camera configurations. The distribution behaviour of the image processing system thereby was abstracted as transmission delay, which was reflected as reduced frame rate.

The results of the image processing test scenarios show the weaknesses and strengths of the movement detection algorithms focussed on. Regarding the COOF algorithm, we saw that it can detect reliable movements under high speed stress conditions, but shows increasing noise behaviour, especially with increasing frame rate, and in reduced form also with increasing image size. In comparison to that, the BMOF algorithm showed serious speed limitations, especially in configurations with low image sizes and frame rates. Furthermore, an algorithm independent but important output signal delay behaviour, related to the image processing, was found in the small area of frame rates.

## CHAPTER 6 CONCLUSIONS AND FURTHER WORK

---

Under consideration of the performance criteria of the designed position and body control system, optimisation experiments were executed to find the best suited parameter configuration for control. The related results show that the realistically designed not-linear physical plant cannot be optimised using linearisation analysis approaches. So the empirical optimisation approach was used with the result of the best suited parameter configuration of the control system used here. Beside this analysis, a strategy for control optimisation was derived, which can be used for further control system developments.

Combined together, and based on the results of the image processing tests and the analysis and optimisation of the control system, the quality of the position control scheme was analysed. This analysis was executed with the aim to show how the complete position correction system reacted under influence of transnational and rotational drifts, and further how it kept the hovering position.

The presented results show that it is possible to build up a distributed position correction scheme with small frame rates, but also with an adequate performance behaviour. Thereby, the test results of the image processing tests also reflected the performances of the position correction tests, and underlined them with visualisation of 3D-Trajectories of the quadrocopter flight. With recapitulating these visualisations, it was found out that the noise of the detected movements had special impact in the area of small movements like these of the hovering state. Afterwards, the speed limitation of image processing algorithms decelerated the reaction behaviour, related to the intensity of the control manoeuvre, and showed that, with decreasing speed limit a bigger flight area is needed to equalise the disturbances.

## 6.1 FURTHER WORK

---

The optical navigation is a strongly growing topic of robotic science. This work showed how the corresponding strengths of this topic can be used for UAV stabilisation, and furthermore how the realisation can be executed systematically using simulation driven MBD. So the optical system realisation of the HSE quadrocopter project can base on a very useful analysis, experience and a flexible simulation structure and test facility.

## 6.1 Further Work

In relation to this Master's Thesis, two of the biggest projects of the Faculty of Information Technology HSE will fuse in the future. These projects are the self-developed and maintained real time operating system Didactic OSEK (DOSEK) and the introduced Quadrocopter Project. The aim thereby is to demonstrate didactically the operation of new technologies that are actually also used in the Automotive-Industry. These projects, the future developments and the exact relation of this Master's Thesis are visualised in the overview graphic ??<sup>1</sup>. As we can see in the black line relations, the Master's Thesis' focus was especially on the simulation of the optical position correction scheme, the control system with the corresponding HIL-facility, and the physical model. In the near future, the optical position correction scheme realisation, presented and analysed here, will start. This process will spawn, nearly parallel, projects for communication, image processing application and camera module development. After that, a future development will be the construction of an MATLAB/Simulink tool-kit for a simulation driven and MBD realisable embedded system application.

---

<sup>1</sup>The blue circles visualise project parts which are scheduled, but not started until now

## 6.1 FURTHER WORK

---

For this purpose, already realised components of this Master's Thesis' software development can be used to realise components that can automatically generate the simulated application into C-code. This source code will be idealised for the target hardware of the quadrocopter and will execute the same time-variant characteristics of control, image processing and so on as designed in the simulation.

For this aim, the generated application source code must be designed as a generic time or event triggered DOSEK application. With this complete tool-chain and the code generation framework, experimental developments could be executed very fast and reliable. This will be the step to a new dimension of possibilities, which also will allow to create very complex developments like an optical autonomous control navigation.

## 6.1 FURTHER WORK

---

graphic/ConclusioMindstorming.pdf

**Figure 6.1:** Overview of project relations and further work

# References

- [1] Hochschule Esslingen University of Applied Sciences. <http://www.hs-esslingen.de>, September 2010.
- [2] Model Based Design, The MathWorks, Inc. <http://www.mathworks.co.uk/model-based-design/>, September 2010.
- [3] OpenCV 2.0 C Reference. <http://opencv.willowgarage.com/>, 2010.
- [4] Matlab, The MathWorks, Inc. <http://www.mathworks.com/products/matlab/>, March 2011.
- [5] Simulink, The MathWorks, Inc. <http://www.mathworks.com/products/simulink/>, March 2011.
- [6] The MathWorks, Inc. <http://www.mathworks.com/>, March 2011.
- [7] Analog Devices. *ADXRS610*, 2007. <http://www.analog.com>.
- [8] Antoine Beyeler, Jean-Christophe Zufferey, Dario Floreano. optiPilot: control of take-off and landing using optic flow. Technical report, Laboratory of Intelligent Systems, École Polytechnique Fédérale de Lausanne (EPFL), 2009.

## REFERENCES

---

- [9] Anton Tratkovski. Prototypische Realisierung und Test einer optischer Flusserkennung auf Basis der OpenCV-Bibliothek, 2010.
- [10] Audsley N. C., Burns A., Richardson M. F., Wellings A. J. HARD REAL-TIME SCHEDULING: THE DEADLINE-MONOTONIC APPROACH. Technical report, Department of Computer Science, University of York, 2001.
- [11] Barry Boehm. A Spiral Model of Software Development and Enhancement. *IEEE Computer*, 21(5):pp.61–72, 1988.
- [12] Beau J. Tippetts. Real-Time Implementation of Vision Algorithms For Control, Stabilization, and Target Tracking, for a Hovering Micro-UAV. Master's thesis, Department of Electrical and Computer Engineering, Brigham Young University, August 2008.
- [13] Bernhard Kleiner. Kameragestuetztes inertiales Navigations-system mit Sensorfusion. Technical report, Fraunhofer Institute for Manufacturing Engineering and Automation IPA, 2009.
- [14] Brian Williams, Georg Klein and Ian Reid. Real-Time SLAM Relocalisation. Technical report, Department of Engineering Science, University of Oxford, 2007.
- [15] Bruce D. Lucas. *Generalized Image Matching by the Method of Differences*. PhD thesis, Robotics Institute, Carnegie Mellon University, July 1984.
- [16] Bruce D. Lucas, Takeo Kanade. An iterative image registration technique

## REFERENCES

---

- with an application to stereo vision. *Proceedings of Imaging Understanding Workshop*, pages pp.121–130, 1981.
- [17] Daniel Gurdan, Jan Stumpf, Michael Achtelik, Klaus-Michael Doth, Gerd Hirzinger, Daniela Rus. Energy-efficient Autonomous Four-rotor Flying Robot Controlled at 1 kHz. *IEEE International Conference of Robotics and Automation, Roma, Italy* , April 2007.
- [18] Daniel Mellinger, Nathan Michael and Vijay Kumar. Trajectory Generation and Control for Precise Aggressive Maneuvers with Quadrotors. *International Symposium on Experimental Robotics, Delhi, India*, December 2010.
- [19] David G. Luenberger. An Introduction to Observers. *IEEE TRANSACTIONS ON AUTOMATIC CONTROL*, VOL. AC-16, NO. 6, December 1971.
- [20] David Morin. *Introduction to classical mechanics: with problems and solutions*. Cambridge University Press, 2007. ISBN 978-0-521-87622-3 First Published Edition 2008.
- [21] Digi International Inc. *XBee*, 2009. <http://www.digi.com/>.
- [22] David H. Douglas and Thomas K. Peucker. Algorithms for the reduction of the number of points required to represent a digitized line or its caricature. *Cartographica: The International Journal for Geographic Information and Geovisualization*, pages 112–122, October 1973.
- [23] Douglas Eastman, Paul Lambrechts and Arkadiy Turevskiy. Design and Ver-

## REFERENCES

---

- ification of Motion Control Algorithms Using Simulation. *The MathWorks, Inc.*, 2009.
- [24] Erdinc, Altug, James P. Ostrowski, Camillo J. Taylor. Quadrotor Control Using Dual Camera Visual Feedback. *IEEE International Conference on Robotics and Automation, Taipei, Taiwan*, 2003.
- [25] Erdinc Altug, James P. Ostrowski, Robert Mahony. Control of a Quadrotor Helicopter Using Visual Feedback. *IEEE International Conference of Robotics and Automation, Washington, DC*, 2002.
- [26] Freescale Semiconductor. *MC9S12XDP512 Data Sheet, HCS12X Microcontrollers, Rev. 2.17*, 2007. <http://www.freescale.com>.
- [27] Gary Bradski and Adrian Kaehler. *Learning OpenCV*. O'Reilly, First Edition edition, 2008.
- [28] George Koharchik. Image Processing with OpenGL and Shaders. <http://www.linuxjournal.com/content/image-processing-opengl-and-shaders>, February 2011.
- [29] Gribbon K.T., Johnston C.T. and Bailey D.G. A Real-time FPGA Implementation of a Barrel Distortion Correction Algorithm with Bilinear Interpolation. Technical report, Institute of Information Sciences and Technology, Massey University, Palmerston North, New Zealand, 2003.
- [30] Hermann Kull. Control Systems 2: Modern Control Structures and Optimiza-

## REFERENCES

---

- sation of Control Systems, July 2011. VZ1.2.
- [31] J.L. Barron, D.J. Fleet and S.S. Beauchemin. Performance of Optical Flow Techniques. Technical report, Dept. of Computer Science, University of Western Ontario, Queen's University, 1994.
- [32] Joachim Schwab, Sreekanth Sundaresh, Nina Vetlugina, Marc Weber, Joerg Fiedrich and Dionysios Satikidis. Project Quadrocopter, Automotive Systems Master Software Based Automotive Systems ASM2-SB / SS 2010 Documentation. Technical report, University of Applied Sciences Esslingen, Department of Information Technology, June 2010.
- [33] John Canny. A Computational Approach to Edge Detection. *IEEE TRANSACTIONS ON PATTERN ANALYSIS AND MACHINE INTELLIGENCE, VOL. PAMI-8, NO. 6*, November 1986.
- [34] John Stowers, Andrew Bainbridge-Smith, Michael Hayes and Steven Mills. Optical Flow for Heading Estimation of a Quadrotor Helicopter. Technical report, University of Canterbury, New Zealand, 2009.
- [35] Juergen Eckert, Falko Dressler and Reinhard German. An Indoor Localization Framework for Four-rotor Flying Robots Using Low-power Sensor Nodes. Technical report, University of Erlangen Dept. of Computer Science, February 2009.
- [36] Karl E. Wenzel, Andreas Masselli and Andreas Zell. Automatic Take Off, Tracking and Landing of a Miniature UAV on a Moving Carrier Vehicle.

## REFERENCES

---

- Technical report, Department of Computer Science, University of Tuebingen, 2010.
- [37] Martin Fach. *Navigation und Lahrensegelung eines Luftschiffes mittels optischer, inertialer und GPS Sensoren*. PhD thesis, Institut für Flugmechanik und Flugregelung, University of Stuttgart, 2008.
- [38] Matlab, The MathWorks, Inc. Simulink Design Optimization. <http://www.mathworks.com/products/sl-design-optimization/index.html>, April 2011.
- [39] Michael Bloesch, Stephan Weiss, Davide Scaramuzza and Roland Siegwart. Vision Based MAV Navigation in Unknown and Unstructured Environments. Technical report, Autonomous Systems Lab, ETH Zuerich, 2010.
- [40] Micron Technology, Inc. *MT9V022: 1/3-Inch Wide-VGA Digital Image Sensor*, 2006. <http://www.micron.com>.
- [41] Nawarat Termtanasombat. Development of Hardware-in-the-Loop Facility for Optical Navigation with the Study of Insect Inspired Algorithm for Spacecraft Landing. Master's thesis, Department of Space Science, Lulea University of Technology, 2010.
- [42] Nirupama Bulusu, John Heidemann and Deborah Estrin. GPS-less Low Cost Outdoor Localization For Very Small Devices. Technical report, University of Southern California / Information Sciences Institute, 2002.

## REFERENCES

---

- [43] Pedro Castillo, Rogelio Lozano and Alejandro Dzul. Stabilization of a Mini Rotorcraft with Four Rotors. *IEEE Control Systems Magazine*, December 2005.
- [44] Pratap Rudra. *Getting started with MATLAB 7 // a quick introduction for scientists and engineers*. Oxford University Press, Inc., 2006. ISBN 978-0-19-517937-8.
- [45] Rachely Esman and Yoad Snapir. OpenCV and MEX-Files Quick Guide, 2010.
- [46] Richard C. Dorf, Robert H. Bishop. *Modern Control Systems*. Prendice-Hall, Inc., ninth edition edition, 2001.
- [47] Robert Czech and Dionysios Satikidis. Project Quadrocopter, Analysis and development of control algorithms. Technical report, University of Applied Sciences Esslingen, Department of Information Technology, 2010.
- [48] Roger R. Pressman. *Software Engineering, A Practitioner's Approach*. McGraw-Hill, Inc., fifth edition edition, 2001.
- [49] Roy Featherstone. *Rigid Body Dynamics Algorithms*. Springer Science+Business Media, LLC, 2008. ISBN 978-0-387-74314-1.
- [50] Samir Bouabdalla, Pierpaolo Murrieri, Roland Siegwart. Design and Control of an Indoor Micro Quadrotor. Technical report, Autonomous Systems Laboratory Swiss Federal Institute of Technology, University of Pisa, 2004.

## REFERENCES

---

- [51] Samir Bouabdallah. *Design and Control of Quadrotors with Application to Autonomous Flying*. PhD thesis, École Polytechnique Fédérale de Lausanne (EPFL), 2007.
- [52] Scott M. Ettinger, Michael C. Nechyba, Peter G. Ifju and Martin Waszak. Vision-Guided Flight Stability and Control for Micro Air Vehicles. Technical report, Intel Corporation, University of Florida, NASA Langley Research Center, March 2004.
- [53] Sebastian Blumenthal, Dirk Holz, Thorsten Linder, Peter Molitor, Hartmut Surmann and Viatcheslav Tretyakov. Teleoperated Visual Inspection and Surveillance with Unmanned Ground and Aerial Vehicles. Technical report, Department of Computer Science, University of Applied Sciences Bonn-Rhein-Sieg, Fraunhofer Institute for Intelligent Analysis and Information Systems (IAIS), 2008.
- [54] Spencer Greg Ahrens. Vision-Based Guidance and Control of a Hovering Vehicle in Unknown Environments. Master's thesis, Department of Mechanical Engineering, Massachusetts Institute of Technology, 2008.
- [55] Steven Kelly. Domain-Specific Modeling 76 cases of MDD that works, 2009.
- [56] Steven Kelly and Juha-Pekka Tolvanen. *Domain-Specific Modeling: Enabling Full Code Generation*. John Wiley & Sons, Inc, 2008. ISBN 978-0-470-03666-2.
- [57] Sven Lange, Niko Sünderhauf, and Peter Protzel. Autonomous Landing for a Multirotor UAV Using Vision. *Intl. Conf. on SIMULATION, MODELING*

## REFERENCES

---

*and PROGRAMMING for AUTONOMOUS ROBOTS, Venice, Italy, November 2008.*

- [58] Sven Lange, Niko Sünderhauf, Peter Protzel. A Vision Based Onboard Approach for Landing and Position Control of an Autonomous Multirotor UAV in GPS-Denied Environments. Technical report, Department of Electrical Engineering and Information Technology, Chemnitz University of Technology, 2009.
- [59] Tommaso Bresciani. Modelling, Identification and Control of a Quadrotor Helicopter. Master's thesis, Department of Automatic Control, Lund University, October 2008.
- [60] Tsai R. Y. and Lenz R. K. . A new technique for fully autonomous and efficient 3D robotics hand-eye calibration. *Robotics and Automation. IEEE Transactions on Robotics and Automation*, Vol. 5, No. 3, June 1989, December 2005.
- [61] Vedran Sikiric. Control of Quadrocopter. Master's thesis, Royal Institute of Technology Sweden, School of Computer Science and Communication, 2008.
- [62] Zhang H. and Ostrowsi J. P. Visual Servoing with Dynamics: Control of an Unmanned Blimp. Technical report, General Robotics, Automation, Sensing, and Perception (GRASP) Laboratory; University of Pennsylvania, 1999.

# Bibliography

- [Ana07] Analog Devices. *ADXRS610*, 2007. <http://www.analog.com>.
- [Ant09] Antoine Beyeler, Jean-Christophe Zufferey, Dario Floreano. optiPilot: control of take-off and landing using optic flow. Technical report, Laboratory of Intelligent Systems, École Polytechnique Fédérale de Lausanne (EPFL), 2009.
- [Ant10] Anton Tratkovski. Prototypische Realisierung und Test einer optischen Flusserkennung auf Basis der OpenCV-Bibliothek, 2010.
- [Aud01] Audsley N. C., Burns A., Richardson M. F., Wellings A. J. HARD REAL-TIME SCHEDULING: THE DEADLINE-MONOTONIC APPROACH. Technical report, Department of Computer Science, University of York, 2001.
- [Bar88] Barry Boehm. A Spiral Model of Software Development and Enhancement. *IEEE Computer*, 21(5):pp.61–72, 1988.
- [Bea08] Beau J. Tippetts. Real-Time Implementation of Vision Algorithms For Control, Stabilization, and Target Tracking, for a Hovering Micro-UAV. Master's thesis, Department of Electrical and Computer Engineering, Brigham Young University, August 2008.

## BIBLIOGRAPHY

---

- [Ber09] Bernhard Kleiner. Kameragestuetztes inertiales Navigations-system mit Sensorfusion. Technical report, Fraunhofer Institute for Manufacturing Engineering and Automation IPA, 2009.
- [Bri07] Brian Williams, Georg Klein and Ian Reid. Real-Time SLAM Relocalisation. Technical report, Department of Engineering Science, University of Oxford, 2007.
- [Bru81] Bruce D. Lucas, Takeo Kanade. An iterative image registration technique with an application to stereo vision. *Proceedings of Imaging Understanding Workshop*, pages pp.121–130, 1981.
- [Bru84] Bruce D. Lucas. *Generalized Image Matching by the Method of Differences*. PhD thesis, Robotics Institute, Carnegie Mellon University, July 1984.
- [Dan07] Daniel Gurdan, Jan Stumpf, Michael Achtelik, Klaus-Michael Doth, Gerd Hirzinger, Daniela Rus. Energy-efficient Autonomous Four-rotor Flying Robot Controlled at 1 kHz. *IEEE International Conference of Robotics and Automation, Roma, Italy*, April 2007.
- [Dan10] Daniel Mellinger, Nathan Michael and Vijay Kumar. Trajectory Generation and Control for Precise Aggressive Maneuvers with Quadrotors. *International Symposium on Experimental Robotics, Delhi, India*, December 2010.
- [Dav71] David G. Luenberger. An Introduction to Observers. *IEEE TRANSACTIONS ON AUTOMATIC CONTROL, VOL. AC-16, NO. 6*, December

## BIBLIOGRAPHY

---

1971.

- [Dav07] David Morin. *Introduction to classical mechanics: with problems and solutions*. Cambridge University Press, 2007. ISBN 978-0-521-87622-3 First Published Edition 2008.
- [Dig09] Digi International Inc. *XBee*, 2009. <http://www.digi.com/>.
- [Dou09] Douglas Eastman, Paul Lambrechts and Arkadiy Turevskiy. Design and Verification of Motion Control Algorithms Using Simulation. *The MathWorks, Inc.*, 2009.
- [DP73] David H. Douglas and Thomas K. Peucker. Algorithms for the reduction of the number of points required to represent a digitized line or its caricature. *Cartographica: The International Journal for Geographic Information and Geovisualization*, pages 112–122, October 1973.
- [Erd02] Erdinc Altug, James P. Ostrowski, Robert Mahony. Control of a Quadrotor Helicopter Using Visual Feedback. *IEEE International Conference of Robotics and Automation, Washington, DC* , 2002.
- [Erd03] Erdinc, Altug, James P. Ostrowski, Camillo J. Taylor. Quadrotor Control Using Dual Camera Visual Feedback. *IEEE International Conference on Robotics and Automation, Taipei, Taiwan*, 2003.
- [Fre07] Freescale Semiconductor. *MC9S12XDP512 Data Sheet, HCS12X Microcontrollers, Rev. 2.17*, 2007. <http://www.freescale.com>.

## BIBLIOGRAPHY

---

- [Gar08] Gary Bradski and Adrian Kaehler. *Learning OpenCV*. O'Reilly, First Edition edition, 2008.
- [Geo11] George Koharchik. Image Processing with OpenGL and Shaders.  
<http://www.linuxjournal.com/content/image-processing-opengl-and-shaders>, February 2011.
- [Gri03] Gribbon K.T., Johnston C.T. and Bailey D.G. A Real-time FPGA Implementation of a Barrel Distortion Correction Algorithm with Bilinear Interpolation. Technical report, Institute of Information Sciences and Technology, Massey University, Palmerston North, New Zealand, 2003.
- [Her11] Hermann Kull. Control Systems 2: Modern Control Structures and Optimisation of Control Systems, July 2011. VZ1.2.
- [HSE10] Hochschule Esslingen University of Applied Sciences. <http://www.hse-esslingen.de>, September 2010.
- [Jea11] Jean-Bernard Hayet. Exploration strategies for simultaneous localization and mapping. <http://www.cimat.mx/jbhayet/temas.php>, February 2011.
- [J.L94] J.L. Barron, D.J. Fleet and S.S. Beauchemin. Performance of Optical Flow Techniques. Technical report, Dept. of Computer Science, University of Western Ontario, Queen's University, 1994.
- [Joa10] Joachim Schwab, Sreekanth Sundaresh, Nina Vetlugina, Marc Weber,

## BIBLIOGRAPHY

---

- Joerg Fiedrich and Dionysios Satikidis. Project Quadrocopter, Automotive Systems Master Software Based Automotive Systems ASM2-SB / SS 2010 Documentation. Technical report, University of Applied Sciences Esslingen, Department of Information Technology, June 2010.
- [Joh86] John Canny. A Computational Approach to Edge Detection. *IEEE TRANSACTIONS ON PATTERN ANALYSIS AND MACHINE INTELLIGENCE, VOL. PAMI-8, NO. 6*, November 1986.
- [Joh09] John Stowers, Andrew Bainbridge-Smith, Michael Hayes and Steven Mills. Optical Flow for Heading Estimation of a Quadrotor Helicopter. Technical report, University of Canterbury, New Zealand, 2009.
- [Jue09] Juergen Eckert, Falko Dressler and Reinhard German. An Indoor Localization Framework for Four-rotor Flying Robots Using Low-power Sensor Nodes. Technical report, University of Erlangen Dept. of Computer Science, February 2009.
- [Kar10] Karl E. Wenzel, Andreas Masselli and Andreas Zell. Automatic Take Off, Tracking and Landing of a Miniature UAV on a Moving Carrier Vehicle. Technical report, Department of Computer Science, University of Tuebingen, 2010.
- [Mar08] Martin Fach. *Navigation und Lahrensegelung eines Luftschiffes mittels optischer, inertialer und GPS Sensoren*. PhD thesis, Institut für Flugmechanik und Flugregelung, University of Stuttgart, 2008.

## BIBLIOGRAPHY

---

- [Mat10] Model Based Design, The MathWorks, Inc. <http://www.mathworks.co.uk/model-based-design/>, September 2010.
- [Mat11a] Matlab, The MathWorks, Inc. <http://www.mathworks.com/products/matlab/>, March 2011.
- [Mat11b] The MathWorks, Inc. <http://www.mathworks.com/>, March 2011.
- [Mat11c] Matlab, The MathWorks, Inc. Simulink Design Optimization. <http://www.mathworks.com/products/sl-design-optimization/index.html>, April 2011.
- [Mic06] Micron Technology, Inc. *MT9V022: 1/3-Inch Wide-VGA Digital Image Sensor*, 2006. <http://www.micron.com>.
- [Mic10] Michael Bloesch, Stephan Weiss, Davide Scaramuzza and Roland Siegwart. Vision Based MAV Navigation in Unknown and Unstructured Environments. Technical report, Autonomous Systems Lab, ETH Zuerich, 2010.
- [Naw10] Nawarat Termtanasombat. Development of Hardware-in-the-Loop Facility for Optical Navigation with the Study of Insect Inspired Algorithm for Spacecraft Landing. Master's thesis, Department of Space Science, Lulea University of Technology, 2010.
- [Nir02] Nirupama Bulusu, John Heidemann and Deborah Estrin. GPS-less

## BIBLIOGRAPHY

---

- Low Cost Outdoor Localization For Very Small Devices. Technical report, University of Southern California / Information Sciences Institute, 2002.
- [Ope10] OpenCV 2.0 C Reference. <http://opencv.willowgarage.com/>, 2010.
- [Ped05] Pedro Castillo, Rogelio Lozano and Alejandro Dzul. Stabilization of a Mini Rotorcraft with Four Rotors. *IEEE Control Systems Magazine*, December 2005.
- [Pra06] Pratap Rudra. *Getting started with MATLAB 7 // a quick introduction for scientists and engineers*. Oxford University Press, Inc., 2006. ISBN 978-0-19-517937-8.
- [Rac10] Rachely Esman and Yoad Snapir. OpenCV and MEX-Files Quick Guide, 2010.
- [Ric01] Richard C. Dorf, Robert H. Bishop. *Modern Control Systems*. Prentice-Hall, Inc., ninth edition edition, 2001.
- [Rob10] Robert Czech and Dionysios Satikidis. Project Quadrocopter, Analysis and development of control algorithms. Technical report, University of Applied Sciences Esslingen, Department of Information Technology, 2010.
- [Rog01] Roger R. Pressman. *Software Engineering, A Practitioner's Approach*. McGraw-Hill, Inc., fifth edition edition, 2001.

## BIBLIOGRAPHY

---

- [Roy08] Roy Featherstone. *Rigid Body Dynamics Algorithms*. Springer Science+Business Media, LLC, 2008. ISBN 978-0-387-74314-1.
- [Sam04] Samir Bouabdalla, Pierpaolo Murrieri, Roland Siegwart. Design and Control of an Indoor Micro Quadrotor. Technical report, Autonomous Systems Laboratory Swiss Federal Institute of Technology, University of Pisa, 2004.
- [Sam07] Samir Bouabdallah. *Design and Control of Quadrotors with Application to Autonomous Flying*. PhD thesis, École Polytechnique Fédérale de Lausanne (EPFL), 2007.
- [Sco04] Scott M. Ettinger, Michael C. Nechyba, Peter G. Ifju and Martin Waszak. Vision-Guided Flight Stability and Control for Micro Air Vehicles. Technical report, Intel Corporation, University of Florida, NASA Langley Research Center, March 2004.
- [Seb08] Sebastian Blumenthal, Dirk Holz, Thorsten Linder, Peter Molitor, Hartmut Surmann and Viatcheslav Tretyakov. Teleoperated Visual Inspection and Surveillance with Unmanned Ground and Aerial Vehicles. Technical report, Department of Computer Science, University of Applied Sciences Bonn-Rhein-Sieg, Fraunhofer Institute for Intelligent Analysis and Information Systems (IAIS), 2008.
- [Sim11] Simulink, The MathWorks, Inc. <http://www.mathworks.com/products/simulink> March 2011.

## BIBLIOGRAPHY

---

- [Spe08] Spencer Greg Ahrens. Vision-Based Guidance and Control of a Hovering Vehicle in Unknown Environments. Master's thesis, Department of Mechanical Engineering, Massachusetts Institute of Technology, 2008.
- [Ste08] Steven Kelly and Juha-Pekka Tolvanen. *Domain-Specific Modeling: Enabling Full Code Generation*. John Wiley & Sons, Inc, 2008. ISBN 978-0-470-03666-2.
- [Ste09] Steven Kelly. Domain-Specific Modeling 76 cases of MDD that works, 2009.
- [Sve08] Sven Lange, Niko Sünderhauf, and Peter Protzel. Autonomous Landing for a Multirotor UAV Using Vision. *Intl. Conf. on SIMULATION, MODELING and PROGRAMMING for AUTONOMOUS ROBOTS, Venice, Italy*, November 2008.
- [Sve09] Sven Lange, Niko Sünderhauf, Peter Protzel. A Vision Based Onboard Approach for Landing and Position Control of an Autonomous Multirotor UAV in GPS-Denied Environments. Technical report, Department of Electrical Engineering and Information Technology, Chemnitz University of Technology, 2009.
- [Tom08] Tommaso Bresciani. Modelling, Identification and Control of a Quadrotor Helicopter. Master's thesis, Department of Automatic Control, Lund University, October 2008.
- [Tsa05] Tsai R. Y. and Lenz R. K. . A new technique for fully autonomous and ef-

## BIBLIOGRAPHY

---

- ficient 3D robotics hand-eye calibration. *Robotics and Automation. IEEE Transactions on Robotics and Automation*, Vol. 5, No. 3, June 1989, December 2005.
- [Ved08] Vedran Sikiric. Control of Quadrocopter. Master's thesis, Royal Institute of Technology Sweden, School of Computer Science and Communication, 2008.
- [Zha99] Zhang H. and Ostrowsi J. P. Visual Servoing with Dynamics: Control of an Unmanned Blimp. Technical report, General Robotics, Automation, Sensing, and Perception (GRASP) Laboratory; University of Pennsylvania, 1999.